



Eidgenössische Technische Hochschule Zürich
Swiss Federal Institute of Technology Zurich

PAUL SCHERRER INSTITUT



Diploma Thesis
Department of Physics

ETHZ - IPP - 2008 - 09

Geometrical Alignment of the Drift Chamber System and Target of the MEG Experiment

SS 2008

Jeanine Adam
ID 03-910-130
<jeanine.adam@psi.ch>

Professor: Prof. Dr. Urs Langenegger
Supervising Tutors: Dr. Malte Hildebrandt
Dr. Stefan Ritt

ETH Zurich, Institute for Particle Physics
PSI - Paul Scherrer Institute, Villigen

Zurich
18th August 2008

Abstract

Optical Survey 2008 of the drift chamber system and the target of the MEG experiment took place in spring 2008. By using the resulting data the placing of the so-called support structure inside MEG detector and the mounting of drift chambers on this support structure are analyzed and compared with data taken in 2007. Additionally the correlation between surveyed measuring points on the drift chamber modules and on the support structure and signal wire positions is derived. The geometrical alignment of the drift chamber system for run 2008 is therefore provided. As improvement compared to last year possible slopes of signal wires depending on z are also implemented in the geometrical alignment. Compared to last year the measuring procedure of the optical survey was upgraded in a way that the z coordinates of measuring points were also determined. Of course these measured z values are also analyzed. Additionally, since spring 2008 it is possible to determine the target position by optical surveying methods. The target data obtained by such measurements is analyzed and among other results the target slant angle is determined to be $\alpha = (20.6 \pm 0.2)^\circ$.

Contents

1	Introduction	1
2	Physics Motivation	3
2.1	Standard Model	3
2.1.1	Standard Model of Particle Physics	3
2.1.2	Lepton Flavor Conservation	4
2.1.3	Muon Decay	5
2.2	$\mu^+ \rightarrow e^+\gamma$ Decay	6
2.2.1	Neutrino Oscillations	6
2.2.2	Physics Beyond the Standard Model	7
2.3	$\mu^+ \rightarrow e^+\gamma$ Decay Search Experiments	8
3	MEG Experiment	11
3.1	Overview	11
3.2	Beam	13
3.2.1	PSI Beam Line π E5	13
3.2.2	MEG Beam Line	13
3.3	Target	14
3.4	COBRA Magnet	17
3.4.1	Design of COBRA	17
3.4.2	Advantages of COBRA	19
3.5	Drift Chamber System	21
3.6	Timing Counters	23

3.6.1	ϕ -Counter	24
3.6.2	z -Counter	25
3.7	Photon Detector	25
4	Drift Chambers	27
4.1	Requirements	27
4.2	MEG Drift Chamber Design	28
4.2.1	Chamber Geometry	28
4.2.2	Left-Right Ambiguity	29
4.2.3	Anode Wires, Potential Wires and Cathodes	30
4.2.4	Assembly	31
4.3	Setup of the Drift Chamber System	34
4.3.1	Drift Chamber System Geometry	34
4.3.2	Support Structure	35
4.3.3	Support Structure Centering inside COBRA	36
5	Optical Survey 2008	39
5.1	Purpose of Optical Survey 2008	39
5.2	Measuring Points	40
5.2.1	Drift Chamber Crosses	40
5.2.2	Support Structure Pins	41
5.2.3	Target Survey Marks	43
5.3	General Measuring Principle	44
5.3.1	Measuring Instrument	44
5.3.2	Survey of Measuring Points	45
5.3.3	Reference Points	46
5.4	Optical Survey 2007	48
5.5	Optical Survey 2008	49
5.5.1	Reference Points	49
5.5.2	Position 1	51
5.5.3	Position 2 / 3	52

5.5.4	Target Extraction and Insertion	53
5.5.5	Remark: Calibration and Errors	54
6	Mechanical Workshop Survey	55
6.1	Mechanical Workshop Survey 2007	55
6.1.1	Measurements No.4/No.5 and No.7/No.8	56
6.1.2	Measurements No.10 and No.11	57
6.1.3	Measurements No.6 and No.9	57
6.2	Anode Wires	59
7	Analysis of Optical Survey 2007 and 2008	61
7.1	Theoretical Positions	62
7.1.1	Theoretical Positions of Support Structure Pins	62
7.1.2	Expected Positions of Drift Chamber Crosses	64
7.2	Support Structure Deformation	67
7.2.1	Support Structure Deformation in 2007	67
7.2.2	Support Structure Deformation in 2008	69
7.2.3	Difference upstream and downstream in 2008	71
7.3	Drift Chamber Mounting	72
7.3.1	Drift Chamber Mounting in 2007	72
7.3.2	Drift Chamber Mounting in 2008	75
7.4	Measured z Coordinates of Crosses and Pins	76
7.4.1	Cross Distance Check	77
7.4.2	Consequence of $+z$ Shift	79
8	Geometrical Alignment of the Drift Chamber System	81
8.1	Calculation of the Corrected Cross Position	81
8.2	Determination of Anode Wire Positions	85
9	Analysis of Target Measurements	89
9.1	Consistency Check	90
9.2	Reproducibility	93

9.3	Target Slant Angle	94
9.3.1	Conventional	95
9.3.2	Photogrammetric	96
9.3.3	Optical Survey 2008	96
10	Conclusion	99
A	Labeling and Numbering	103
A.1	Orientation in Area $\pi E5$	103
A.2	MEG Coordinate System	104
A.3	Drift Chamber Labeling and Numbering	104
A.3.1	upstream / downstream	104
A.3.2	Drift Chamber Numbering	104
A.3.3	plane A / plane B	105
A.3.4	Anode Wire Numbering	105
B	Data Mechanical Workshop Survey 2007	107
B.1	Data No.4/No.5 and No.7/No.8	107
B.2	Data No.10/No.11 and No.6/No.9	108
C	Data Optical Survey 2007	109
C.1	Pins with given z Positions	109
C.2	DC Crosses with given z Positions	111
D	Data Optical Survey 2008	113
D.1	Pins with given z Positions	113
D.2	DC Crosses with given z Positions	115
D.3	Pins with measured z Positions	117
D.4	DC Crosses with measured z Positions	118
E	Data Theoretical Positions	121
E.1	Theoretical Positions Pins	121
E.2	Expected Positions DC Crosses	123

F Data Target Measurements	125
F.1 Target Crosses in Local Coordinate System	125
F.2 Measured Target Crosses in 2008	126
Bibliography	128

List of Figures

2.1	Feynman Diagrams of Michel Decays	5
2.2	$\mu^+ \rightarrow e^+\gamma$ Decay induced by Neutrino Oscillation	7
2.3	$\mu^+ \rightarrow e^+\gamma$ Decay induced by Slepton Flavor Mixing	8
3.1	Schematic of a $\mu^+ \rightarrow e^+\gamma$ Decay	12
3.2	Schematics of two possible Background Events	12
3.3	Outline of MEG Beam Line Devices	14
3.4	Photograph and Schematic Drawing of the Target	15
3.5	Photographs of the Target mounted on the Support Structure	16
3.6	Lateral View of the Positron Spectrometer	17
3.7	Cross-Sectional View of the Positron Spectrometer	18
3.8	Schematic Drawing and Photograph of COBRA	19
3.9	Advantage of COBRA: Particles emitted close to 90°	20
3.10	Advantage of COBRA: Constant Bending Radius	20
3.11	Schematic Drawing of a MEG Drift Chamber	21
3.12	Cross-Sectional View of a MEG Drift Chamber with Details	22
3.13	Photographs of the Support Structure	23
3.14	Lateral View of Timing Counters	23
3.15	Cross-Sectional View of Timing Counters	24
3.16	Schematic Drawing of the Liquid Xenon Detector	26
4.1	Schematic Drawing of one MEG Drift Chamber	29
4.2	Left-Right Ambiguity in Single and Double Layer Drift Chambers	29

4.3	Cross-Sectional View of the final Drift Chamber Setup	30
4.4	Schematic of a z Position Measurement with Vernier Pads . . .	31
4.5	Schematic Drawing of a general Drift Chamber Frame	32
4.6	Schematic Drawing of the Cathode Frame	32
4.7	Schematic Drawings of Anode Wire Frames	33
4.8	Schematic Drawings of the Hood Frame and the Cathode Foil "hood"	34
4.9	Schematic Drawing of the Drift Chamber System Geometry . .	34
4.10	Photograph of the Support Structure	35
4.11	Photographs of the Cabling Situation upstream and downstream	36
4.12	Schematic Drawing of the Support Structure Centering 2007 . .	37
4.13	Schematic Drawing of the Support Structure Centering 2008 . .	37
5.1	Photograph of Drift Chamber Crosses viewed from downstream	41
5.2	Photograph and Schematic Drawing of Flags	41
5.3	Photograph of Support Structure Pins viewed from downstream	42
5.4	Schematic of Support Structure Pins and Drift Chambers . . .	42
5.5	Schematic Drawing of the Target with Cross Coordinates . . .	43
5.6	Photograph of Total Station TC2002 and Schematic of Optical Survey from downstream	44
5.7	Photograph of a Corner Cube Reflector	45
5.8	Photograph of COBRA with labeled Reference Points	47
5.9	Schematic Drawing of the Theodolite Position used for Optical Survey 2007	48
5.10	Photographs of some Temporary Reference Points used for Optical Survey 2008	50
5.11	Outline of Area $\pi E5$ with marked Reference Points used for Optical Survey 2008	50
5.12	Schematic of Position 1	51
5.13	Schematic of Position 2 and Position 3	52
5.14	Schematic of Position 4 and Position 5	53
6.1	Schematic of the Mechanical Workshop Survey Setup	55

6.2	Schematics of Measurements No.4/No.5 and No.7/No.8	56
6.3	Schematics of Measurements No.10 and No.11	57
6.4	Schematics of Measurements No.6 and No.9	58
6.5	Results of Cross Distance Measurements	58
6.6	Schematics of the Distance between outermost Anode Wire and Drift Chamber Bolt	59
7.1	Schematic of Support Structure Pins with Geometrical Spec- ifications	63
7.2	Theoretical z Positions of Support Structure Pins	64
7.3	Schematic with Variables and Geometrical Specifications to calculate Expected Drift Chamber Cross Positions	66
7.4	Theoretical z Positions of Drift Chamber Crosses	67
7.5	2007 Pins downstream: Theoretical and Measured Coordinates	68
7.6	2007 Pins upstream: Theoretical and Measured Coordinates .	69
7.7	2008 Pins downstream: Theoretical and Measured Coordinates	70
7.8	2008 Pins upstream: Theoretical and Measured Coordinates .	70
7.9	2008 Pins upstream - downstream: Measured x Coordinates .	71
7.10	2008 Pins upstream - downstream: Measured y Coordinates .	71
7.11	2008 Pins upstream - downstream: Measured Two Dimen- sional Distances	72
7.12	2007 Crosses downstream and upstream: Expected and Mea- sured Coordinates	73
7.13	Drift Chamber Mounting downstream in 2007	74
7.14	Drift Chamber Mounting upstream in 2007	74
7.15	2008 Crosses downstream and upstream: Expected and Mea- sured Coordinates	75
7.16	Drift Chamber Mounting downstream in 2008	75
7.17	Drift Chamber Mounting upstream in 2008	76
7.18	2008 Crosses downstream: Theoretical and Measured z	77
7.19	2008 Crosses upstream: Theoretical and Measured z	77
7.20	Measured Cross Distances with Error Bars of 0.7 mm	78
7.21	Measured Cross Distances with Error Bars of 0.3 mm	78

7.22	2008 Crosses downstream: x and y Coordinates determined by Theoretical and Measured z Coordinates	79
7.23	2008 Crosses upstream: x and y Coordinates determined by Theoretical and Measured z Coordinates	80
8.1	Schematics of the Cross Displacement χ	82
8.2	Schematic with Variables mentioned in Section 8.1	83
8.3	Schematic Drawing to calculate the Angle ψ	84
8.4	Schematics to determine Anode Wire Positions	86
8.5	Schematic to calculate the Center of each Anode Wire	87
8.6	Anode Wire Positions at $z = 480.5$ mm	88
9.1	Schematic of the Target with Cross Coordinates in a Local Coordinate System	89
9.2	Consistency Check: Target Crosses before Movements	91
9.3	Consistency Check: Target Crosses after Movements	92
9.4	Reproducibility of the Target Position x Coordinate	93
9.5	Reproducibility of the Target Position y Coordinate	93
9.6	Reproducibility of the Target Position z Coordinate	94
9.7	Schematic of the Conventional Measuring Method to determine the Target Slant Angle	95
9.8	Schematic of the xz Plane with marked Angle α	97
9.9	Schematics of xy and zy Planes with marked Angles β and γ	97
A.1	Area $\pi E5$ Outline with Labels upstream, downstream, berg and aare	103
A.2	Labels upstream and downstream used for Drift Chambers	104
A.3	Schematic Drawing of the Drift Chamber System with numbered Modules	105
A.4	Schematic Drawing of two Drift Chambers with labeled Planes and Anode Wires	106

List of Tables

2.1	Branching Ratios of Muon Decay Modes	6
2.2	Upper Limits for the Branching Ratio $B(\mu^+ \rightarrow e^+ \gamma)/B(\mu^+ \rightarrow e^+ \bar{\nu}_\mu \nu_e)$ reached by other Experiments	9
3.1	Summarized Specifications of the Target	16
3.2	Summarized Specifications of COBRA Coils	19
3.3	Summarized Specifications of Drift Chambers	21
3.4	Summarized Specifications of Timing Counters	25
4.1	Length of each Anode Wire in Plane A and B	33
4.2	Specifications about the asymmetric Cable Disposition	36
5.1	Theoretical z Positions of Measuring Points	49
5.2	List of Reference Points used for Optical Survey 2008	50
9.1	Axis Intercepts and Angles of the Target Plane	98
9.2	Target Slant Angle	98
B.1	Data of Measurements No.4/No.5 and No.7/No.8	107
B.2	Data of Measurements No.10/No.11 and No.6/No.9	108
C.1	Data of Support Structure Pins downstream obtained by Optical Survey 2007 with given z Positions	109
C.2	Data of Support Structure Pins upstream obtained by Optical Survey 2007 with given z Positions	110
C.3	Data of Drift Chamber Crosses downstream obtained by Optical Survey 2007 with given z Positions	111

C.4	Data of Drift Chamber Crosses upstream obtained by Optical Survey 2007 with given z Positions	112
D.1	Data of Support Structure Pins downstream obtained by Optical Survey 2008 with given z Positions	113
D.2	Data of Support Structure Pins upstream obtained by Optical Survey 2008 with given z Positions	114
D.3	Data of Drift Chamber Crosses downstream obtained by Optical Survey 2008 with given z Positions	115
D.4	Data of Drift Chamber Crosses upstream obtained by Optical Survey 2008 with given z Positions	116
D.5	Data of Support Structure Pins downstream obtained by Optical Survey 2008 with measured z Positions	117
D.6	Data of Support Structure Pins upstream obtained by Optical Survey 2008 with measured z Positions	117
D.7	Data of Drift Chamber Crosses downstream obtained by Optical Survey 2008 with measured z Positions	118
D.8	Data of Drift Chamber Crosses upstream obtained by Optical Survey 2008 with measured z Positions	119
E.1	Theoretical Positions of Support Structure Pins downstream	121
E.2	Theoretical Positions of Support Structure Pins upstream	122
E.3	Expected Positions of Drift Chamber Crosses downstream	123
E.4	Expected Positions of Drift Chamber Crosses upstream	124
F.1	Data of Target Crosses in a Local Coordinate System	125
F.2	Data of Target Crosses measured by the Optical Survey 2008 before Movements	126
F.3	Data of Target Crosses measured by the Optical Survey 2008 after Movements	126

Chapter 1

Introduction

The MEG experiment is located at the Paul Scherrer Institute (PSI) in Villigen, Switzerland. Physicists from Italy, Japan, Russia, Switzerland and the United States collaborate on this experiment to measure the branching ratio of the lepton flavor violating decay $\mu^+ \rightarrow e^+\gamma$. The goal of the MEG Collaboration is to lower the current experimental upper limit of this branching ratio by two orders of magnitude to $1.0 \cdot 10^{-13}$. To reach the required sensitivity the track and the timing of the positron are measured by drift chambers and timing counters whereas the photon is detected by a liquid xenon calorimeter.

To reconstruct the track of the positron it is necessary to know where exactly the drift chambers and therefore the signal wires are placed inside the MEG detector. This alignment is usually done by using measurements with cosmic rays or Michel decays. But nevertheless a certain starting point of the drift chamber positions is absolutely essential to determine signal wire positions with the help of these measurements and software algorithm. Because only geometrical considerations but no particle or decay data are involved to this starting point, it is called geometrical alignment. Of course it is possible to use theoretical drift chamber positions as geometrical alignment but to improve the alignment it is reasonable to survey the drift chamber positions by optical methods which is done by the PSI Survey Group.

The goal of this thesis is to provide the geometrical alignment for the run 2008. This means that the position of each drift chamber and therefore each signal wire has to be determined by using geometrical data provided by the Survey Group.

To derive this geometrical alignment it is necessary to understand the drift chamber construction and the mounting of the chambers inside the MEG detector. Additionally it is important to understand the measuring procedure used by the Survey Group.

Since spring 2008 it is possible to determine the target position inside the MEG detector by using optical surveying methods. This thesis will therefore also deal with the analysis of the target position especially with the target slant angle.

After a brief introduction to physics motivation in chapter 2, the MEG experiment with all its components as beam line, target, drift chambers, timing counters and liquid xenon detector will be introduced in chapter 3. The drift chambers will be discussed in detail in chapter 4 followed by a description of the optical surveys 2007 and 2008 (chapter 5) and the mechanical workshop survey 2007 (chapter 6). Then, the results of the analysis of optical surveys 2007 and 2008 will be presented in chapter 7. After this discussion, chapter 8 will describe the calculation of the signal wire positions for the geometrical alignment 2008. Finally, target measurements will be analyzed in chapter 9 followed by a short conclusion (chapter 10).

Chapter 2

Physics Motivation

To highlight the importance of the MEG experiment, it is necessary to consider some aspects of theoretical physics as for example the Standard Model of particle physics and neutrino oscillations. Of course theories about physics beyond the Standard Model are also important because the discovery of the $\mu^+ \rightarrow e^+\gamma$ decay will corroborate or falsify such theories.

This chapter will only give a short introduction in these theoretical aspects: In section 2.1 is a short overview about fundamentals of the Standard Model with special attention to the Lepton Flavor Conservation. The decay $\mu^+ \rightarrow e^+\gamma$ will be discussed in detail in section 2.2 with a focus on physics beyond the Standard Model. Finally, a short summary about $\mu^+ \rightarrow e^+\gamma$ decay search experiments and the current experimental upper limit of the corresponding branching ratio will be given in section 2.3. For more detailed information about these theoretical aspects, please see basic literature about particle physics or the original papers.

2.1 Standard Model

2.1.1 Standard Model of Particle Physics

In physics, there are four known fundamental interactions between elementary particles, namely the electromagnetic, the weak, the strong and the gravitational force. The first two can be combined with the electroweak theory whereas quantum chromodynamics is the description of the strong interaction. The combination of electroweak theory and quantum chromodynamics is called the Standard Model¹ of particle physics. The Standard

¹Fundamentals about the Standard Model of particle physics mentioned in these sections are based on [1] and [2].

Model describes three of these four fundamental forces, whereas gravitation is neglected in particle physics.

In the Standard Model, the elementary particles are six leptons and six quarks, respectively. A lepton is a spin 1/2 particle² which interacts electromagnetically and weakly but not strongly with other elementary particles. At present, six leptons are known: electron e , muon μ , tau τ , electron neutrino ν_e , muon neutrino ν_μ and tau neutrino ν_τ . These particles are classified in three lepton flavors:

$$\begin{pmatrix} \nu_e \\ e \end{pmatrix} \quad \begin{pmatrix} \nu_\mu \\ \mu \end{pmatrix} \quad \begin{pmatrix} \nu_\tau \\ \tau \end{pmatrix}$$

A quark is a spin 1/2 particle too, but it interacts through all fundamental forces. There are also six known quarks called up u , down d , strange s , charm c , bottom (sometimes also called beauty) b and top t classified in three quark families³:

$$\begin{pmatrix} u \\ d \end{pmatrix} \quad \begin{pmatrix} c \\ s \end{pmatrix} \quad \begin{pmatrix} t \\ b \end{pmatrix}$$

2.1.2 Lepton Flavor Conservation

In the Standard Model of particle physics, weak decays of a quark into another quark and a so-called W boson are possible even if the two corresponding quarks are not in the same quark family (see subsection 2.1.1). The theoretical foundation of this physics phenomenon is given by the Cabibbo-Kobayashi-Maskawa (CKM) matrix, which describes the mixing of flavor and mass eigenstates in the quark sector. Each entry of this 3×3 unitary matrix gives the transition probability between two quarks.

The presumption of a corresponding transition matrix for the lepton sector is obvious. But because neutrino masses are not measurable at the moment, it is assumed that all neutrinos have mass equal zero. This assumption leads in theoretical calculations to vanishing transition probabilities between leptons from different lepton flavors and thus to the so-called Lepton Flavor Conservation (LFC). This principle describes the conservation of the lepton flavor quantum number in every decay or interaction with leptons:

²Every particle with a half-integer spin is called fermion.

³Note that the listing order used in the text represents increasing quark masses.

$$\begin{array}{rcc}
 & \begin{pmatrix} \nu_e \\ e^- \end{pmatrix} & \begin{pmatrix} \nu_\mu \\ \mu^- \end{pmatrix} & \begin{pmatrix} \nu_\tau \\ \tau^- \end{pmatrix} \\
 L_e & = & 1 & 0 & 0 \\
 L_\mu & = & 0 & 1 & 0 \\
 L_\tau & = & 0 & 0 & 1
 \end{array}$$

And for antiparticles:

$$\begin{array}{rcc}
 & \begin{pmatrix} e^+ \\ \bar{\nu}_e \end{pmatrix} & \begin{pmatrix} \mu^+ \\ \bar{\nu}_\mu \end{pmatrix} & \begin{pmatrix} \tau^+ \\ \bar{\nu}_\tau \end{pmatrix} \\
 L_e & = & -1 & 0 & 0 \\
 L_\mu & = & 0 & -1 & 0 \\
 L_\tau & = & 0 & 0 & -1
 \end{array}$$

2.1.3 Muon Decay

Muons are unstable particles and in the Standard Model they decay through the weak interaction into other leptons. In most cases the muon decays into a muon neutrino and a virtual W boson which decays then into an electron and an electron antineutrino. The lepton flavor quantum number is conserved at each decay vertex during this interaction and the principle of Lepton Flavor Conservation is therefore fulfilled. The corresponding decay of an antimuon can be derived by using charge conjugation and parity transformation:

$$\mu^- \rightarrow e^- \nu_\mu \bar{\nu}_e, \quad \mu^+ \rightarrow e^+ \bar{\nu}_\mu \nu_e.$$

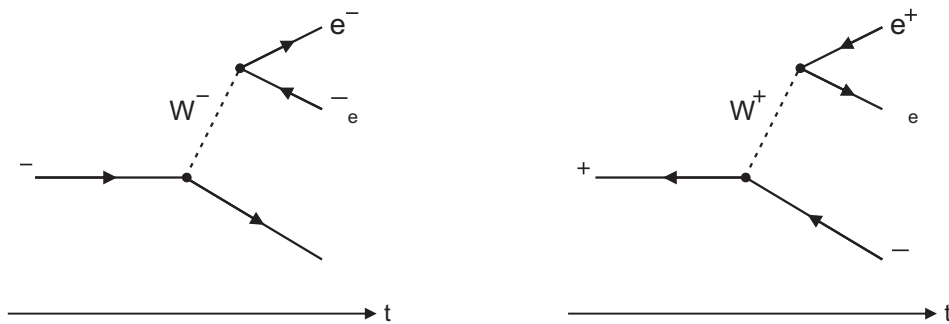


Figure 2.1: Feynman diagrams of Michel decays for muons (left) and antimuons (right).

These processes are known as Michel decays of muons or antimuons and the corresponding Feynman diagrams are shown in figure 2.1. Even if it is the dominant process, this Michel decay is not the only decay mode of muons. There are also radiative decay modes

$$\mu^- \rightarrow e^- \nu_\mu \bar{\nu}_e \gamma, \quad \mu^+ \rightarrow e^+ \bar{\nu}_\mu \nu_e \gamma$$

and $e^+ e^-$ pair associated decay modes

$$\mu^- \rightarrow e^- \nu_\mu \bar{\nu}_e e^+ e^-, \quad \mu^+ \rightarrow e^+ \bar{\nu}_\mu \nu_e e^+ e^-.$$

The corresponding branching ratios for muons are listed in table 2.1. The antimuon modes are charge conjugates of the modes listed in this table.

Table 2.1: Branching ratios of muon decay modes [3].

Decay Mode	Branching Ratio
$\mu^- \rightarrow e^- \nu_\mu \bar{\nu}_e$	$\approx 100\%$
$\mu^- \rightarrow e^- \nu_\mu \bar{\nu}_e \gamma$	$(1.4 \pm 0.4)\%$
$\mu^- \rightarrow e^- \nu_\mu \bar{\nu}_e e^+ e^-$	$(3.4 \pm 0.4) \times 10^{-5}$

2.2 $\mu^+ \rightarrow e^+ \gamma$ Decay

In the previous section 2.1 we discussed about the Standard Model and the muon decay in this theory but not about the $\mu^+ \rightarrow e^+ \gamma$ decay. This will be done in this section.

2.2.1 Neutrino Oscillations

As described in section 2.1, the lepton flavor quantum number is conserved in the Standard Model if massless neutrinos are assumed. The decay $\mu^+ \rightarrow e^+ \gamma$ is therefore not allowed in the Standard Model. But data from the Sudbury Neutrino Observatory [4] and from the Super-Kamiokande detector [5], [6] show that lepton flavor violation exists in the neutrino lepton sector. These neutrino oscillations⁴ reveal the basic fact that neutrinos have different masses and that the assumption of massless neutrinos is wrong. With the consequence that $\mu^+ \rightarrow e^+ \gamma$ decays can be induced by $\bar{\nu}_\mu \rightarrow \bar{\nu}_e$ neutrino oscillations as shown in figure 2.2.

⁴For general information about neutrino physics and especially neutrino oscillations, please see [7].

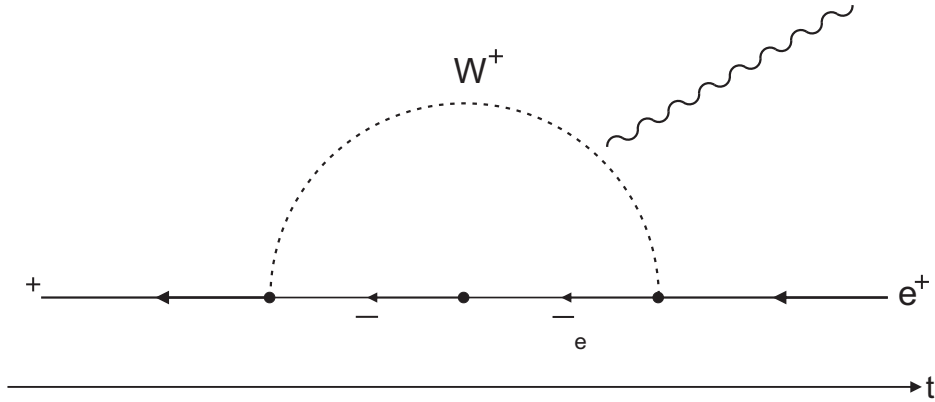


Figure 2.2: $\mu^+ \rightarrow e^+ \gamma$ decay induced by $\bar{\nu}_\mu \rightarrow \bar{\nu}_e$ neutrino oscillation.

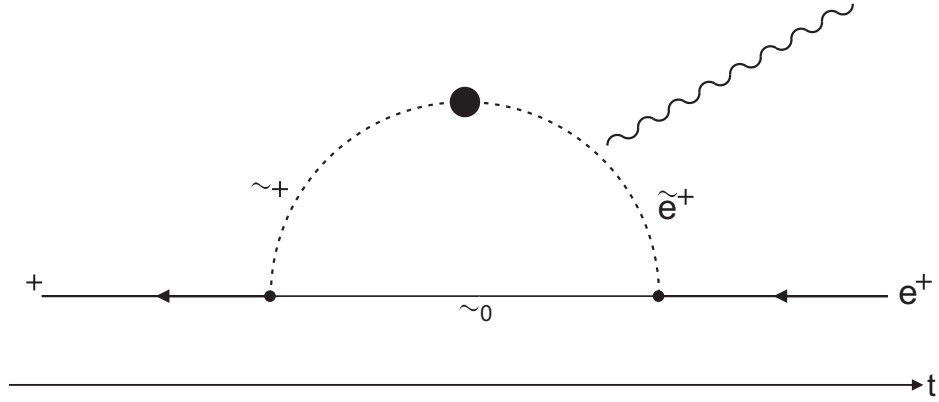
In case of finite neutrino masses, it is possible to calculate the estimated transition rate of the $\mu^+ \rightarrow e^+ \gamma$ decay. The normalization to the Michel decay gives a very small branching ratio of $B(\mu^+ \rightarrow e^+ \gamma) \leq 10^{-40}$ due to the suppression by small neutrino masses [8]. Of course, it is at the moment not possible to verify this theoretical result with experimental methods.

2.2.2 Physics Beyond the Standard Model

As already mentioned in subsection 2.1.1, the Standard Model of particle physics does not describe gravitation. Of course it is desirable to derive a more general theory which includes gravitation as well as the other three fundamental interactions. Different theoretical extensions of the Standard Model are currently known, for example Grand Unified Theories (GUT) or Supersymmetry (SUSY). With these theories, it is possible to introduce supersymmetric partners of all known leptons, so-called sleptons which are identified by tildes over particle shortcuts. With the help of these particles the decay $\mu^+ \rightarrow e^+ \gamma$ can be explained as shown in figure 2.3.

The antimuon μ^+ decays into its supersymmetric partner $\tilde{\mu}^+$ and a hypothetical, uncharged elementary particle called neutralino $\tilde{\chi}^0$. This particle, which is predicted by supersymmetric theories, is a linear combination of supersymmetric partners of uncharged gauge and higgs fields. Then the particle $\tilde{\mu}^+$ converts into a spositron \tilde{e}^+ , the supersymmetric partner of a positron, by slepton flavor mixing. The exact procedure at this intersection depends on the used supersymmetric theory. A direct change

$$\tilde{\mu}^+ \rightarrow \tilde{e}^+$$

Figure 2.3: $\mu^+ \rightarrow e^+\gamma$ decay induced by slepton flavor mixing.

is possible as well as an indirect transition over one or two stauons

$$\tilde{\mu}^+ \rightarrow \tilde{\tau}^+ \rightarrow \tilde{e}^+, \quad \tilde{\mu}^+ \rightarrow \tilde{\tau}^+ \rightarrow \tilde{\tau}^+ \rightarrow \tilde{e}^+.$$

Finally, the spositron and the neutralino combine to a positron while a photon is emitted by the spositron.

Note that the calculated branching ratio of a $\mu^+ \rightarrow e^+\gamma$ decay induced by slepton flavor mixing is much larger than the one calculated for neutrino oscillations because it does not depend on tiny neutrino masses. As the transitions before, the predicted branching ratios for $\mu^+ \rightarrow e^+\gamma$ depend on the used supersymmetric theory. For example [9] investigated five predictive supersymmetric SO(10) models with the result that at least three of these models give rise to prediction for $\mu^+ \rightarrow e^+\gamma$ that can be tested with the MEG experiment. The predicted branching ratios are in the range of $B(\mu^+ \rightarrow e^+\gamma) < 10^{-11}$ which is just below the current experimental upper limit of $1.2 \cdot 10^{-11}$ [10]. The other two models with a prediction of $B(\mu^+ \rightarrow e^+\gamma) < 10^{-15}$ are beyond the limit that can be reached by the MEG experiment. It is therefore not possible to probe these models with this experiment.

If an experiment is able to measure the branching ratio $B(\mu^+ \rightarrow e^+\gamma)$ with such a precision to lower the current experimental limit by two orders of magnitude to 10^{-13} , it is possible to corroborate or disprove some of these theories about physics beyond the Standard Model.

2.3 $\mu^+ \rightarrow e^+\gamma$ Decay Search Experiments

The MEG Collaboration is not the first experiment which is interested in the decay $\mu^+ \rightarrow e^+\gamma$ as you can see in table 2.2. The name of the experiment

and the reached upper limit for the branching ratio $B(\mu^+ \rightarrow e^+ \gamma)/B(\mu^+ \rightarrow e^+ \bar{\nu}_\mu \nu_e)$ are listed in this table. The goal of the MEG experiment is to lower the current upper limit of $1.2 \cdot 10^{-11}$ by two orders of magnitude to 10^{-13} . How the required sensitivity can be obtained is described in the next chapter.

Table 2.2: Upper limits for the branching ratio $B(\mu^+ \rightarrow e^+ \gamma)/B(\mu^+ \rightarrow e^+ \bar{\nu}_\mu \nu_e)$ at a 90% confidence level reached by other experiments.

Experiment	Year	Upper Limit	Ref
TRIUMF	1977	$< 3.6 \cdot 10^{-9}$	[11]
SIN	1980	$< 1.0 \cdot 10^{-9}$	[12]
LANL	1982	$< 1.7 \cdot 10^{-10}$	[13]
Crystal Box	1988	$< 4.9 \cdot 10^{-11}$	[14]
MEGA	1999	$< 1.2 \cdot 10^{-11}$	[10]

Chapter 3

MEG Experiment

The goal of the MEG experiment¹ is to measure the branching ratio of the decay $\mu^+ \rightarrow e^+\gamma$ with a sensitivity of 10^{-13} . The importance of this experiment for basic physics is discussed in the previous chapter 2, whereas this chapter gives a rough overview about the MEG experiment. First, the general measuring principle will be discussed in section 3.1. After this overview, the focus will be on the different components of the MEG experiment, namely the beam line (section 3.2) with the target (section 3.3), the positron spectrometer and finally the photon detector, see section 3.7. The description of the positron spectrometer is split into different parts: COBRA magnet (section 3.4), drift chamber system (section 3.5) and timing counters (section 3.6).

3.1 Overview

To measure the branching ratio of the $\mu^+ \rightarrow e^+\gamma$ decay, an antimuon beam is stopped by a target. A negatively charged muon beam is not suitable for this experiment, because these muons will form muonic atoms and may be captured by nuclei of the target. The stopped antimuon decays at rest into a positron and a photon each carries an energy equal to half of the antimuon mass, i.e. 52.8 MeV. Because of kinematic reasons the two particles are emitted back-to-back as shown in figure 3.1.

There are mainly two different kinds of possible background events. The first is a radiative antimuon decay $\mu^+ \rightarrow e^+ \bar{\nu}_\mu \nu_e \gamma$ with positron and photon emitted nearly back-to-back and low-energy neutrinos (see figure 3.2(a)).

¹For more information about the MEG experiment itself and the different sub-detectors, please see [15]. On this website one can find a large number of publications, documentations, photographs and much more.

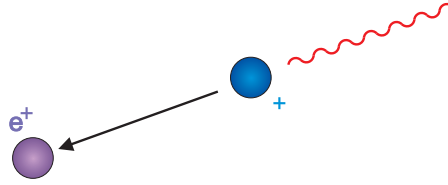


Figure 3.1: Schematic of a $\mu^+ \rightarrow e^+\gamma$ decay with the antimuon decaying at rest into a positron and a photon which are emitted back-to-back.

Secondly, an accidental coincidence of a Michel decay of an antimuon $\mu^+ \rightarrow e^+ \bar{\nu}_\mu \nu_e$ and a photon with nearly the right energy can wrongly be identified as $\mu^+ \rightarrow e^+\gamma$ decay (see figure 3.2(b)). Unfortunately there are different sources for such photons as radiative antimuon decays, bremsstrahlung of positrons in the detector, annihilation in flight and so on.

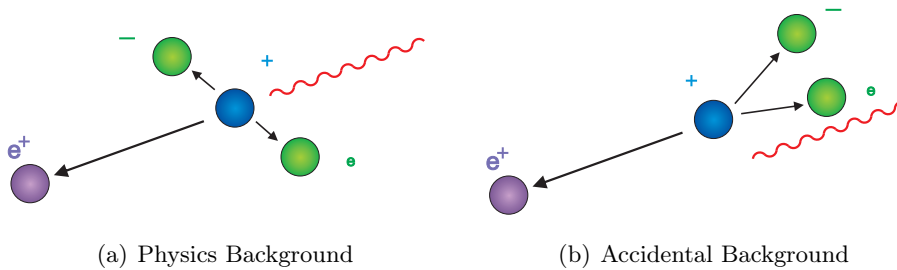


Figure 3.2: Schematics of two possible background events. In figure 3.2(a) is a physics background event shown: A Michel decay with positron and photon emitted nearly back-to-back whereas neutrinos carry only low energies. An accidental background event with a Michel decay and a photon emitted by another physics source is shown in figure 3.2(b).

To reject all background events from real $\mu^+ \rightarrow e^+\gamma$ decays, a precise measurement of the energy, fly direction and timing of each emitted particle is necessary. In the MEG experiment all properties of the photon are measured with the liquid xenon detector whereas the positron spectrometer consists of drift chambers, timing counters and the so-called COBRA magnet provide momentum, direction and timing measurements of positrons.

3.2 Beam

The beam used in the MEG experiment is produced in a way described in subsection 3.2.1, whereas in subsection 3.2.2 the specific beam line devices of the MEG experiment will be discussed.

3.2.1 PSI Beam Line π E5

Protons are produced and then accelerated to energies of 860 keV by the Cockcroft-Walton Pre-Injector². The next step is the Injector 2 ring cyclotron with a proton beam injection energy of 860 keV and an extraction energy of 72 MeV. These protons are then injected over a transfer beam line into the Ring Cyclotron which accelerates them to an extraction energy of 590 MeV. The generated proton beam current with 2.0 mA is one of the highest in the world and is therefore perfectly suited for this experiment, because the searching of rare $\mu^+ \rightarrow e^+\gamma$ decays needs a high intense muon beam to increase the event rate. After the acceleration, the proton beam is guided with bending magnets and quadrupoles to the target E where protons produce a large amount of secondary particles for example pions. These particles can be bunched in several beam lines guided to different experiment areas where the beams can be used for particle physics experiments. For instance the π E5 beam line extracts low energy pions and muons (with momenta of 10 to 120 MeV/c) from this production target E. For the MEG experiment the π E5 beam line is tuned to positively charged particles with momenta of about 28 MeV/c to capture the so-called surface antimuons. These particles are antimuons produced by pions decaying at rest on the production target surface. But note that this antimuon beam has always a particle contamination. A source for this contamination are for example positrons produced by decaying antimuons.

3.2.2 MEG Beam Line

Of course the quality of the composite beam described in subsection 3.2.1 is not good enough for the MEG experiment which requires a high-quality pure antimuon beam, i.e. the fraction of positron contamination has to be reduced. Additionally it is necessary to degrade the antimuon momentum to ensure that they stop in a thin target (see section 3.3). To achieve these features, several additional devices have to be installed between the beam extraction into area π E5 and the COBRA magnet (see section 3.4). See figure 3.3 for an overview of these devices in the π E5 outline.

²More information about PSI accelerators and beam lines can be found in [16].

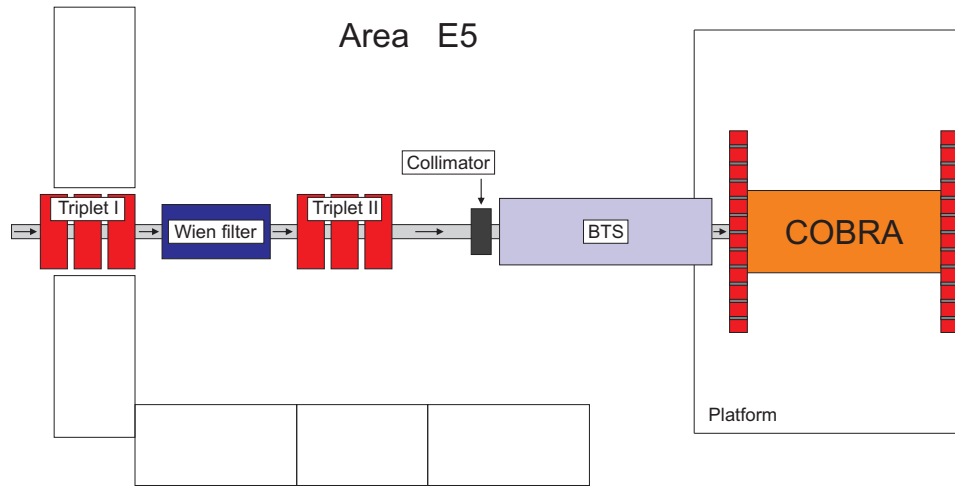


Figure 3.3: Outline of the MEG beam line with Triplet I, Wien filter, Triplet II, collimator and BTS with implemented degrader and collimator system. Additionally the COBRA magnet and the platform are also shown.

A triplet of quadrupoles called Triplet I is mounted at the beam extraction to focus the beam to the next device, a Wien filter. Using such a filter, it is possible to select particles of a certain velocity from a composite beam with the help of homogeneous magnetic and electric fields and an aperture. In the MEG experiment this Wien filter is used to separate antimuons and positrons to reduce the positron contamination and improve the beam quality. After this device another quadrupole triplet, called Triplet II, is mounted to refocus the antimuon beam after separation to the collimator system. This device is necessary to ensure a small beam spot size at the target position. At last, there is a so-called Beam Transport Solenoid (BTS) to guide the antimuon beam to the COBRA magnet and therefore to the target. A momentum degrader and another collimator system is implemented inside of this BTS. The purpose of this momentum degrader is to reduce the antimuon momentum to ensure that the beam is stopped in the target.

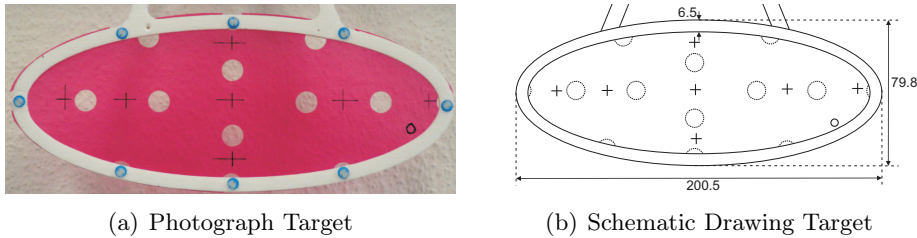
With these devices an antimuon beam which is as pure as possible can be focused at the target position in an ellipsoidal spot with an antimuon stopping rate of $3 \cdot 10^7 \mu^+$ per second.

3.3 Target

As mentioned before, the antimuon beam is focused to the target, which has to satisfy the following criteria: It should be as thin as possible because

otherwise the track of the produced positron could be affected by multiple scattering or the positron could be annihilated which leads to photons increasing the background. But on the other side a maximum number of antimuons should be stopped in the target. The solution for this problem is given by using a thin target which is mounted with a slant angle in respect to the beam line.

As target material a $205\ \mu\text{m}$ thick ellipsoidal polyethylene foil is used which is clamped between a support frame consists of ROHACELL. With this construction the target has a length of $200.5\ \text{mm}$ and a height of $79.8\ \text{mm}$ whereas the frame has a thickness of $2 \times 5.25\ \text{mm}$ and a wideness of $6.5\ \text{mm}$. A photograph and a schematic drawing of the target and its support frame are shown in figures 3.4(a) and 3.4(b), respectively³.



(a) Photograph Target

(b) Schematic Drawing Target

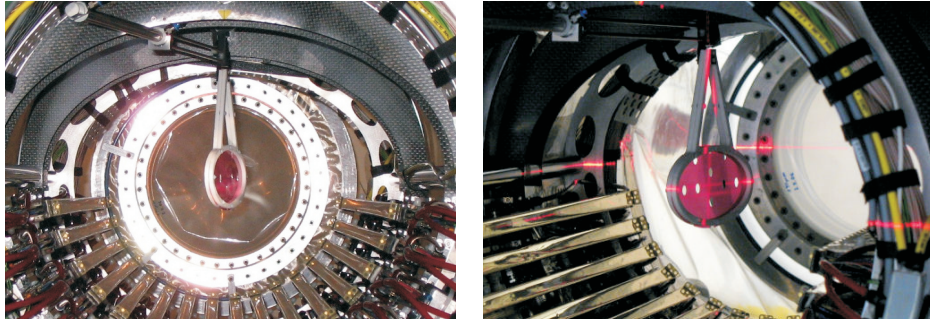
Figure 3.4: A photograph of the target outside of COBRA with holes and crosses is shown in 3.4(a) whereas in 3.4(b) is a schematic drawing of the target with geometrical information.

The holes and crosses in the polyethylene foil, which are visible in these two figures, have an important physical relevance. The crosses are used to determine the position of the target inside COBRA by optical surveying methods (see later in this thesis). The relation between cross coordinates and location of holes is well known with the consequence that all hole positions can be calculated. With the help of these holes the precision of the positron track reconstruction algorithm can be checked.

During the run 2007, the target was mounted on the support structure of the drift chamber system (see section 3.5) with a slant angle of $(12.8 \pm 0.5)^\circ$ in respect to the beam line. But this angle was not optimized and recent calculations and simulations show that an angle of about 20° is better suited. Hence the mounting was changed in April 2008 in a way to reach this slant angle. There exist several methods to measure the target slant angle which will be described later in section 9.3. The mean value of all these results obtained by the different measuring methods is used as target slant angle for run 2008: $\alpha_{2008} = (20.5 \pm 0.3)^\circ$.

³Geometrical specifications shown in this and all following schematic drawings are given in unit millimeter.

Photographs of the situation with target, drift chambers and support structure inserted into COBRA are shown in figure 3.5. Additionally all specifications mentioned in this section are summarized in table 3.1.



(a) Target: Camera on Beam Axis

(b) Target: Camera away from Beam Axis

Figure 3.5: Photographs of the target mounted on the support structure which was already inserted into COBRA when these pictures were taken. Photograph 3.5(a) was taken with camera position on beam axis whereas in 3.5(b) the camera was away from beam axis. Additionally the drift chamber system is also visible, see section 3.5 and chapter 4 for more information.

Table 3.1: Summarized specifications of the target (for more information about the target slant angle, please see section 9.3).

Material foil:	polyethylene
Foil thickness:	205 μm
Foil shape:	ellipsoidal
Material support frame:	ROHACELL
Support frame thickness:	$2 \times 5.25 \text{ mm}$
Support frame wideness:	6.5 mm
Target length:	200.5 mm
Target height:	79.8 mm
Target slant angle 2007:	$(12.8 \pm 0.5)^\circ$
Target slant angle 2008:	$(20.5 \pm 0.3)^\circ$

3.4 COBRA Magnet

The MEG positron spectrometer consists of a specially designed superconducting solenoidal magnet called CONstant Bending RADIUS COBRA magnet (see later in this section), a drift chamber system (see section 3.5) and timing counters (see section 3.6). This spectrometer should provide momentum, track and timing information about the positron. Schematic drawings of the positron spectrometer are shown in figures 3.6 and 3.7. Note that the identifiers upstream and downstream are used in the MEG collaboration for the region from the center of the target up and down to the beam line, whereas berg and aare are PSI terms. For more information about used labeling and numbering see appendix A.

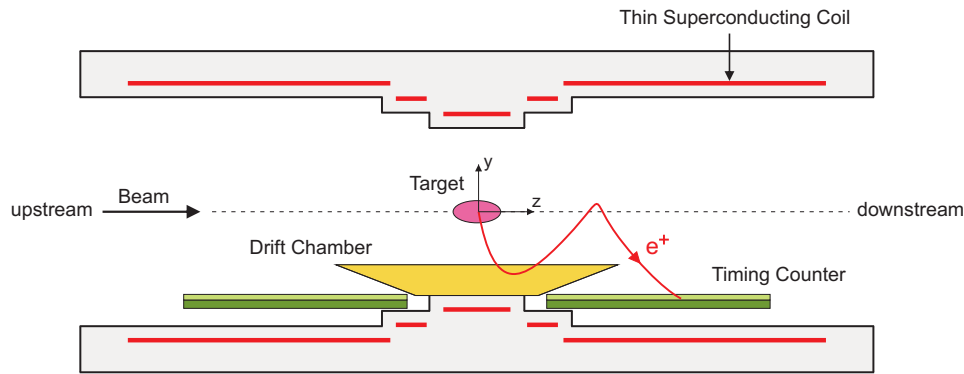


Figure 3.6: Schematic drawing of the positron spectrometer with drift chambers, timing counters and the main magnet of COBRA. In addition, the y and z axis of the used right-handed coordinate system are also shown in this picture.

3.4.1 Design of COBRA

COBRA consists of a superconducting main magnet and a pair of big resistive compensation coils placed at the upstream and downstream end of the main magnet. These compensation coils should reduce the stray field of the main magnet around the photon detector, because its photomultipliers can not operate in a strong magnetic field (see section 3.7). The main magnet is composed of five superconducting coils with altogether three different radii as shown in figure 3.8. All specifications about COBRA coils which are shown in this figure are summarized in table 3.2.

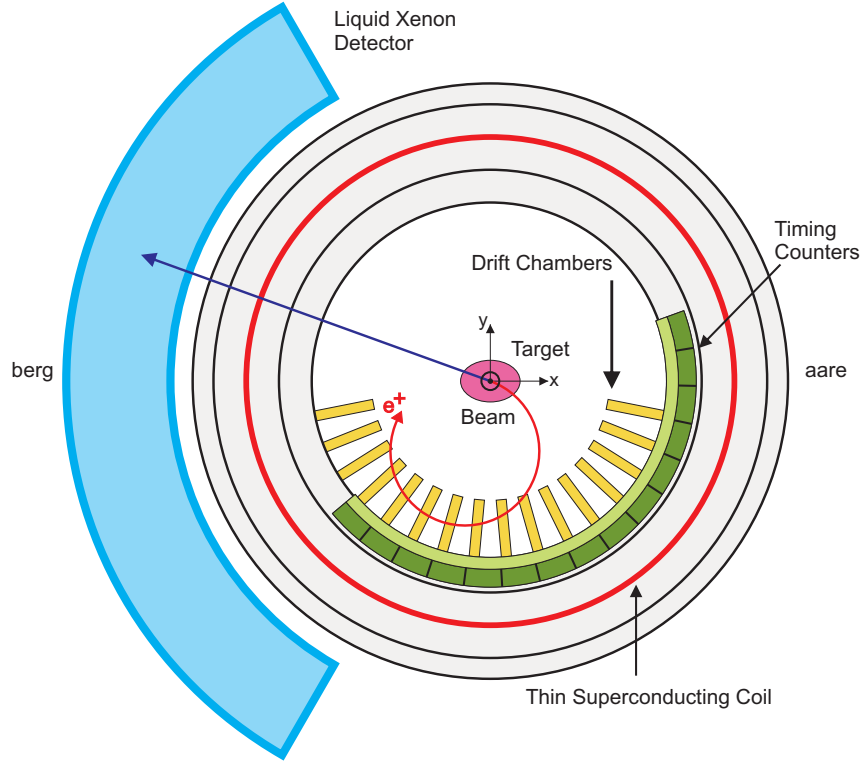


Figure 3.7: Cross-sectional view of the positron spectrometer with drift chambers, timing counters and the main magnet of COBRA. The x and y axis of the used coordinate system are also shown. Additionally the liquid xenon detector is also shown, but it has nothing to do with positron measurements.

The strength of the produced magnetic field reaches its highest value of 1.27 T at the target position $z = 0$. The field decreases with increasing $|z|$, for example at $z = \pm 1.25$ m it has a strength of about 0.49 T. Outside of the main magnet at the place of the photon detector the magnetic field is reduced by compensation coils to less than 50 Gauss.

The volume of the COBRA main magnet is filled and flushed with helium to reduce the amount of material between target and the sub-detectors drift chambers and timing counters, respectively. This helium atmosphere inside COBRA provides additionally that the beam is not disturbed by atoms until it stops into the target.

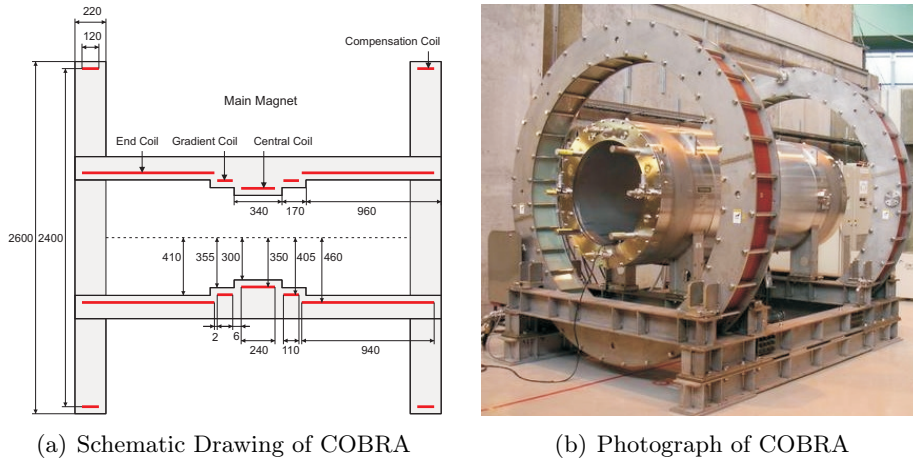


Figure 3.8: In 3.8(a) is a schematic drawing of COBRA with main magnet and compensation coils. Additionally, some geometrical specifications are also shown. In 3.8(b) is a photograph of COBRA.

Table 3.2: Summarized specifications of COBRA central, gradient, end and compensation coils. Note that these given values have only an accuracy of one millimeter.

Coil	Diameter [mm]	Length [mm]	Conductivity
Central	700	240	super
Gradient	810	110	super
End	920	940	super
Compensation	2400	120	resistive

3.4.2 Advantages of COBRA

In this subsection the physics advantages of the specially designed COBRA magnet over a normal solenoidal magnet will be shown.

In a normal uniform solenoidal magnetic field antimuon decay positrons emitted close to 90° with respect to the z axis undergo many turns in the drift chamber system as shown in figure 3.9(a). With such many hits it is very difficult to reconstruct positron tracks resulting in bad resolutions of time and place determinations. With a specially designed magnet it is possible to create a magnetic field in which positrons are swept away very quickly from the sensitive drift chamber and timing counter volume (see figure 3.9(b)).

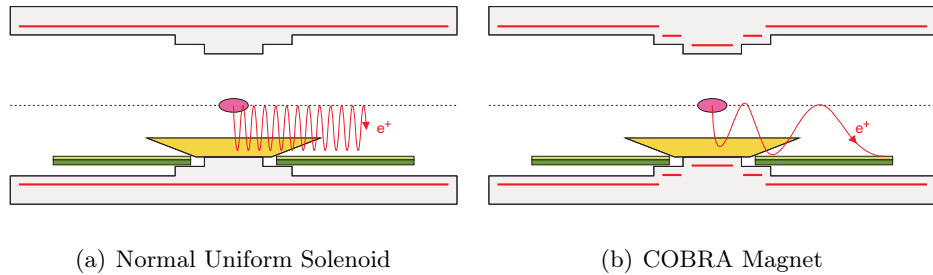


Figure 3.9: Advantage of COBRA if a positron is emitted close to 90° . In a normal solenoid magnet 3.9(a) this particle undergoes many turns in the drift chambers, whereas in COBRA 3.9(b) it is swept away very quickly.

The second important advantage of the used magnet is given by the fact that in this field $\mu^+ \rightarrow e^+\gamma$ positrons with the same momentum follow trajectories with constant projected bending radii independent of the emission angle. In a uniform solenoidal magnetic field the bending radius of monochromatic positrons depends on the emission angle (see figures 3.10(a) and 3.10(b)). It is therefore possible to create a special magnet to constrain positrons with a momentum of about $52.8 \text{ MeV}/c$ on tracks crossing the sensitive volume of the drift chamber system. With such a magnet the amount of Michel positrons strongly decrease at radii larger than 20 cm from the beam axis where the drift chamber system is placed. This means that most of the Michel positrons never reach a drift chamber and can therefore not cause accidental coincidences, i.e. background.

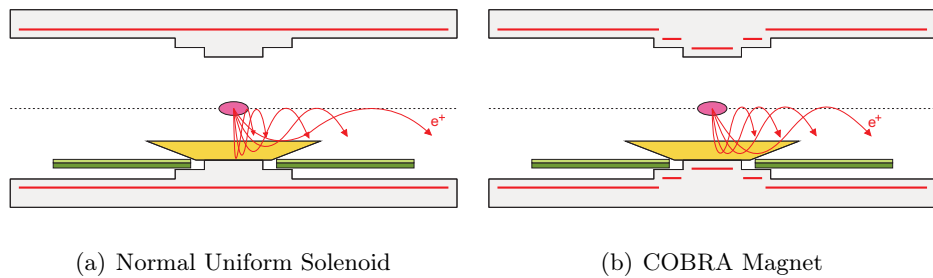


Figure 3.10: In the magnetic field of COBRA particles with the same momentum follow tracks with constant bending radius, whereas in a uniform solenoid the bending radius depends on the emission angle.

3.5 Drift Chamber System

Tracks of positrons from Michel or $\mu^+ \rightarrow e^+\gamma$ decays in the target should be measured with high precision with the help of drift chambers. To satisfy such requirements a special drift chamber system, which is part of the MEG positron spectrometer, was developed and constructed. This section gives a rough overview about this system, whereas in chapter 4 the drift chambers are discussed in detail.

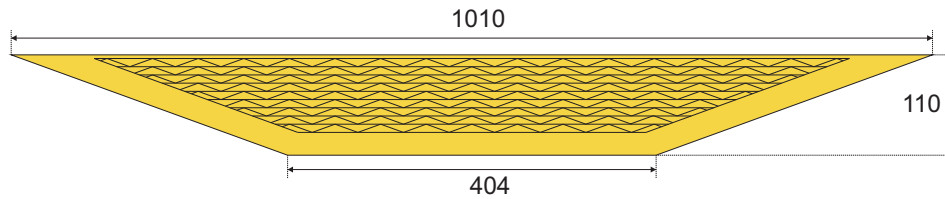


Figure 3.11: Schematic drawing of a MEG drift chamber with geometrical information (the so-called cathode Vernier pads are also visible, see later in subsection 4.2.3).

The drift chamber system consists of totally 16 drift chambers, sometimes also called modules, each with the shape of an isosceles trapezoid as shown in figure 3.11. Each chamber has a height of 110 mm, the top edge has a length of 1010 mm while the bottom edge is 404 mm long. All specifications mentioned in this section are summarized in table 3.3.

Table 3.3: Summarized specifications of drift chambers.

Drift chamber shape:	isosceles trapezoid
Length of top edge:	1010 mm
Length of bottom edge:	404 mm
Drift chamber height:	110 mm
Number of drift layers:	2 (called A and B)
Shift distance:	4.5 mm
Number of drift cells per layer:	9
Dimensions of one drift cell:	$(9 \times 7) \text{ mm}^2$
Cathode foil material:	polyimide, deposited with aluminium
Cathode foil thickness:	$12.5 \mu\text{m}$ with 250 nm deposition

Each module consists of two drift layers called A and B which are shifted against each other with a distance of 4.5 mm, corresponding exactly to half a drift cell. This displaced design, whose cross section is shown in figure 3.12, is necessary to solve left-right ambiguity. One layer is built by 9 drift cells each with one anode wire in the center. Such a drift cell is delimited by ultrathin cathode foils and potential wires.

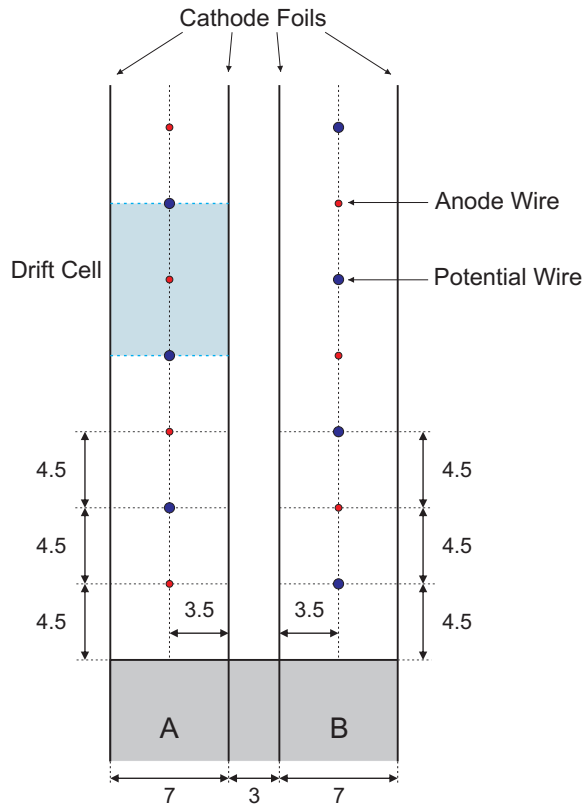


Figure 3.12: Cross-sectional view of a MEG drift chamber with geometrical information. Note that only a few drift cells of a completed drift chamber are shown.

The drift chambers are mounted on a specially designed carbon fiber frame called support structure. See figure 3.13 for two photographs of this structure. With this construction the drift chambers align radially from 11.25° to 168.75° with respect to $+x$ direction, each module separated by an angle of 10.5° . The active volume of the drift chamber system extends from 190 mm to 300 mm in radial direction from the target (see figure 3.7). Please see chapter 4 for more details about the drift chamber mounting, schematic drawings and general information about MEG drift chambers.

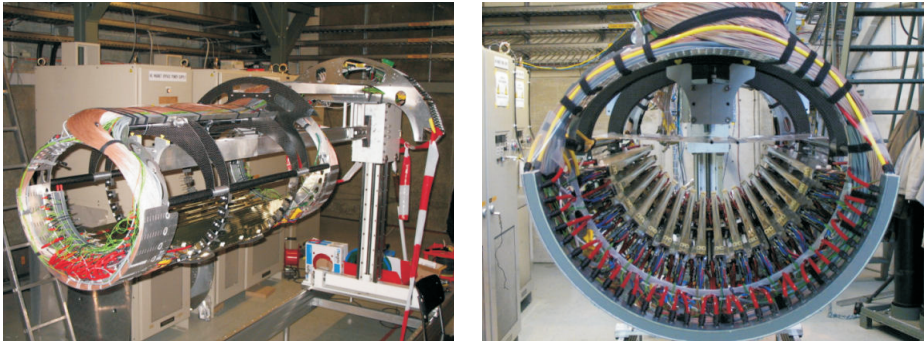


Figure 3.13: On the left side, a photograph of the support structure with mounted drift chambers is shown. Note that this picture was taken before the insertion into COBRA. On the right side, the support structure outside of COBRA is shown with camera position on beam axis. In these pictures the target is not yet mounted on the support structure.

3.6 Timing Counters

The timing of positrons emitted in the target is measured by two timing counters mounted inside COBRA at the upstream and downstream side. Each timing counter is designed in the same way and consists of two layers of different time measuring sub-detectors. The inner sub-detector is called z -counter whereas ϕ -counter is the name of the outer layer. For more details about properties and geometry of these two sub-detectors, see subsections 3.6.1 and 3.6.2.

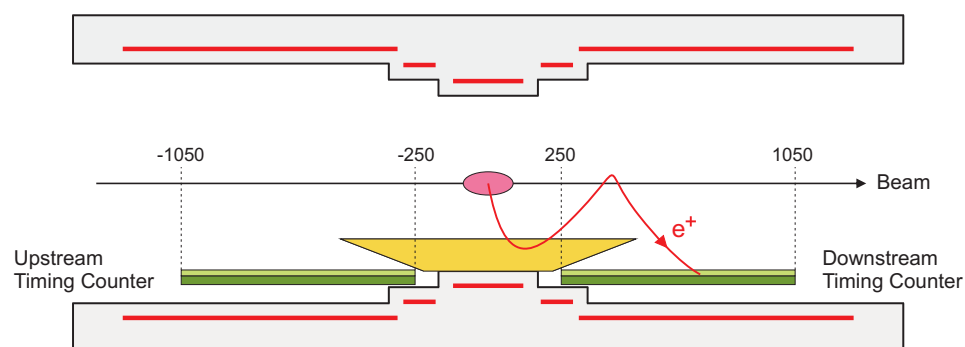


Figure 3.14: Schematic drawing of COBRA with target, drift chambers and the two timing counters at the upstream and downstream end. The two different sub-detector layers are indicated by using different colors.

The active volume of timing counters reaches from $250 \text{ mm} < |z| < 1050 \text{ mm}$ along the z axis where the target describes as usual the $z = 0$ point (please see appendix A for more information about the used coordinate system). In azimuthal direction each detector covers an angle of $220^\circ < \phi < 380^\circ$ whereas in radial direction, the z - and ϕ -counter are placed at a radius of $r = 292.4 \text{ mm}$ and $r = 320 \text{ mm}$, respectively. All these specifications are shown in figures 3.14 and 3.15 and are summarized in table 3.4.

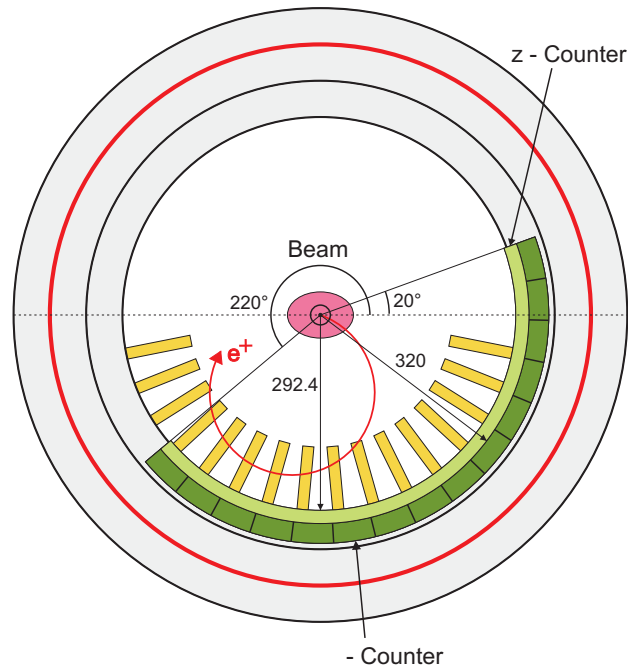


Figure 3.15: Schematic drawing of COBRA with target, drift chambers and one timing counter viewed from the downstream side of COBRA. Specifications about radius and angle coverage of the two sub-detectors are also shown.

3.6.1 ϕ -Counter

With the so-called ϕ -counter the timing and the ϕ position of the emitted positron should be measured as precisely as possible. The needed information is provided by 15 plastic scintillation bars aligned in z direction. Each bar has dimensions of about $(40 \times 40 \times 900) \text{ mm}^3$ and covers 10.5° in azimuthal direction resulting in a total coverage of 160° . Signals induced by passing charged particles are read out by 2" photomultiplier tubes (PMTs) on each plastic scintillation bar side.

3.6.2 z -Counter

Of course the purpose of the other sub-detector z -counter is the timing determination too, but additionally the z coordinate of the positron when it passes through the timing detector should be measured. The measurement of these kinematic parameters is done by 256 scintillating fiber bunches aligned radially to the beam line with a cross-section of $(6 \times 6) \text{ mm}^2$. The fibers are read out on both sides by $(5 \times 5) \text{ mm}^2$ silicon avalanche photo-diodes (APDs).

As mentioned in section 3.4, the COBRA volume is filled with helium to reduce the amount of material. This helium atmosphere damages sensitive photomultipliers resulting in a short life time of these read out devices. The solution for this problem is to isolate each timing counter with a bag filled and flushed with nitrogen gas (the so-called Nitrogen Bag).

Table 3.4: Summarized specifications of timing counters.

Active volume timing counters:	$250 \text{ mm} < z < 1050 \text{ mm}$
Covered angle:	$220^\circ < \phi < 380^\circ$
Radius ϕ -counter:	320 mm
Detector material:	plastic scintillation bars
Number of bars:	15
Dimensions of one bar:	$(40 \times 40 \times 900) \text{ mm}^3$
Read out devices:	PMTs
Radius z -counter:	292.4 mm
Detector material:	scintillating fiber bunches
Number of bunches:	256
Dimensions of one bunch:	$(6 \times 6) \text{ mm}^2$
Read out devices:	APDs

3.7 Photon Detector

Photons from decays in the target are, compared to positrons, not affected by magnetic fields and fly straight ahead from their emission places away and pass through the superconducting coil of COBRA. After this passage photons are detected with the help of a liquid xenon scintillation detector. This detector is filled with 0.8 m^3 of liquid xenon corresponding to total 800 liter of this expensive substance. Scintillation light signals induced by photons entering and converting in the liquid xenon are picked up by 846

photomultiplier tubes surrounding the photon calorimeter. With this photon detector it is possible to determine direction, timing and energy of photons coming from $\mu^+ \rightarrow e^+\gamma$ decays in the target.

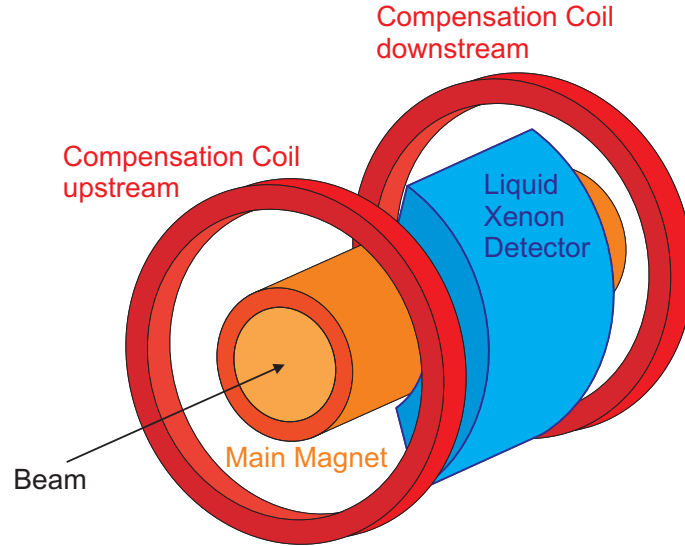


Figure 3.16: Schematic drawing of the liquid xenon detector, the COBRA magnet and a schematic beam line.

The MEG photon detector is placed outside of the main magnet at berg side between the two compensation coils. See figure 3.16 for a schematic drawing of the situation. The detector is C shaped to achieve best fit to outer casing of COBRA resulting in a sensitive volume between 650 mm and 1120 mm in radial direction from the target. The detector's depth of 470 mm is chosen because of the requirement that showers induced by photons with energies of 52.8 MeV from $\mu^+ \rightarrow e^+\gamma$ decays should be located completely inside the sensitive volume. Note that the liquid xenon detector has to be shielded from the strong magnetic stray field produced by the main magnet because photomultipliers are used as read out devices. To reduce the stray field to less than 50 Gauss the big compensation coils of COBRA described in section 3.4 have been designed and constructed.

A crucial factor of liquid xenon is given by the pureness of the xenon because impurities cause a bad transparency for the scintillation light of xenon itself. This problem was solved by the development and installation of a unique purification system.

Chapter 4

Drift Chambers

Because the topic of this thesis is about the geometrical drift chamber alignment, it is necessary to discuss geometry as well as physics and mechanical considerations about the design of these chambers in more details. This chapter will give an extensive description of the MEG drift chamber system starting with a discussion about requirements in section 4.1. In section 4.2 the design of one MEG drift chamber will be described by considering the requirements mentioned before. Finally, the focus in section 4.3 will be on the support structure and the setup of the drift chamber system. For labeling and numbering conventions used in this and all following chapters, see appendix A.

4.1 Requirements

As already mentioned in chapter 3, the drift chamber system should determine positron tracks with high precision. To reach this purpose some physics aspects have to be considered for example high counting rates, background or multiple scattering. In this section, the requirements on the drift chamber system will be discussed with the attention on these aspects.

With a desired antimuon stopping rate of about $3 \cdot 10^7 \mu^+/\text{s}$ in the target it is obvious that there is the same amount of positrons in the COBRA volume due to antimuon decays. The drift chamber system should be able to operate even with such a high counting rate, which is of course exceedingly difficult for a drift chamber detector. But with the great advantages of the COBRA magnet most of low energy Michel positrons never reach a drift chamber and the counting rate is therefore dramatically suppressed. Nevertheless, it is still quite high especially in the innermost drift chamber region, i.e. the region nearest to the target.

The resolution of particle track measurements always depends on Coulomb scattering leading to inexact track determination. To suppress this scattering it is necessary to minimize the amount of spectrometer material which is traversed by positrons. Because the highest counting rate is observed in the innermost region of the drift chamber system, the amount of material has to be minimized on the top of each drift chamber. The reduction of detector material has another advantage, namely the suppression of background and hence accidental coincidences.

If it is possible to implement all these requirements in the development and construction of the MEG drift chamber system, one can achieve the required resolution of track determination.

4.2 MEG Drift Chamber Design

After a lot of experimental research and computer simulations, the PSI Detector Group [17] of the Laboratory for Particle Physics¹ designed and constructed the MEG drift chamber system. Note that the description of the exact production process of the chambers would go beyond the scope of this thesis. For more details about the production, please see [20].

The general geometry of a MEG drift chamber will be described in subsection 4.2.1, followed by a detailed discussion about the so-called left-right ambiguity in subsection 4.2.2. The focus in subsection 4.2.3 will be on anode wires, potential wires and cathodes with Vernier pads with a discussion about how the position of a particle track can be determined. After these subsections the theoretical setup of a drift chamber and hence a drift cell is clear, but a description about how this setup can be achieved mechanically, i.e. the assembly, is still missing. This will be caught up in subsection 4.2.4.

4.2.1 Chamber Geometry

This subsection will give a description of the general MEG drift chamber geometry and is therefore a repetition of section 3.5.

Every drift chamber is designed in the same way and has the shape of an isosceles trapezoid with a height of 110 mm and a top edge length of 1010 mm whereas the bottom edge is 404 mm long. A schematic drawing of one drift chamber with some geometrical specifications is shown in figure 4.1.

¹The Laboratory for Particle Physics (LTP) [18] is part of the Research Department Particles and Matter (TEM) [19] at PSI.

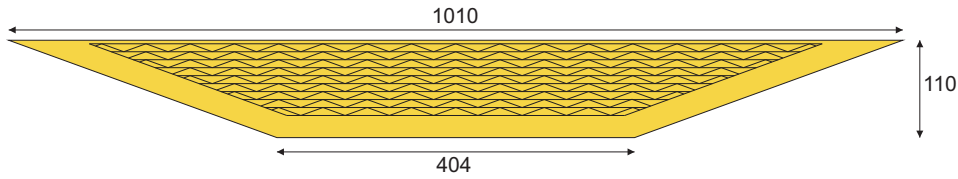


Figure 4.1: Schematic drawing of one MEG drift chamber with geometrical information.

4.2.2 Left-Right Ambiguity

After this rough overview about the general external geometry of one drift chamber, it is necessary to think about how the drift chamber should be designed inside. This means that one has to discuss the setup of a single drift cell and how several drift cells can be arranged to reach best positron track resolution. An important point in this consideration is of course the so-called left-right ambiguity if a drift chamber contains only one layer of anode wires as in figure 4.2(a). With such single layer drift chambers it is impossible to say whether a charged particle passed the detector on the left or the right side of the anode wire resulting in bad track resolution.

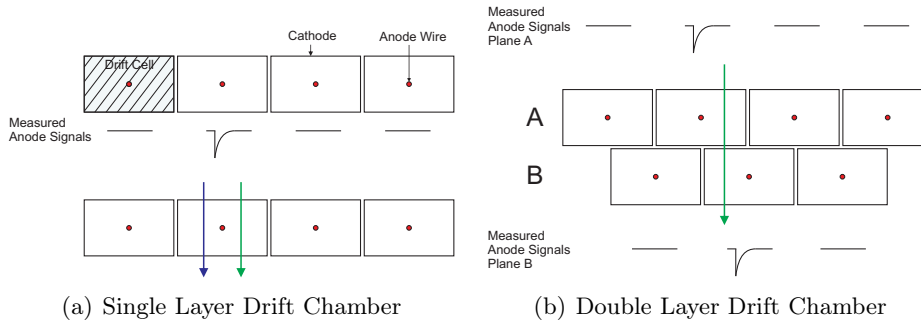


Figure 4.2: Schematic 4.2(a) shows the problem of left-right ambiguity in a single layer drift chamber whereas 4.2(b) shows the solved problem in a double layer detector.

The solution for this ambiguity problem is given by drift chambers containing two drift layers shifted against each other by half a drift cell as shown in figure 4.2(b). Now it is much easier to reconstruct tracks of charged particles and is therefore the reason, why this principle is used for the MEG experiment.

4.2.3 Anode Wires, Potential Wires and Cathodes

After the decision to build up one MEG drift chamber by two drift layers shifted to each other, the design of one single drift cell has to be discussed. Resistive anode wires composed of Ni/Cr with a diameter of $25\ \mu\text{m}$ which are aligned along the beam line are used as signal wires in the center of each drift cell. The boundary cathode of any drift layer is provided by ultrathin cathode foils consist of a $12.5\ \mu\text{m}$ polyimide foil deposited with $250\ \text{nm}$ aluminium. In one drift layer, adjacent drift cells are not separated by material planes but by so-called potential wires between two anodes. For the MEG experiment, potential wires consist of Be/Cu with a diameter of $50\ \mu\text{m}$ are used.

Positive high voltage of about $1800\text{-}1900\ \text{V}$ is applied to each anode wire while cathode foils and potential wires are connected to ground to achieve potential differences. Each drift chamber is filled and flushed with a $\text{He}:\text{C}_2\text{H}_6$ (50:50) gas mixture to lower the amount of material in the spectrometer.

After additional computer simulations and measurements with prototype drift chambers, parameters as the ideal drift cell volume or the optimal number of drift cells in one layer were optimized. A cross-sectional view of the final design of a MEG drift chamber is shown in figure 4.3. Please note the different naming of cathode foils: the outer cathode consists of one foil is called "hood" whereas the two cathodes inside of the drift chamber are simply called "cathode". The gap of $3\ \text{mm}$ between the two inner cathodes shown in figure 4.3 is necessary to avoid cross talk.

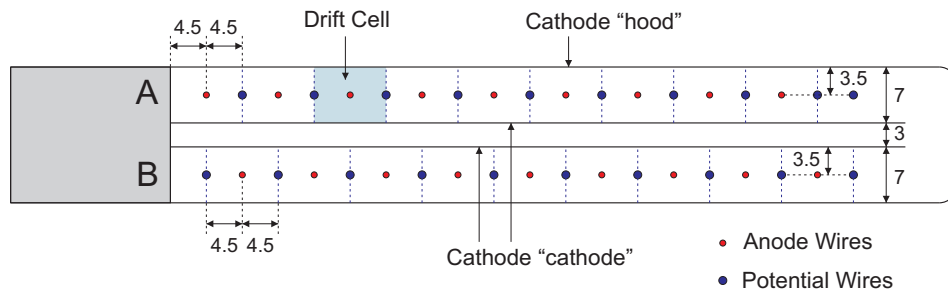


Figure 4.3: Cross-sectional view of the drift chamber setup with geometrical information. The outer cathode consists of one single foil and is called "hood" whereas "cathode" is the name of the two inner cathodes.

Anode wires are read out on the upstream and downstream side of the chamber, i.e. every anode wire provides two signals. By comparing the charge of these signals the z position of the positron passage through the chamber can be determined with an accuracy of about $10\ \text{mm}$. To improve the resolution of the z position measurement all cathodes are divided into so-called Vernier

pads. Such pads can be obtained by shaping the aluminium deposition on the polyimide foil in a zig-zag fashion with a period of 50 mm into two strips as shown in figure 4.4. These two strips of one Vernier pad are read out on opposite ends of the drift chamber.

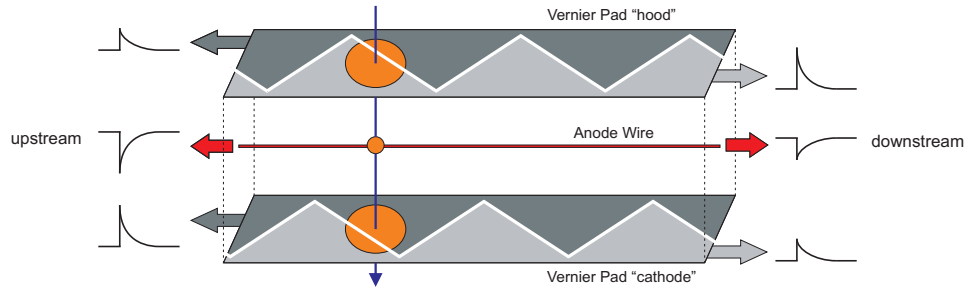


Figure 4.4: One single drift cell is shown in this figure with anode wire and Vernier pads of both "hood" and "cathode". Signals induced by charged particles passing this drift cell are shown on the upstream and downstream side of the cell. With the charge ratio of both anode signals the corresponding period of the Vernier pad can be determined and then the z position of the positron passage can be calculated by analyzing Vernier pad signals.

One single drift cell provides therefore two anode signals from one anode wire read out on both sides and total four cathode signals, two from the Vernier pad "hood" and two provided by the Vernier pad "cathode".

With charge ratios from anode signals one can determine the track position of a positron with an accuracy of 10 mm as mentioned before. With this information the corresponding Vernier pad period can be located. By comparing the read out signals of each strip one can calculate the positron passage position with an accuracy of $900 \mu\text{m}$. In figure 4.4 is a schematic of the principle of a z position measurement with Vernier pads.

4.2.4 Assembly

With the help of previous considerations the general setup of one drift chamber is already known but now one has to find out how this theoretical geometry can be realized mechanically. Additionally all requirements described in section 4.1 have to be achieved for example the minimization of material in the innermost drift chamber region. A possibility to reduce the material to an absolute minimum is given by a so-called open-frame structure. The drift chamber is therefore built up by carbon fiber frames shaped as shown

in figure 4.5. With this construction only the ultrathin cathode foil and a small ROHACELL frame (to keep the foil in form) is placed between the target and the innermost signal wires and Vernier pads.

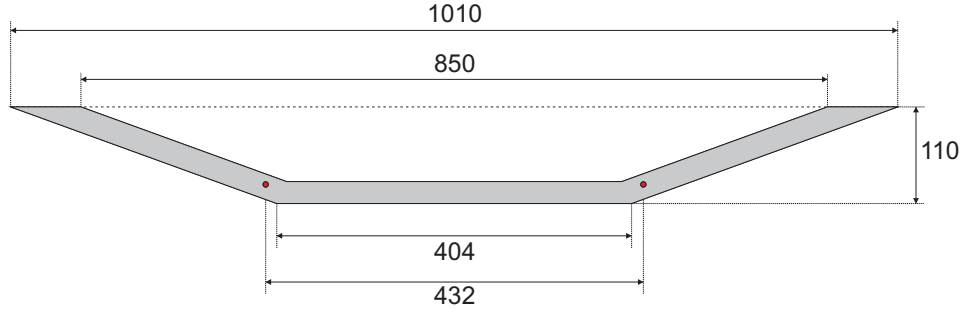


Figure 4.5: Schematic drawing of a general drift chamber frame with geometrical information. Additionally, the so-called drift chamber bolts are also shown (red points). See chapter 6 for more information about the importance of these bolts.

A single MEG drift chamber can now be built up layer by layer starting with a so-called cathode frame in the middle of each chamber. This cathode frame consists of two mirror-inverted frames which are glued to each other. Cathode foils are glued to this frame with a resulting gap of 3 mm between the foils (this gap was already mentioned in subsection 4.2.3). A schematic of a cathode frame with drift chamber bolts and some printed circuits boards (PCB) for read out channels is shown in figure 4.6.

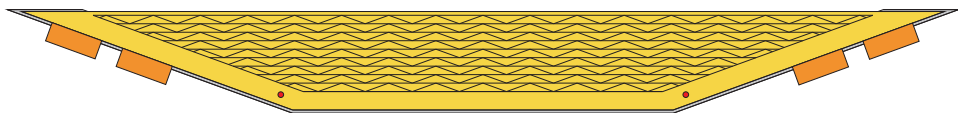


Figure 4.6: Schematic drawing of a cathode frame with drift chamber bolts, some printed circuits boards for read out channels and Vernier pads (see subsection 4.2.3).

As we discussed in subsection 4.2.2, the two drift layers should be shifted against each other with the consequence that two different anode wire frames are necessary to build one drift chamber (see figure 4.7). One frame is designed for the so-called plane A whereas the other one is for plane B (see later in appendix A.3). This means that every anode wire of one drift chamber has a different length as shown in table 4.1.

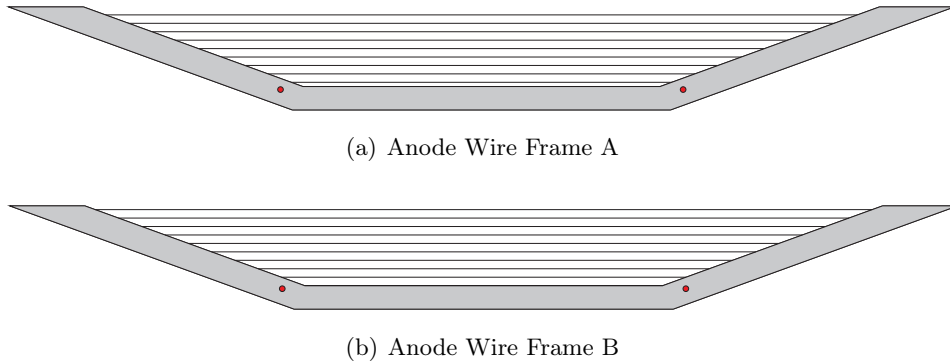


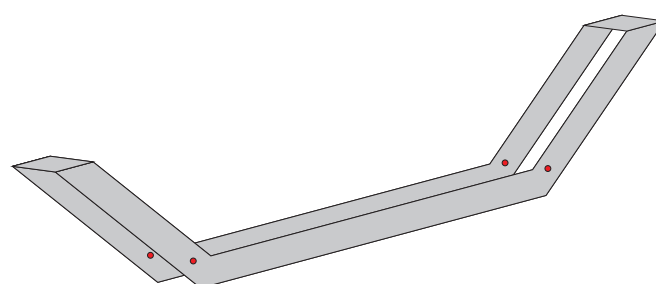
Figure 4.7: Because of the used drift chamber layout with two drift layers shifted to each other, two different anode wire frames are necessary, one for plane A and one for plane B.

Table 4.1: Length of each anode wire in plane A and B (see appendix A for more information about the used wire numbering).

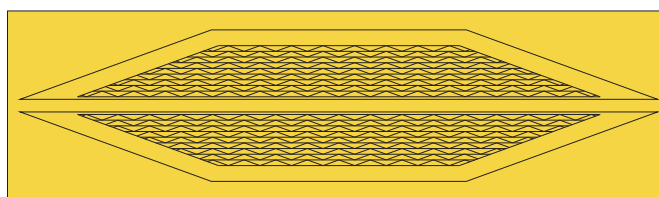
Anode Wires Frame A		Anode Wires Frame B	
wire a8	402.60 mm	wire a8	427.53 mm
wire a7	452.43 mm	wire a7	477.35 mm
wire a6	502.28 mm	wire a6	527.20 mm
wire a5	552.12 mm	wire a5	577.04 mm
wire a4	601.96 mm	wire a4	626.91 mm
wire a3	651.80 mm	wire a3	676.71 mm
wire a2	701.64 mm	wire a2	726.52 mm
wire a1	751.47 mm	wire a1	776.40 mm
wire a0	801.32 mm	wire a0	826.19 mm

The final component is the hood frame composed by two separated frames and two small connection pieces as shown in figure 4.8(a). Note that the thickness of this construction is given by 17 mm corresponding to the thickness of a drift chamber. The cathode foil named "hood" consists of one single foil which is glued over this hood frame. In figure 4.8(b) is a schematic of this foil as it is delivered from production, of course the spare foil has to be cut away.

All frames described before can now be sandwiched between the hood frame. To fix all these layers there are holes in each frame in which adjusting pins and bolts can be implemented. Note that in previous pictures only holes for so-called drift chamber bolts are shown. See chapter 6 for more information about the importance of these bolts.



(a) Hood Frame



(b) Cathode Foil "hood"

Figure 4.8: In 4.8(a) is a schematic drawing of the so-called hood frame whereas 4.8(b) shows a schematic of the cathode foil "hood" which can be glued over the hood frame.

4.3 Setup of the Drift Chamber System

After the detailed description of one single MEG drift chamber given in section 4.2, the focus in this section will be on the drift chamber system, i.e. the arrangement of all 16 modules.

4.3.1 Drift Chamber System Geometry

The drift chamber system with some geometrical specifications is shown in figure 4.9.

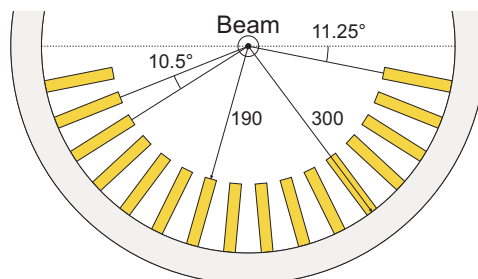


Figure 4.9: Schematic drawing of the drift chamber system geometry.

The drift chambers are aligned from 11.25° to 168.75° with respect to the $+x$ direction. Between adjacent drift chambers is therefore an angular separation of 10.5° . The active volume of the drift chamber system extends from 190 mm to 300 mm in radial direction from beam axis.

4.3.2 Support Structure

To achieve the geometrical specifications described in subsection 4.3.1, the drift chambers are mounted on a carbon fiber frame called support structure. A picture of this structure before the insertion into COBRA is shown in figure 4.10. This support structure with all drift chambers can be extracted out of COBRA to test for example pre-amplifier cards, gas system connections etc. With this extractable construction it is necessary that the entire cabling can be extracted too. All cables are therefore guided along the support structure to the downstream edge of COBRA.

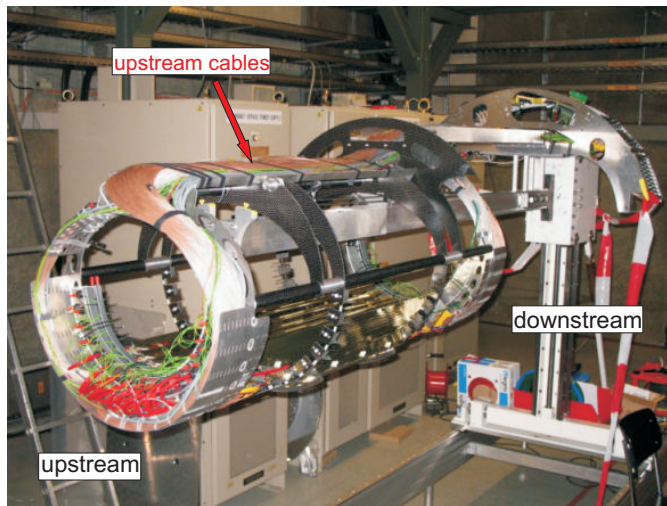


Figure 4.10: Picture of the support structure with already mounted drift chambers before the insertion into COBRA. All upstream cables are guided along the support structure to the downstream edge of COBRA.

Because the liquid xenon detector is installed at the berg side of COBRA, a photon from the $\mu^+ \rightarrow e^+\gamma$ decay can only be detected at this side of COBRA. Therefore, the corresponding positron fly initially in direction aare. To reduce the amount of material in this aare region an asymmetric cable disposition is chosen which is specified in table 4.2 and illustrated in figure 4.11.

Table 4.2: Specifications about the asymmetric cable disposition.

upstream	aare	cables of 5 modules
	berg	cables of 11 modules
downstream	aare	cables of 5 modules
	berg	cables of 11 modules

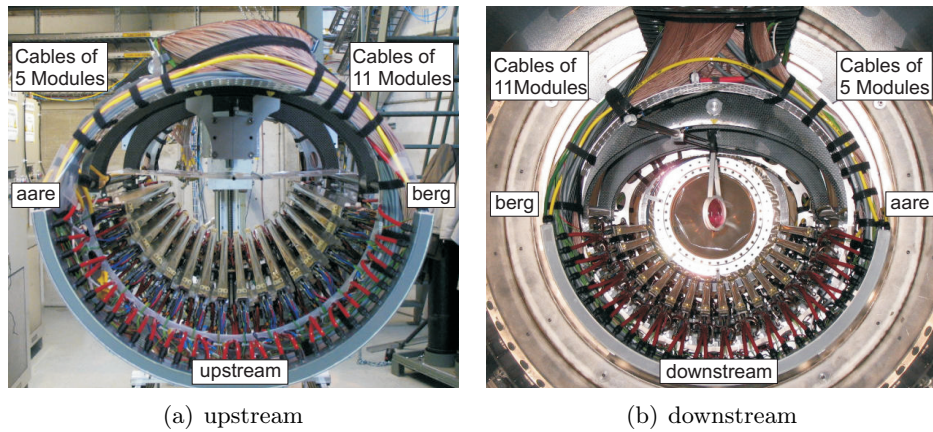


Figure 4.11: Photographs of the cabling situation at the 4.11(a) upstream and 4.11(b) downstream side of the support structure. These pictures should illustrate the asymmetric cable disposition.

4.3.3 Support Structure Centering inside COBRA

It is desirable to ensure reproducibility of the drift chamber system position inside COBRA even after several extraction and insertion movements of the support structure. This means that an effective centering mechanism mounted inside COBRA is necessary to fix the support structure at the correct position.

The centering mechanism used for the run 2007 is illustrated in figure 4.12 with drift chambers (golden), support structure (orange) and COBRA (light gray). On the upstream side, the centering was achieved by pins (black) mounted on the carbon frame which rested on small platforms (dark gray) mounted inside COBRA. On the downstream side, the support structure was fixed by pins (black) mounted inside COBRA. At the bottom part of the upstream and downstream side of the support structure are centering devices in the form of plates (green). These plates ensure centering of the support structure at the bottom. But note that with this construction small shifts of

the support structure in horizontal direction are possible. Additionally the drift chambers touched the inner surface of COBRA even if there should be a gap of about 1 mm between COBRA and bottom edge of the chambers.

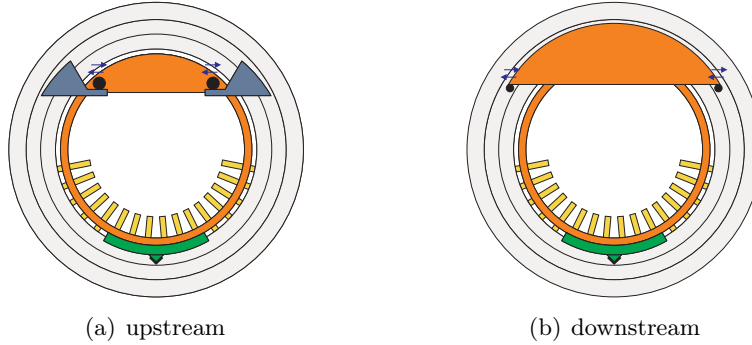


Figure 4.12: Schematic drawing of the support structure centering mechanism 2007 viewed from 4.12(a) upstream and 4.12(b) downstream.

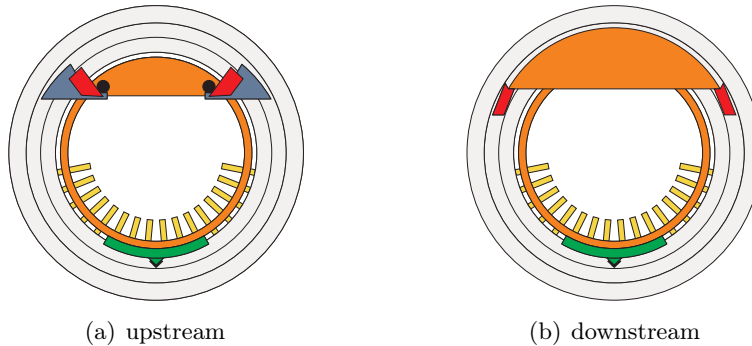


Figure 4.13: Schematic drawing of the support structure centering mechanism 2008 viewed from 4.13(a) upstream and 4.13(b) downstream.

This is the reason why in spring 2008 the centering mechanism was improved (see figure 4.13 for a schematic drawing). The centering on the upstream and downstream side is now done by small wedge-shaped aluminium plates (red) which avoid horizontal shifts. Additionally the entire support structure was raised by 1 mm to avoid contact between drift chambers and COBRA.

The optical survey 2008 should show if these efforts were successful (see later in this thesis).

Chapter 5

Optical Survey 2008

Optical surveys for the MEG experiment are usually done by the Survey Group of the Paul Scherrer Institute¹. This group is for example responsible for the survey of the Synchrotron Lichtquelle Schweiz (SLS) and the proton accelerator, which is described in subsection 3.2.1. But also the surveying of experiments on beam lines belongs to their assignment if such a measurement is desired.

This chapter should give a detailed description of the optical survey 2008 starting with a discussion about the purpose of this survey in section 5.1. After this introduction possible measuring points on drift chambers, support structure and target will be described in section 5.2. Of course an overview about general measuring principles of optical surveys must be included which will be done in section 5.3. Finally the optical surveys of 2007 and 2008 will be described in detail in sections 5.4 and 5.5, respectively.

5.1 Purpose of Optical Survey 2008

The most important intention of the optical survey 2008 is to provide the positions of all anode wires in the MEG coordinate system. These positions designate the starting point for the software wire alignment 2008 with particle tracks and is therefore an indispensable contribution to positron track reconstructions.

In 2007 and before the position of the target inside COBRA was always assumed to be ideal. Since spring 2008 it is possible to measure the target position by optical surveys with the help of survey marks painted on the polyethylene foil (see subsection 5.2.3). To provide the target position inside COBRA is therefore the second purpose of the optical survey 2008.

¹For more information about the PSI Survey Group, please see [21].

To calibrate the photon detector, a LiF target has to be inserted into COBRA from the downstream side several times during the run. To avoid conflicts between these two targets, an extraction and insertion system for the usual target was developed. This system moves the target from the beam axis away to a park position and after the calibration the target is moved back to its origin position. A very crucial question is of course if the target position is reproducible even after extraction and insertion movements. The optical survey 2008 should answer this question.

After last years run, it turned out that the support structure is maybe deformed and distorted inside COBRA with the consequence that the drift chambers are not at expected positions. The analysis of the optical survey 2008 should show if this suspicion is true and then determine the extent of this deformation. With the results of this analysis it is maybe possible to improve the situation for run 2009.

5.2 Measuring Points

Before the optical survey can start, some possible measuring points have to be defined. It is clear that these points should provide a precise measurement with optical methods, i.e. point-like objects on drift chambers or the support structure would be perfectly suited. Another requirement on such a point is that its theoretical position should be known with the advantage that variations from ideal values can be identified. Last but not least an exact calculation from such points to each anode wire position has to be possible to provide the starting point for the software wire alignment.

In 2007 and before, there were two different kinds of measuring points: small plates with crosses glued on drift chambers (see subsection 5.2.1) and pins on the support structure as described in subsection 5.2.2. The target was till spring 2008 not surveyed with optical methods but now there are measuring points in the form of crosses painted on the polyethylene foil (see subsection 5.2.3 for more details).

5.2.1 Drift Chamber Crosses

To allow a determination of a possible sloping position of the drift chamber, at least two different measuring points on the upstream and downstream side of each module are necessary. But on the chambers as described in chapter 4 are no suitable points which could be surveyed by optical methods. That is the reason why especially for optical surveys small printed circuit board (PCB) plates are glued on the upstream and downstream side of each drift chamber. In figure 5.1 is a photograph of some drift chambers with these

flags. On each plate are PCB tracks of a width of $200\ \mu\text{m}$ in the form of small targets as shown in figure 5.2(a). In 5.2(b) is a schematic drawing of such a flag with important geometrical information: The distance between bull's eye and upper flag edge is given by $1.5\ \text{mm}$ whereas the distance to each side edge is $8.5\ \text{mm}$ long, corresponding to half a drift chamber width.

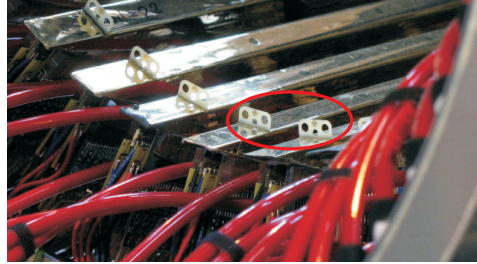
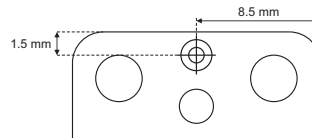


Figure 5.1: Photograph of drift chamber crosses viewed from downstream while the drift chambers are already mounted on the support structure.

With these total $2 \times 16 = 32$ drift chamber crosses a precise optical survey is possible because it is very easy to target at these measuring points with the theodolite eyeglass. Another advantage of these flags is given by the fact that if the positions of the crosses is known, it is possible to determine the center of the corresponding drift chambers (see chapter 6 and 8 for more information). Additionally, the expected positions of these crosses are perfectly known (see subsection 7.1.2) and it is possible to calculate each anode wire position if the coordinates of these crosses are measured (see chapter 8).



(a) Photograph of two Flags



(b) Schematic Drawing of a Flag

Figure 5.2: In 5.2(a) is a photograph of PCB plates of adjacent drift chambers mounted on the support structure. A schematic drawing of one flag with some geometrical specifications is shown in figure 5.2(b).

5.2.2 Support Structure Pins

With coordinate measurements of drift chamber crosses (see subsection 5.2.1), it is only possible to determine the upper edge position of each module but not the exact drift chamber slant angle. This means that other measuring points on the bottom edge of each drift chamber are necessary to measure

this angle. But because there are all pre-amplifier cards and signal cables it is impossible to add a survey target as for example a PCB flag.

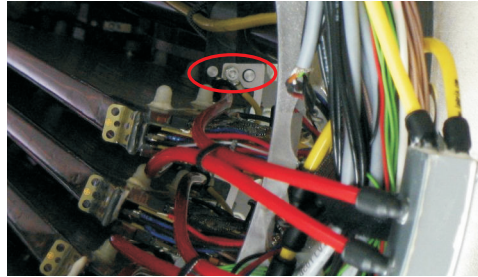


Figure 5.3: Photograph of the outermost pair of support structure pins viewed from downstream.

The drift chambers are mounted on the support structure by clamping them between carbon blocks. On each block are two pins, the ones with a smaller and bigger radius from beam axis are called inner and outer pins, respectively. Because both pins of a block are identical it does not matter if the inner or outer pins are used for optical surveys. In figure 5.3 is a photograph of the outermost pair of pins viewed from downstream. A schematic drawing of three pairs of pins with two clamped drift chambers is shown in figure 5.4. Note that totally 34 blocks are necessary to clamp 16 drift chambers on the support structure (17 blocks at the downstream side and 17 blocks at the upstream side of the support structure).

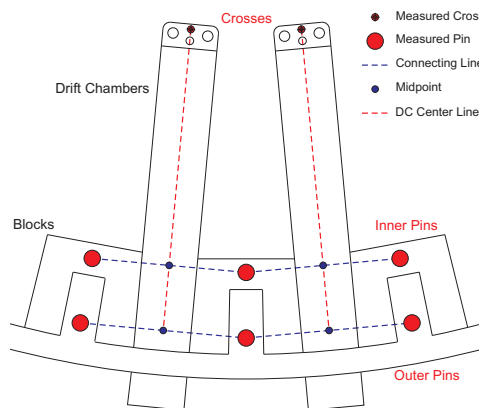


Figure 5.4: Schematic drawing of three pairs of support structure pins with two clamped drift chambers. The midpoint of the connecting line between adjacent pin pairs and the measured drift chamber cross determine the center line of the corresponding drift chamber.

With these pins a precise optical survey is possible because concentric circles resulting from the pin production are visible on the pin surface. Of course it is very easy to determine the center of these pins with the help of a theodolite eyeglass with implemented crosshairs.

To determine the drift chamber slant angle, it has to be assumed that the midpoint of the connecting line between adjacent pins corresponds to the center of the drift chamber. This means that the midpoint of the connecting line between adjacent pin pairs and the measured drift chamber cross determine the center line of the corresponding drift chamber as shown in figure 5.4.

5.2.3 Target Survey Marks

In spring 2008 it was decided that the target position should be determined by optical surveying. Of course it is impossible to glue PCB plates on the ROHACELL frame or the foil because otherwise tracks of positrons and photons coming from decays in the target would be affected by this additional material. But it is possible to draw crosses with a super-fine pen on the foil as already shown in figure 3.4(a). Before the target was mounted on the support structure, the relative positions of these crosses to each other were measured. The resulting coordinates are shown in figure 5.5 but note that they are in reference to a local coordinate system.

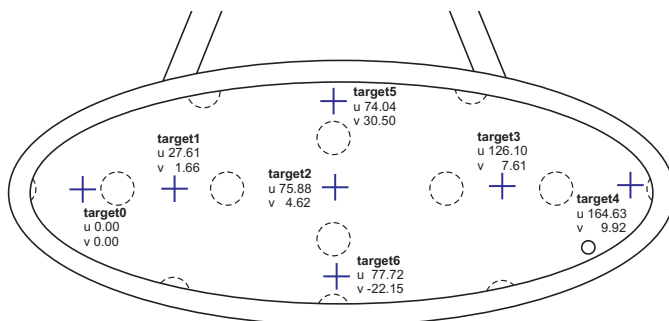


Figure 5.5: Schematic drawing of the target with cross positions which are in reference to a local coordinate system with origin in cross named target0.

Unfortunately the target foil is not perfectly fixed in the ROHACELL frame with the consequence that the foil can be shifted by one or two millimeters in target plane direction. This means that the two lines formed by target crosses target0 - target4 and target5 - target6 are not exactly the major and minor axis of the ellipsoid shaped target.

5.3 General Measuring Principle

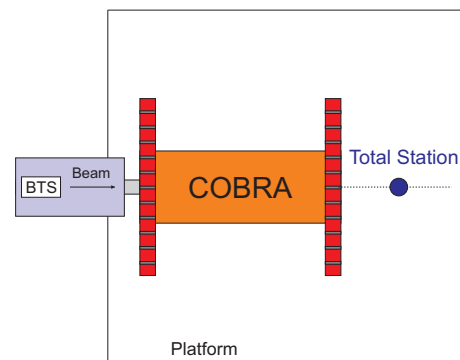
After the detailed description of measuring points on drift chambers, the support structure and the target given in section 5.2, the general measuring principle of an optical survey will be discussed in this section. First, the measuring instrument and its features will be described in subsection 5.3.1 following by some words about how coordinates of measuring points can be determined (see subsection 5.3.2). Finally, subsection 5.3.3 will give a short overview about reference points and why they are important.

5.3.1 Measuring Instrument

A so-called total station was used for the optical survey 2008 of the drift chamber system and the target. With this device one can measure the horizontal and vertical angles of a measuring point but additionally it is possible to determine the distance between this point and the total station. This means that the used measuring instrument is a combination of a theodolite and an electronic distance meter.



(a) Total Station TC2002



(b) Optical Survey from downstream

Figure 5.6: In 5.6(a) is a photograph of a total station TC2002 from Leica Geosystems which was used for the optical survey 2008 (picture originates from [22]). A schematic of optical surveys from downstream is shown in figure 5.6(b). Note that optical surveys from upstream are impossible because COBRA is closed at this side.

The used measuring instrument was a total station TC2002 from Leica Geosystems², see figure 5.6(a) for a picture of this device. The direction measurement with the TC2002 has an accuracy of 0.1 mm for a distance of 30 m corresponding to an error of 0.15 milligon. Gon is a unit for angles which is normally used by surveyors with one gon corresponds to 1/400 of

²See [23] for more information about Leica Geosystems and surveying instruments.

a full circle. The distance measurement has an accuracy of about 0.25 mm and is therefore the limiting factor for optical surveys with this measuring instrument.

The TC2002 is mounted on a tripod with massive legs to minimize twisting due to the weight of the measuring instrument. The tripod with the TC2002 is installed at the downstream side of COBRA, i.e. against the beam direction as shown in figure 5.6(b). An optical survey from upstream is impossible because COBRA is closed at this side and the BTS is connected to the upstream edge of COBRA.

5.3.2 Survey of Measuring Points

As mentioned in subsection 5.3.1 the used measuring instrument TC2002 can determine distances to measuring points. But of course this is only possible if the measurement light beam of the total station is reflected by the measuring point because the distance can only be calculated by measuring delay and phase shift of the reflected beam. One possibility to reflect a light beam is to use a corner cube reflector consisting of three perpendicular mirrors. Such a reflector is a so-called retroreflector which reflects light beams back towards the light source which can be for example a total station. In figure 5.7 is a photograph of such a corner cube reflector which is used by the PSI Survey Group.



Figure 5.7: Photograph of the corner cube reflector which was used by the PSI Survey Group for the optical survey 2008 (picture originates from [24]).

Of course it is impossible to mount such a reflector on drift chambers or the target. This means that only horizontal and vertical angles of the points described in section 5.2 can be measured with the total station but not the distance. Nevertheless, the x , y and z coordinates (in the MEG coordinate system) of all these measuring points can be calculated by two different methods.

Method 1: Given Distances of Measuring Points

As mentioned before the direction of a drift chamber cross, a support structure pin or a target cross can be measured by the total station but not the distance. This means that a determination of the x , y and z coordinate in the MEG coordinate system is impossible. But if the distance between such a measuring point and any point with already determined coordinates is known, it is possible to calculate the position of the measuring point in the MEG coordinate system. If we know for example where the total station is located with respect to the COBRA magnet and if the theoretical z coordinates of all measuring points are known, the x and y coordinates can be calculated. For more details about the theoretical z coordinates of the used measuring points, please see section 7.1.

How the location of the total station with respect to the COBRA magnet can be determined is described in subsection 5.3.3.

Method 2: Measured Direction from at least two different Total Station Positions

If horizontal and vertical angles of a measuring point are determined from at least two spatially distributed positions of the total station and if the coordinates of these two positions are known, it is possible to calculate the coordinates of the measuring point by geometrical considerations. Of course it is necessary that the measurements from these two total station positions can be merged together. This can be reached by surveying the same reference points (see subsection 5.3.3) from the first and the second position. The PSI Survey Group has special software at their disposal which can merge all available data together and can calculate the coordinates of the measuring points.

5.3.3 Reference Points

Before the survey of the measuring points can start, one has to determine the location of the total station in the experimental hall of the Paul Scherrer Institute, i.e. the position in an absolute coordinate system has to be known. The position determination can be done by using so-called reference points on which a reflector (see previous subsection) can be mounted. This means that not only a horizontal and vertical angle determination is possible, the distance between reference point and total station can also be measured. At least three spatially distributed reference points are necessary to determine the position of the measuring instrument and to minimize instrument errors as for example axis errors. Another possibility to minimize such errors is

given by measuring reference points two times: first with the normal instrument orientation and the second time with the total station turned by 200 gon. But the most important advantage of such reference points for the optical survey 2008 is that they can be used to merge surveys from different total station positions together. Of course this is only possible if from all these positions the same reference points are measured.

Possible reference points are for example PSI points on the floor of the experimental hall which have known coordinates. After the installation of COBRA, the Survey Group determined the coordinates of some points on the main magnet and on the compensation coils which can now be used as reference points too. Some COBRA points are labeled and marked in figure 5.8. Of course there are more such points on COBRA but they are not visible in this picture. Additionally, due to these COBRA points the MEG coordinate system has a well known location in the experimental hall with the consequence that the two coordinate systems MEG and experimental hall can be transferred to each other.

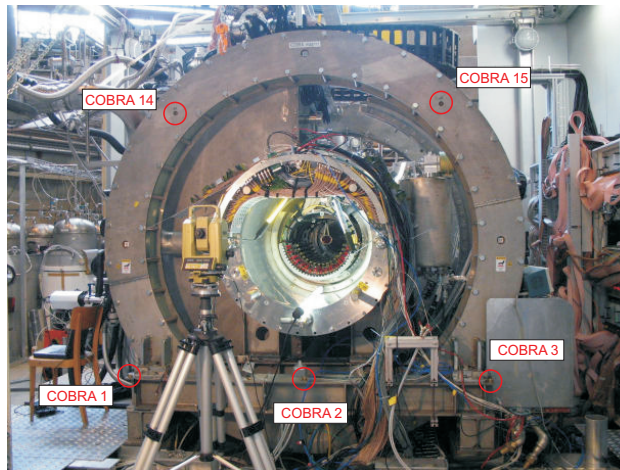


Figure 5.8: Photograph of COBRA viewed from downstream with labeled reference points. Additionally the total station used for optical survey 2008 is also shown in this picture.

If the total station has to be installed on positions from where not enough of these reference points are visible, it is also possible to use temporary reference points which have no known coordinates. These points can be used to merge measurements from different positions together but not to determine the location of the total station in the experimental hall. The resulting coordinates of the measuring points are therefore only in a local coordinate system but not in the MEG or the experimental hall system.

5.4 Optical Survey 2007

In 2007 the measuring instrument was a theodolite and not a total station. This means that with this device distance measurements with reflectors were not possible but nevertheless distances for example from the theodolite to COBRA can be determined by using a ruler. The measuring instrument was installed exactly on beam axis with the help of laser devices. The distance between theodolite and COBRA magnet was measured to be 519.76 mm. All drift chamber crosses and support structure pins were visible from this position. In figure 5.9 is a schematic drawing of the situation with drift chamber, COBRA magnet and the position of the theodolite.

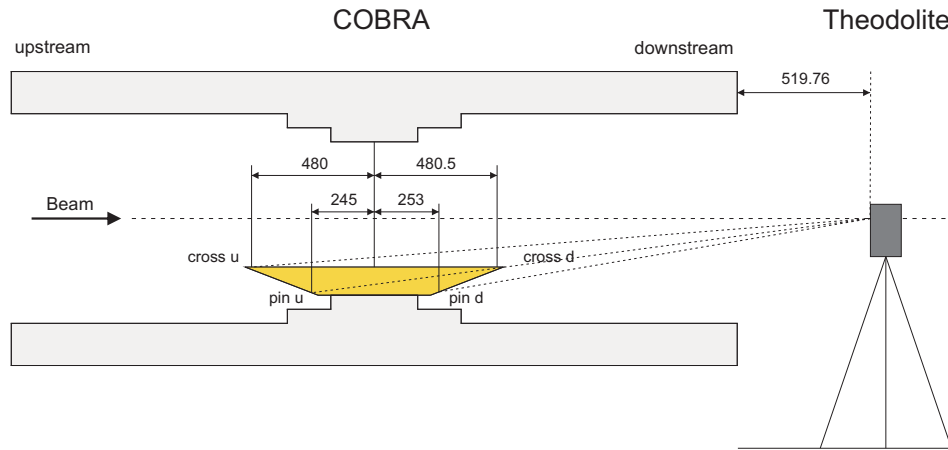


Figure 5.9: Schematic drawing of the theodolite position used for the optical survey 2007. All drift chamber crosses and support structure pins were visible from this position. The given theoretical z positions of all measuring points are also shown in this figure.

From this position the horizontal and vertical angles of the following measuring points were determined:

- 16 drift chamber crosses upstream
- 16 drift chamber crosses downstream
- 17 inner support structure pins upstream
- 17 outer support structure pins downstream

With this measurement only the angles of all measuring points are known but of course no distances. In 2007 this problem was solved by giving theoretical z coordinates in the MEG coordinate system which are summarized in table

5.1. The asymmetry between upstream and downstream will be described later in section 7.1. With these given z positions and the measured horizontal and vertical angles the x and y coordinates of every measuring point can be calculated. The results from this survey were used as starting point for the drift chamber alignment 2007.

Table 5.1: Theoretical z positions of the drift chamber crosses and the support structure pins.

Measuring Point	Theoretical z Coordinate
Drift chamber cross upstream:	$z = -480.0$ mm
Drift chamber cross downstream:	$z = 480.5$ mm
Support structure pin upstream:	$z = -245.0$ mm
Support structure pin downstream:	$z = 253.0$ mm

5.5 Optical Survey 2008

Of course it is very dissatisfying if one has to assume theoretical z positions to get results from optical surveys. Is this assumption actually good? What can we do if it is bad? These questions are the reason why in 2008 an upgraded optical survey should take place.

An improvement of the optical survey 2007 as described in section 5.4 can be achieved by surveying all measuring points from at least two different total station positions. In the following subsections the exact procedure of the optical survey 2008 will be described.

5.5.1 Reference Points

Four temporary reference points and a PSI reference point on the floor were used as reference points for the survey 2008 (see table 5.2). The temporary reference points were installed by the Survey Group only for this optical survey and were dismantled right after the measurements (see figure 5.10 for some pictures). The temporary points were mounted on support columns of the high stage and of the COBRA wood barrack. The high stage is used for electronic crates whereas the wood barrack shields the COBRA magnet from the environment and provides an effective air conditioning.

As shown in figure 5.11, the arrangement of these reference points is spatially distributed and therefore best suited to merge surveys from different total station positions together.

Table 5.2: List of reference points used for optical survey 2008 with T and R as shortcuts for temporary point and reference point, respectively.

ID	Mounted On	Location	Bottom/Top
T1:	support high stage	downstream	top
T2:	support COBRA wood barrack	berg	bottom
T3:	support COBRA wood barrack	aare, downstream	bottom
T4:	support COBRA wood barrack	aare, upstream	bottom
R5:	PSI point on the floor	downstream	



(a) Temporary Reference Point T1



(b) Temporary Reference Point T4

Figure 5.10: Photographs of some temporary reference points used for optical survey 2008.

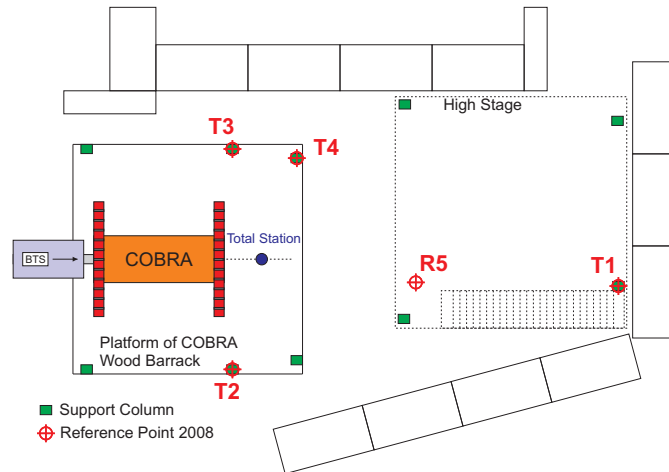


Figure 5.11: Outline of area $\pi E5$ with beam line devices, COBRA magnet with platform, total station position and high stage. Additionally the locations of the reference points used for optical survey 2008 are also marked.

With these reference points a determination of the measuring point positions is only possible in a local coordinate system, but we are interested in the positions of crosses and pins in the MEG coordinate system. This means that an additional relation to COBRA is necessary which can be achieved by measuring as many reference points on the COBRA magnet as possible (see subsection 5.3.3).

5.5.2 Position 1

At the beginning of the optical survey 2008 the total station was installed approximately on beam axis, the so-called Position 1. It is important to note that the measuring device is, compared with 2007, not exactly on beam axis. In figure 5.12 is an outline of this situation in area $\pi E5$.

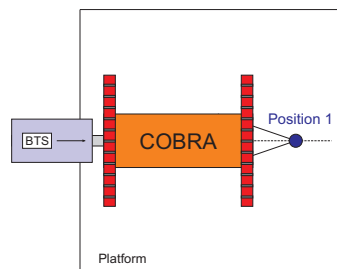


Figure 5.12: Schematic of the survey situation 2008 with the total station installed at Position 1.

After the installation, all reference points described in subsection 5.5.1 and as many COBRA points as possible were surveyed. After that the Survey Group measured the horizontal and vertical angles of the following points:

- 16 drift chamber crosses upstream
- 16 drift chamber crosses downstream
- 17 inner support structure pins upstream
- 17 inner support structure pins downstream
- 7 target crosses

Note that in 2007 the outer support structure pins at the downstream side were measured while in 2008 the coordinates of the inner ones were determined. The reason for this change is that in 2008 some of the outer pins were covered by drift chamber cables (signal cables, high voltage cables etc).

For the drift chamber crosses and support structure pins this measurement is already enough to obtain measured x and y coordinates if the z position of the measuring point is given. But with this procedure we do not get any information about the target because the z positions of the target crosses are not known.

5.5.3 Position 2 / 3

To determine the coordinates of the target crosses in the MEG system and to achieve the desired improvement compared to the optical survey 2007, the measuring points were surveyed from two additional total station positions. Position 2 and Position 3 are also placed on beam high but approximately +500 mm and -500 mm shifted along the MEG x axis as shown in figure 5.13.

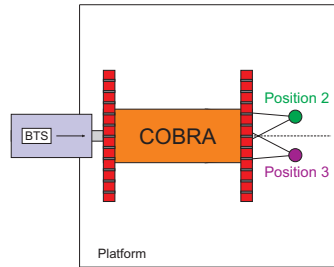


Figure 5.13: Schematic of the survey situation 2008 with the total station installed at Position 2 and Position 3. With these additional positions the x , y and z coordinates of measuring points can be determined.

The purpose of these two additional positions is to measure as many drift chamber crosses, support structure pins and target crosses as possible. The Survey Group surveyed the following measuring points from at least two different total station positions:

- 16 drift chamber crosses upstream (cross00 - cross15)
- 16 drift chamber crosses downstream (cross00 - cross15)
- 5 inner support structure pins upstream (pin00, pin01, pin14, pin15, pin16)
- 3 inner support structure pins downstream (pin00, pin01, pin16)
- 7 target crosses (target0 - target6)

In summary, all measuring points were surveyed from Position 1 of the total station. Additionally all drift chamber crosses and target crosses were

measured either from Position 2 or Position 3 but unfortunately only 8 support structure pins were measured from a secondary position. The reason for this disappointing result is that the view from Position 2 or Position 3 to these pins is limited by the COBRA geometry but mostly by the support structure, drift chambers, cables, pre-amplifier cards etc. To demonstrate the difficulty of this pin measurement, please see figure 5.3. This picture was taken away from beam axis with the consequence that only the outermost pair of pins is visible.

To improve the support structure pin measurements in 2009, it is maybe interesting to analyze the consequences if Position 2 and Position 3 are located less than 500 mm away from beam axis. Of course the angles between direction measurements will be more flat than the ones in 2008 with the consequence that the error of a measured point will be bigger than in 2008 (see subsection 5.5.5 for more information about errors). But on the other side, the Survey Group will be able to measure more support structure pins. It is maybe possible to find an optimum for the optical survey 2009.

The x , y and z coordinate of all measuring points listed before can be determined and then compared with the results which were obtained by using theoretical z positions. For more information about the outcome of this comparison, please see chapter 7.

5.5.4 Target Extraction and Insertion

As already mentioned in section 5.1 one important purpose of the optical survey 2008 is to check the reproducibility of the target position after extraction and insertion movements. With the survey procedure described in the previous subsections the current position of the target was known.

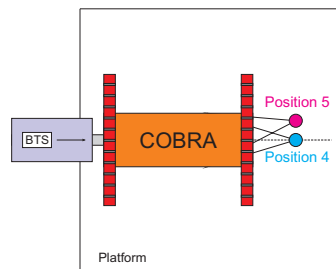


Figure 5.14: Schematic of the survey situation 2008 with the total station installed at Position 4 and Position 5. With these two positions the coordinates of the target after several extraction and insertion movements can be measured. Note that these two positions are close to Positions 1 and 2.

After several extraction and insertion movements, the target crosses were measured again from two different positions as shown in figure 5.14. Position 4 and Position 5 are close to the previous Positions 1 and 2 but they are not exactly at the same place. After these measurements the coordinates of the target crosses before and after extraction/insertion movements are known and can be compared. The results will be presented in chapter 9.

5.5.5 Remark: Calibration and Errors

After the optical survey 2008 the Survey Group analyzed the measured angles to obtain the coordinates of the measuring points. During this analysis, the Survey Group realized that measurements of the horizontal angle before and after turning the total station with 200 gon give a discrepancy of 6 mgon. This means that during the optical survey 2008 the horizontal scale of the total station was not perfectly calibrated. Usually the Survey Group calibrates the measuring instruments every month but unfortunately the optical survey 2008 took place at the end of such a calibration period which is the reason for this angle discrepancy. The Survey Group minimized this error during their analysis with compensation software.

As already mentioned in subsection 5.3.1, measurements with the total station which was used for the optical survey 2008 have a small uncertainty. These uncertainties have also consequences for the calculated coordinates of the measuring points which were surveyed from three different total station positions. By considering this measuring instrument uncertainty as well as a certain error due to the calibration problem described before, the Survey Group determined the following errors (standard deviation σ):

$$x \text{ coordinate: } \Delta x = 0.3 \text{ mm} \quad (5.1)$$

$$y \text{ coordinate: } \Delta y = 0.3 \text{ mm} \quad (5.2)$$

$$z \text{ coordinate: } \Delta z = 0.5 \text{ mm} \quad (5.3)$$

The error in z is bigger than the other ones because of flat angles between direction measurements from the used total station positions.

Chapter 6

Mechanical Workshop Survey

The PCB plates with the crosses used as measuring points for optical surveys (see subsection 5.2.1) were glued on drift chambers with the help of positioning devices. But nevertheless, it cannot be precluded that the flags are not at theoretical positions. Additionally, we still do not know how the position of all anode wires can be determined if the coordinates of all measuring points are surveyed. This chapter should clarify all these open questions.

In section 6.1 the mechanical workshop survey which took place in summer 2007 will be explained in detail whereas the obtained data is tabulated in appendix B. How the position of the anode wires can be determined will be described in section 6.2.

6.1 Mechanical Workshop Survey 2007

To measure a possible displacement of the PCB flag from theoretical position, the so-called mechanical workshop survey took place in summer 2007.

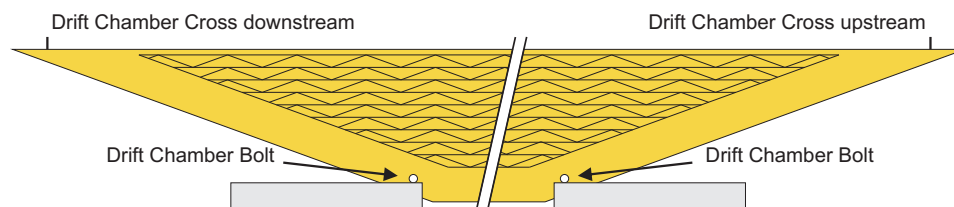


Figure 6.1: Schematic of the measuring setup which was used for the mechanical workshop survey 2007.

Before the mounting on the support structure each drift chamber was placed on blocks in a way that the chamber rests on the drift chamber bolts as shown in figure 6.1. After this installation, 8 different distances for each drift chamber were measured with a stereoscopic touch sensitive sensor. In the following subsections these 8 measurements will be described in more details.

6.1.1 Measurements No.4/No.5 and No.7/No.8

It could be possible that the PCB plate is shifted against the drift chamber with the consequence that the bull's eye does not mark the center of the chamber. Two different distances have to be measured to disclose such a shift and of course it is necessary to do this measurement twice for upstream and downstream. The first distance is from an arbitrary chosen point to the upper side edge of the drift chamber (measurement No.4 for downstream and measurement No.7 for upstream) whereas the second distance is from the same arbitrary point to the side edge of the flag (measurement No.5 for downstream and measurement No.8 for upstream). In figures 6.2(a) and 6.2(b) are schematics of the situation for downstream and upstream, respectively.

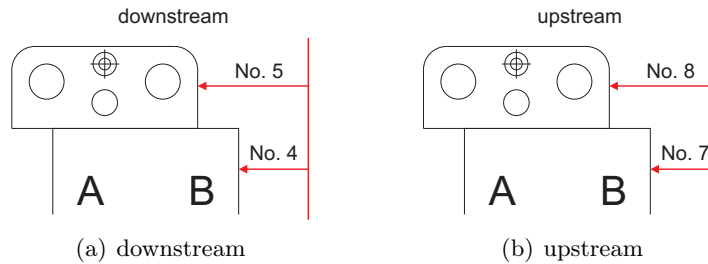


Figure 6.2: In 6.2(a) is a schematic of measurements No.4 and No.5 at the downstream side whereas figure 6.2(b) shows the principle of measurements No.7 and No.8 at the upstream side of the chamber.

With the difference of the corresponding measurements for upstream and downstream one can calculate how much the flag is displaced with respect to the drift chamber:

$$\text{downstream: } \chi_d = \text{No.5} - \text{No.4} \quad (6.1)$$

$$\text{upstream: } \chi_u = \text{No.8} - \text{No.7} \quad (6.2)$$

The maximum deviation from the theoretical value $\chi_{d,u} = 0$ mm shows drift chamber dc07 with 0.376 mm for downstream and 0.197 mm for upstream. As consequence of these results it is necessary to consider these measurements for the calculation of the anode wire positions.

6.1.2 Measurements No.10 and No.11

As you will see later in this thesis, the height between top edge of the PCB flag and bottom edge of the drift chamber bolt is very important for the calculation of the anode wire positions. This is the reason why this value has to be measured during the mechanical workshop survey. It is clear that this measurement has to be done at the downstream (measurement No.10) and the upstream (measurement No.11) side of each drift chamber as shown in figure 6.3. The theoretical value of these two measurements is given by 110.26 mm.

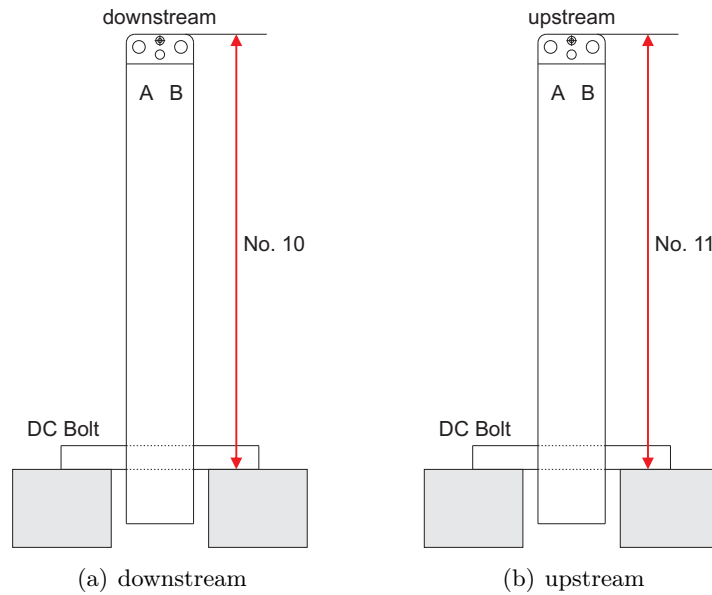


Figure 6.3: Schematics of measurement No.10 at the 6.3(a) downstream side and measurement No.11 at the 6.3(b) upstream side of the drift chamber.

The data obtained from these measurements shows deviations of up to 0.5 mm for dc11 at the upstream side of this chamber. Of course it is again necessary to consider these measurements for the anode wire position calculation.

6.1.3 Measurements No.6 and No.9

For the optical survey 2007 it was assumed that all crosses on the downstream and upstream side have the same z coordinate. To check if this assumption is tenable or not, it is necessary to know the exact distance between two corresponding flags. During measurement No.6 the distance between leading edge of the downstream flag to the center of the upstream drift chamber bolt is surveyed (see figure 6.4(a)). The distance between leading edge of the

upstream flag to the center of the upstream drift chamber bolt is determined by measurement No.9 as shown in figure 6.4(b). Note that the sensor always measures the distance by touching the flag from downstream, i.e. from the same side as the Survey Group targets the flag during the optical survey.

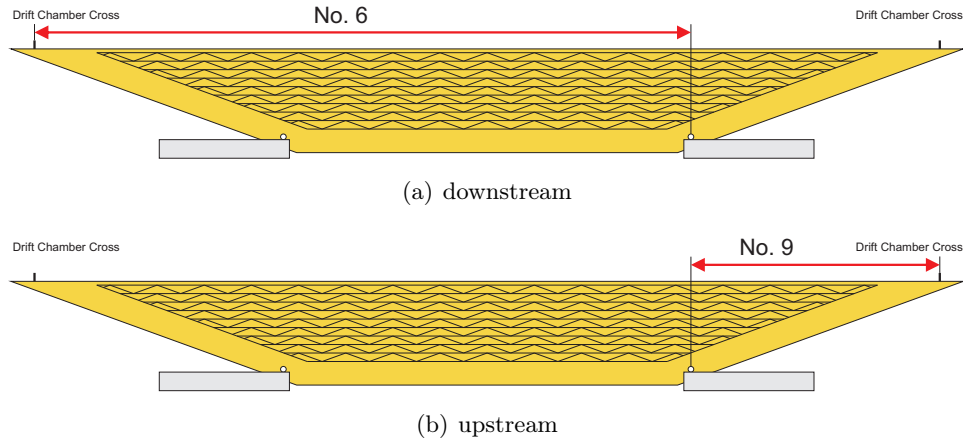


Figure 6.4: Schematics of measurement No.6 and measurement No.9.

The diagram in figure 6.5 shows the result of this cross distance measurement for each drift chamber, i.e. the difference of measurement No.9 and No.6 is shown in this figure.

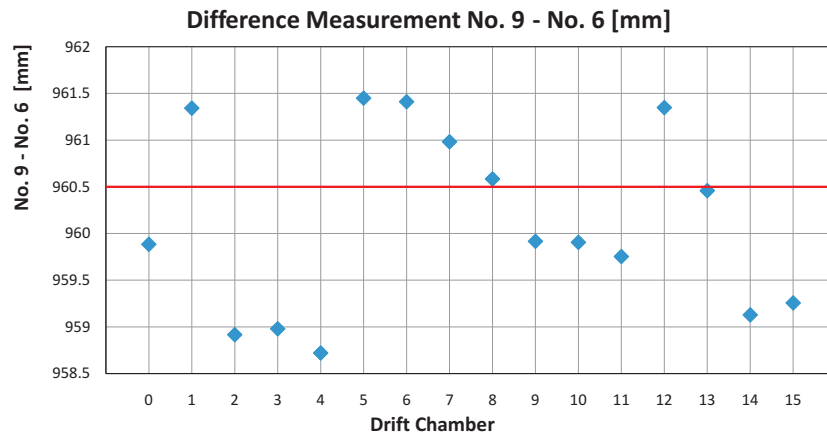


Figure 6.5: Diagram with the results of the cross distance measurement, i.e. the difference from measurements No.9 and No.6 is shown in this figure. Additionally the theoretical value $No.9 - No.6 = 960.5\text{ mm}$ is marked by a red line.

Additionally, the following theoretical value for measurement No.9 - No.6 is marked in this diagram:

$$\begin{array}{rcl} \text{downstream:} & \text{No.6} & = -696.25 \text{ mm} \\ \text{upstream:} & \text{No.9} & = 264.25 \text{ mm} \\ \text{upstream - downstream:} & \text{No.9 - No.6} & = 960.50 \text{ mm} \end{array}$$

These results show clearly that the assumption of fixed cross distances is not tenable.

6.2 Anode Wires

Whereas the previous section described the mechanical workshop survey 2007 in detail this section should answer the question how the position of the anode wires can be calculated. The coordinates of the drift chamber crosses and the support structure pins are already known from the optical survey 2007 / 2008 and with the help of the results from the mechanical workshop survey 2007 the positions of the drift chamber bolts can be calculated. From technical drawings we know the distance between the outermost anode wire of each plane to the center of the drift chamber bolt:

$$\begin{array}{rcl} \text{Plane A:} & 7.76 \text{ mm} \\ \text{Plane B:} & 12.26 \text{ mm} \end{array}$$

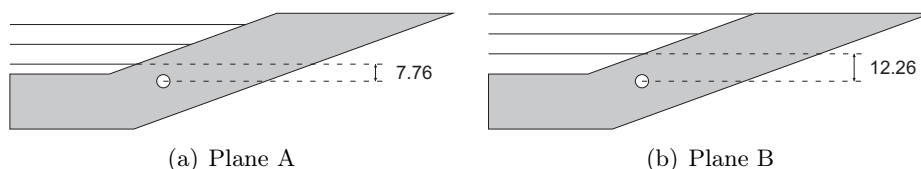


Figure 6.6: Schematic drawings of the outermost anode wires and the drift chamber bolts with important geometrical specifications.

In figures 6.6(a) and 6.6(b) are schematic drawings of the situation for plane A and plane B, respectively. If the positions of the outermost anode wires are known, the other wires can be calculated using given distances between each wire as shown for example in figure 3.12. For more details about the anode wire calculation, please see chapter 8.

Of course it would be advantageous to use measured distances between wires and bolts instead of theoretical values. But random checks of these distances gave differences of about $\pm 50 \mu\text{m}$ from theoretical positions which are quite smaller than the accuracy of an optical survey.

Chapter 7

Analysis of Optical Survey 2007 and 2008

This chapter will describe the analysis of the data provided by the optical survey 2007 and 2008 and of course the results of this analysis will be also presented in this chapter. The measured coordinates of the drift chamber crosses and support structure pins are tabulated in appendix C for optical survey 2007 and in appendix D for optical survey 2008.

To determine variations of measured coordinates of the drift chamber crosses and support structure pins from theoretical positions, these values have to be known firstly. The theoretical positions of the measuring points are therefore discussed in section 7.1. The resulting theoretical coordinates of support structure pins and drift chamber crosses for 2007 and 2008 are tabulated in appendix E.

With these theoretical values it is possible to analyze the measured pin positions to determine a possible support structure deformation. Of course this analysis can be applied to data obtained by the optical survey 2007 and 2008 which will be done in section 7.2. Additionally it is also possible to calculate expected drift chamber cross positions and to compare these with the results of the optical survey 2007 and 2008. The aim of this analysis is to draw conclusions about the mounting of drift chambers on the support structure (see section 7.3).

Because in 2007 the measuring points were surveyed from only one theodolite position it was necessary to give theoretical z positions to get x and y coordinates. A direct comparison of data sets from 2008 with last year is therefore only possible by using survey data with given z coordinates.

Of course it will be very interesting to compare cross and pin coordinates from the optical survey 2008 which were calculated by using theoretical z

positions with the ones which were surveyed from at least two different total station positions. Are there any differences? Which conclusions can be drawn with the measured z positions of crosses and pins? Is it possible to reconstruct the drift chamber cross distances which were measured during the mechanical workshop survey 2007? All these questions will be answered in section 7.4.

7.1 Theoretical Positions

In this section the calculation of the theoretical positions of the support structure pins and the expected positions of the drift chamber crosses will be described. The results are tabulated in appendix E.

7.1.1 Theoretical Positions of Support Structure Pins

x and y Coordinates

The following specifications are necessary to calculate the theoretical position of all support structure pins:

$$\begin{array}{ll} \text{radius inner pins:} & R = 257.5 \text{ mm} \\ \text{radius outer pins:} & R = 277.5 \text{ mm} \\ \text{angle between adjacent pins:} & \alpha = 10.5^\circ \end{array}$$

In figure 7.1 is a schematic drawing of the situation with all these theoretical specifications. Additionally the labeling of the support structure pins is also shown in this figure. The pin labeling follows the same principle as the one for drift chambers with the only difference that there are 17 pins instead of 16 drift chambers.

With the specifications from above the theoretical x and y coordinates of each support structure pin can be calculated:

$$\begin{array}{lll} \text{pin08:} & \text{pin07:} & \text{pin09:} \\ x = 0 & x = R \cdot \sin(\alpha) & x = R \cdot \sin(-\alpha) \\ y = -R & y = -R \cdot \cos(\alpha) & y = -R \cdot \cos(-\alpha) \\ & \text{pin06:} & \text{pin10:} \\ & x = R \cdot \sin(2\alpha) & x = R \cdot \sin(-2\alpha) \\ & y = -R \cdot \cos(2\alpha) & y = -R \cdot \cos(-2\alpha) \\ & \vdots & \vdots \end{array}$$

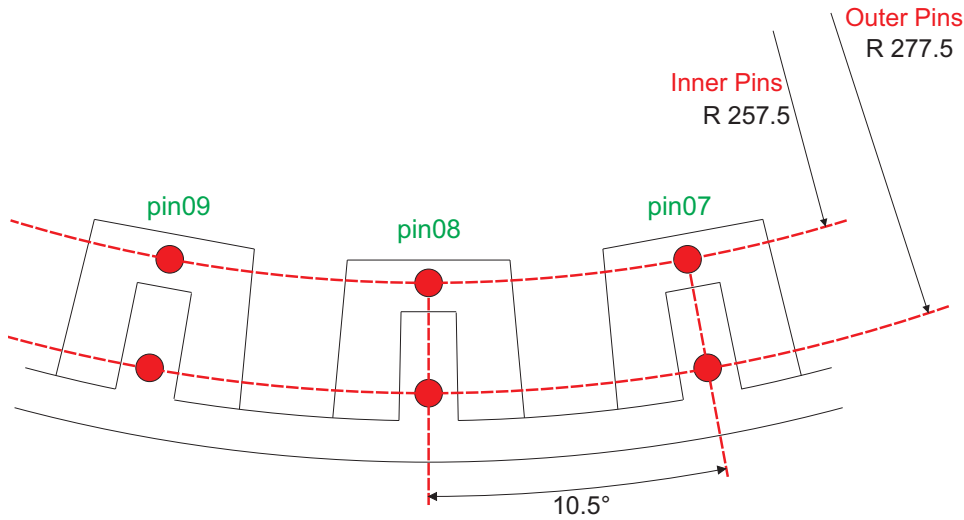


Figure 7.1: Schematic drawing of some support structure pins shown from downstream. Additionally some important geometrical specifications and the used pin labeling are also shown in this figure.

Note that the pins have the same x and y coordinate independent of the fact if they are at the upstream or downstream side of the support structure.

These theoretical x and y coordinates are true for the run 2007 but in spring 2008 the support structure was raised by 1 mm to avoid contact between drift chambers and COBRA. This fact leads to the following consequence for the theoretical positions of the support structure pins:

$$y_{\text{pin2008}} = y_{\text{pin2007}} + 1 \text{ mm.} \quad (7.1)$$

z Coordinate

If the Survey Group could measure drift chamber crosses and support structure pins from upstream and downstream, the situation would be mirror-inverted to the $z = 0$ plane. But because COBRA is closed at the upstream side, an optical survey is only possible from downstream. In figure 7.2 is a schematic of the situation with important geometrical specifications. In summary, the following theoretical z coordinates are used for the upstream and downstream support structure pins:

$$\begin{aligned} \text{pin upstream:} & \quad z = -245 \text{ mm} \\ \text{pin downstream:} & \quad z = 253 \text{ mm} \end{aligned}$$

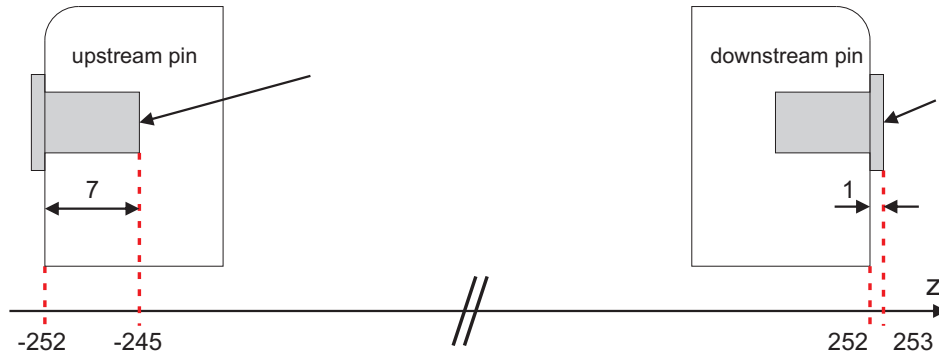


Figure 7.2: Detailed schematic drawing of upstream and downstream support structure pins with specified theoretical z positions.

7.1.2 Expected Positions of Drift Chamber Crosses

Of course it is possible to calculate the theoretical position of each drift chamber cross. But as shown in chapter 6 the PCB plates and hence the drift chamber crosses are not at theoretical positions. It is therefore necessary to consider the results of the mechanical workshop survey 2007 to calculate the expected (not theoretical) position of each drift chamber cross. Another important fact which has to be considered is given by a possible support structure deformation: It is clear that the drift chambers are not at theoretical positions if the support structure is deformed. This is the reason why the results of the mechanical workshop survey 2007 as well as a possible support structure deformation have to be considered to calculate the expected drift chamber cross positions.

x and y Coordinates

As already mentioned in subsection 5.2.2 it is assumed that the middle of the connecting line of adjacent support structure pins marks the center of the drift chamber. To start the calculation of the expected position of a drift chamber cross it is therefore necessary to know the corresponding measured pin coordinates:

$$\vec{\text{pin}}_i = (x_{\text{pin}i}, y_{\text{pin}i}), \quad (7.2)$$

$$\vec{\text{pin}}_{i+1} = (x_{\text{pin}i+1}, y_{\text{pin}i+1}). \quad (7.3)$$

This information is provided by the optical survey 2007 and 2008. The center of the drift chamber defined by adjacent support structure pins is given by:

$$\vec{M} = \vec{\text{pin}}_i + 1/2 \cdot (\vec{\text{pin}}_{i+1} - \vec{\text{pin}}_i). \quad (7.4)$$

In the following calculations the index i for the drift chamber dci is skipped to simplify formulas.

If the drift chamber is perfectly clamped between the two corresponding blocks, the normalized center line of the drift chamber \vec{l} is perpendicular to the normalized connecting line of adjacent pins \vec{p} :

$$\vec{p} = \frac{\vec{\text{pin}}_{i+1} - \vec{\text{pin}}_i}{|\vec{\text{pin}}_{i+1} - \vec{\text{pin}}_i|} = (x_p, y_p), \quad (7.5)$$

$$\vec{l} = (y_p, -x_p). \quad (7.6)$$

Two steps are necessary to calculate the expected position of the drift chamber cross. First, the coordinates of the cross have to be calculated if it is assumed that the PCB plate is not shifted against the drift chamber. Of course one has to distinguish between crosses at the upstream and downstream side of the support structure. The coordinates of the not shifted cross which are calculated by using inner pins are given by:

$$\vec{\text{cross}}'_u = \vec{M} + (-25.76 - 3 + \text{No.11} - 1.5) \cdot \vec{l}, \quad (7.7)$$

$$\vec{\text{cross}}'_d = \vec{M} + (-25.76 - 3 + \text{No.10} - 1.5) \cdot \vec{l}, \quad (7.8)$$

whereas the following formulas are true for outer pins:

$$\vec{\text{cross}}'_u = \vec{M} + (-5.84 - 3 + \text{No.11} - 1.5) \cdot \vec{l}, \quad (7.9)$$

$$\vec{\text{cross}}'_d = \vec{M} + (-5.84 - 3 + \text{No.10} - 1.5) \cdot \vec{l}. \quad (7.10)$$

The values 25.76 mm and 5.84 mm are the theoretical distances between the center of the inner and outer support structure pin to the center of the drift chamber bolt while 3 mm defines the radius of the drift chamber bolt. It is necessary to use the measured values No.10 and No.11 of the mechanical workshop survey 2007 (see subsection 6.1.2) for the downstream and upstream side of the chamber. Finally the value 1.5 mm corresponds to the distance between top edge of PCB plate and bull's eye of the drift chamber cross (see figure 5.2(b)). In figure 7.3 is a schematic drawing with all these specifications.

As already mentioned in subsection 6.1.1, it was measured during the mechanical workshop survey if the PCB plate is shifted against the drift chamber or not. Of course it is necessary to implement this information in the

calculation of the expected cross position:

$$\overrightarrow{\text{cross}}_u = \overrightarrow{\text{cross}}'_u + \chi_u \cdot \vec{p}, \quad (7.11)$$

$$\overrightarrow{\text{cross}}_d = \overrightarrow{\text{cross}}'_d + \chi_d \cdot \vec{p}. \quad (7.12)$$

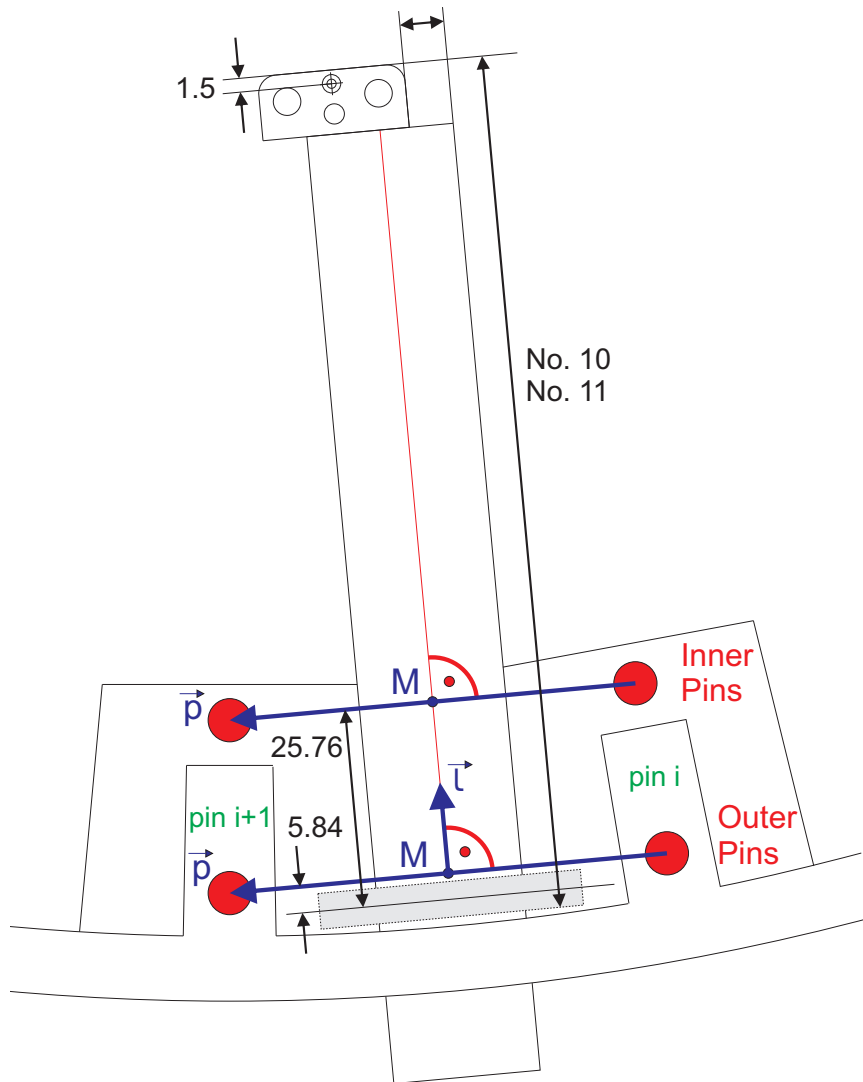


Figure 7.3: Schematic drawing of one drift chamber and two pairs of pins which are viewed from downstream. Additionally, variables and geometrical specifications mentioned in subsection 7.1.2 are shown in this figure.

z Coordinate

As already mentioned in subsection 7.1.1 an optical survey of measuring points is only possible from the downstream side of COBRA. The situation of the drift chamber crosses is therefore similar to the one of the support structure pins as shown in figure 7.4. The following theoretical z coordinates are used for the upstream and downstream drift chamber crosses:

$$\begin{aligned} \text{cross upstream:} & \quad z = -480.0 \text{ mm} \\ \text{cross downstream:} & \quad z = 480.5 \text{ mm} \end{aligned}$$

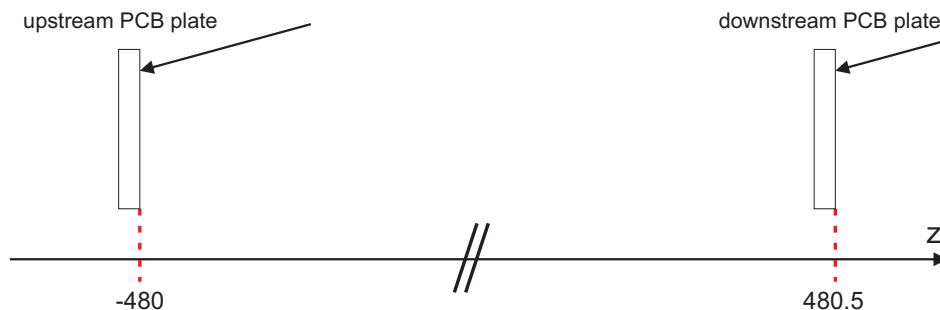


Figure 7.4: Schematic drawing of upstream and downstream drift chamber crosses with marked theoretical z positions.

7.2 Support Structure Deformation

To show if the support structure is deformed inside COBRA, one has to compare measured coordinates of support structure pins with the calculated theoretical pin positions (see subsection 7.1.1). The support structure positions which were measured in 2007 and 2008 will be analyzed in this section. Because in 2007 the z coordinates of the pins were not measured, it is necessary to use only data with given z values to compare the support structure position in 2007 with the one in 2008.

7.2.1 Support Structure Deformation in 2007

Recall that in 2007 the inner pins at the upstream side of the support structure but the outer pins at the downstream side were surveyed. It is therefore necessary to use the corresponding theoretical values (see appendix E).

In figure 7.5 is a diagram of the downstream situation 2007. Additionally to the theoretical positions (blue) the measured values (red) are also shown in

this figure. Of course it is impossible to see differences between theory and measurement in a diagram with such big ranges. This is the reason why in this figure the measured values are shown with 50 times displacement. Note that this diagram shows only x and y coordinates because the z coordinate is always constant and therefore not interesting for this analysis.

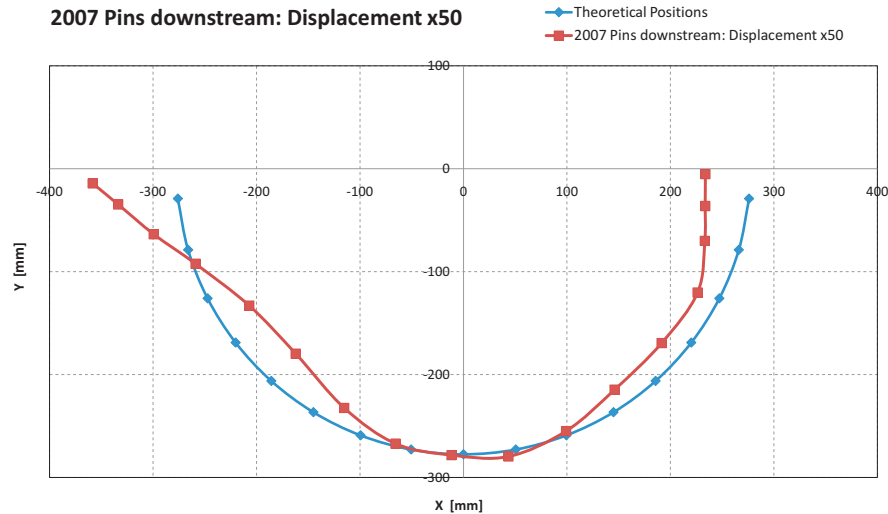


Figure 7.5: Diagram with theoretical and measured coordinates of downstream support structure pins 2007.

It is obvious that the support structure shows big deviations from the theoretical positions, especially at the outermost regions berg and aare with deviations of up to 1.7 mm. Additionally, some indentations at pin04 / pin05 and pin11 / pin12 are also visible in figure 7.5. These indentations will be discussed later in this section.

The situation at the upstream side of the support structure is shown in figure 7.6. Again, the measured coordinates of the support structure pins show big deviations from theoretical values. It seems that the support structure is squeezed in a way that it forms an oval instead of a perfect circle. Additionally the added weight of cables at berg side (i.e. in $-x$ direction) seems to be responsible for a certain rotation. As already mentioned in subsection 4.3.2, upstream cables of 11 modules are guided outside of COBRA at the berg side of the support structure whereas at the aare side are cables of 5 drift chambers.

Finally, it is necessary to discuss about errors of measured pin coordinates. The Survey Group calculated an error of 0.1 mm for the x and y coordinates of each pin. It is comparatively small because for the optical survey 2007 only one measurement was done. The error consists therefore of the uncertainty of

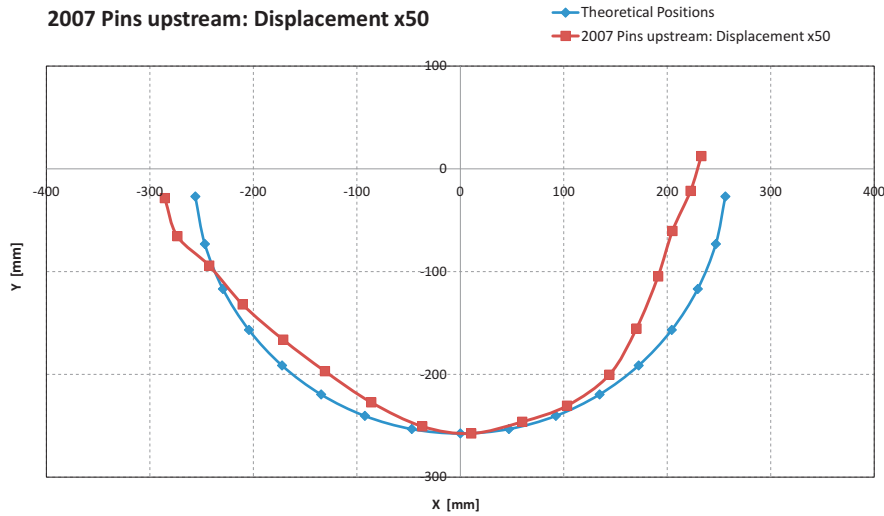


Figure 7.6: Diagram with theoretical and measured coordinates of upstream support structure pins 2007.

the theodolite measurement and the uncertainty of the measuring instrument position. But of course the pin coordinates were determined by using given z coordinates. If the assumption of constant z values is bad it is therefore possible that this error is much bigger.

7.2.2 Support Structure Deformation in 2008

Recall that in 2008 only inner pins were surveyed and that the support structure was raised by 1 mm. It is therefore necessary to use the correct theoretical values which are tabulated in appendix E.

In figure 7.7 is a diagram of pin positions 2008 at the downstream side of the support structure. Compared to the support structure position of last year, the situation in 2008 seems to be better: The support structure is centered inside COBRA and the biggest deviation is given by pin16 with $\Delta x = -0.72$ mm and $\Delta y = -0.07$ mm. It is interesting to note that there are again indentations at pin05 and pin11.

The upstream situation is shown in figure 7.8. Again it is obvious that the support structure is rotated by the additional weight of cables (see subsection 4.3.2). Additionally it seems that the pins are lifted at the upstream side. It is possible that the support structure is raised by the upstream timing counter or the upstream Nitrogen Bag.

Of course a discussion about errors is again important. As already mentioned in subsection 5.5.5 the Survey Group calculated an error of 0.3 mm for the x and y coordinates. Recall that the data used for this analysis was obtained by assuming theoretical z positions.

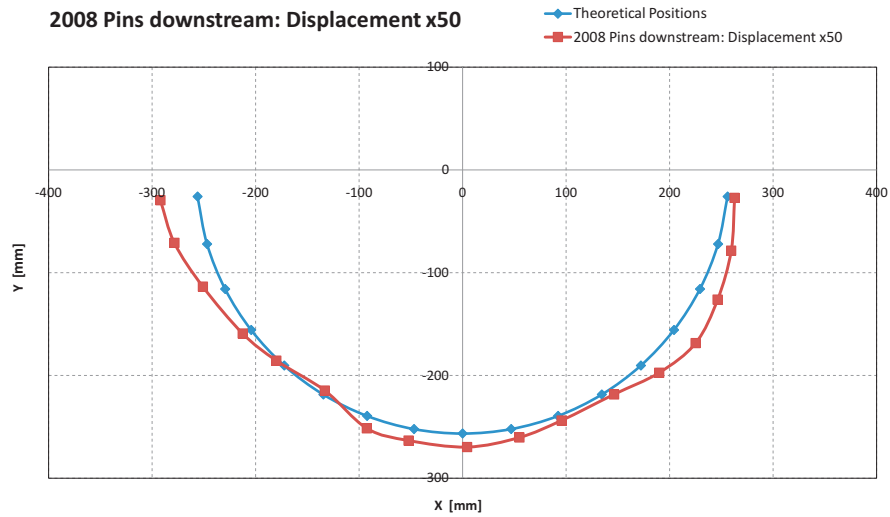


Figure 7.7: Diagram with theoretical and measured coordinates of downstream support structure pins 2008.

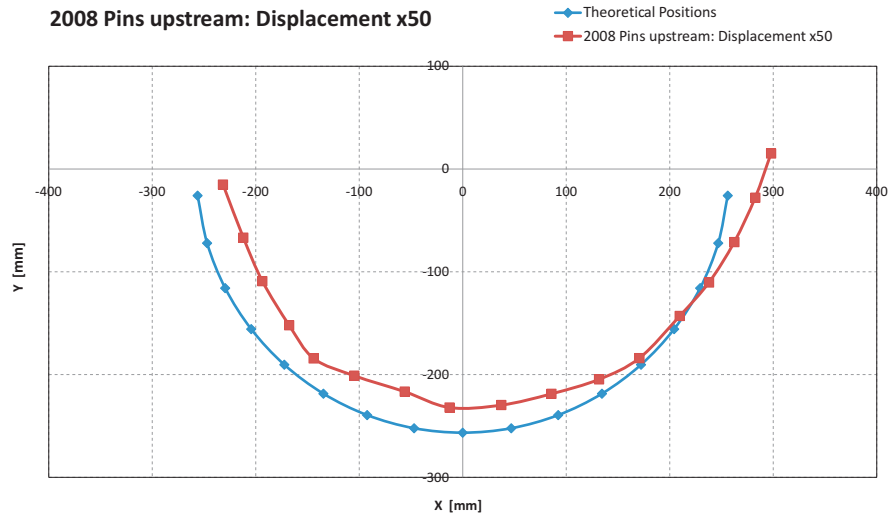


Figure 7.8: Diagram with theoretical and measured coordinates of upstream support structure pins 2008.

7.2.3 Difference upstream and downstream in 2008

It could be interesting to compare the measured pin positions 2008 at the upstream and downstream side of the support structure. In figures 7.9 and 7.10 are diagrams with marked differences upstream - downstream of the x and y coordinate of each support structure pin. It seems that the pins at the upstream side are generally shifted to aare, i.e. in $+x$ direction, whereas pin positions at the upstream side are higher than the ones at the downstream side.

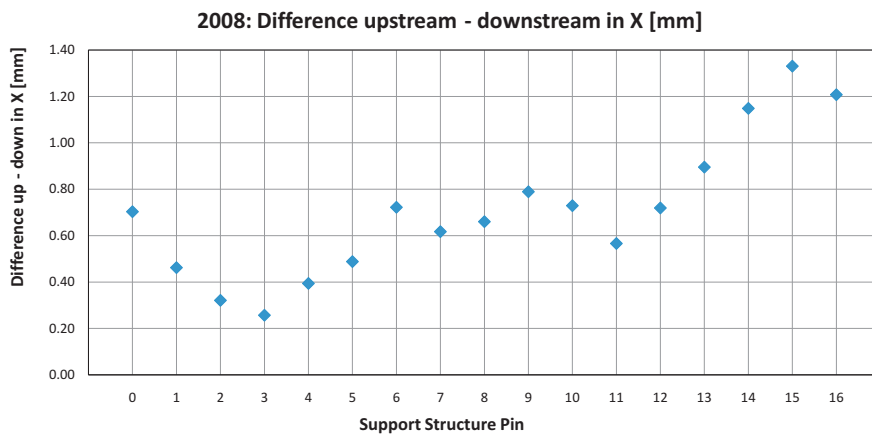


Figure 7.9: Diagram with measured differences upstream - downstream of the x coordinates of each support structure pin in 2008.

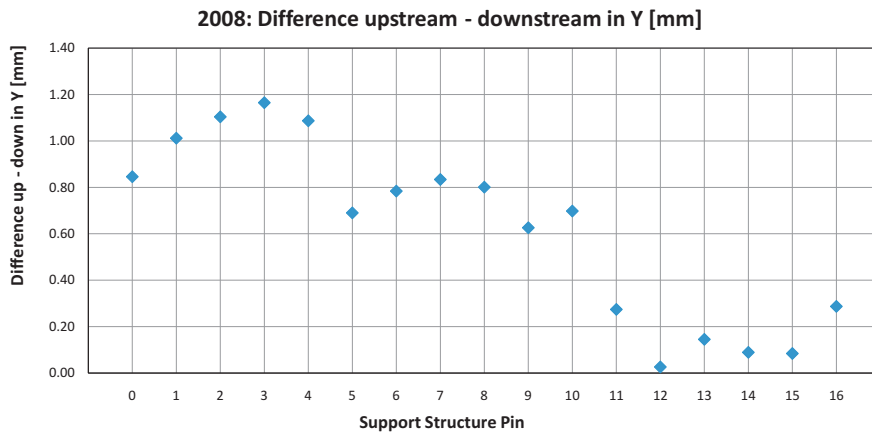


Figure 7.10: Diagram with measured differences upstream - downstream of the y coordinates of each support structure pin in 2008.

Additionally, in figure 7.11 is a diagram with the calculated two dimensional distances between upstream and downstream pins. All three diagrams presented in this subsection as well as the figures in the subsections before show indentations at pin04 / pin05 and pin11 / pin12. Exactly at these positions are rods between the upstream and downstream side to stabilize the support structure. It seems that these rods have an effect on the position of the support structure inside COBRA. With enhanced stabilization methods it is maybe possible to improve the support structure position for next years run.

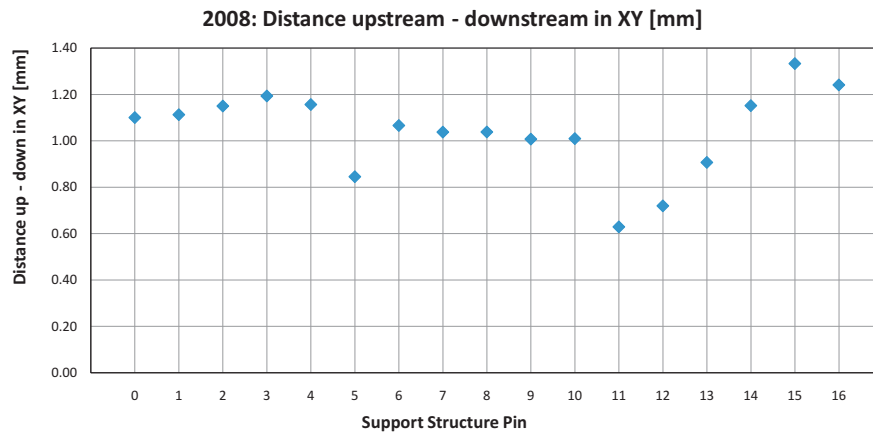


Figure 7.11: Diagram with measured two dimensional distances between upstream and downstream support structure pins in 2008.

7.3 Drift Chamber Mounting

In the previous section 7.2 the position of the support structure inside COBRA in 2007 and 2008 was analyzed in detail. Now, it is interesting to find out where exactly the drift chambers are located inside COBRA and to determine the deviation from expected values. As already mentioned in subsection 7.1.2, not theoretical values are used to determine deviations but so-called expected values. The calculation of these expected drift chamber cross positions can be found in subsection 7.1.2.

7.3.1 Drift Chamber Mounting in 2007

The analysis of drift chamber positions is done in a similar way as before the one of the support structure pins. In figures 7.12(a) and 7.12(b) are diagrams which show the expected values and measured cross positions for

downstream and upstream in 2007. To visualize deviations from expected values, the measured cross positions are marked with 10 times displacement. If a bigger magnification would be chosen (as for example for the support structure pins in the previous section) these diagrams would be too confusing because of big deviations.

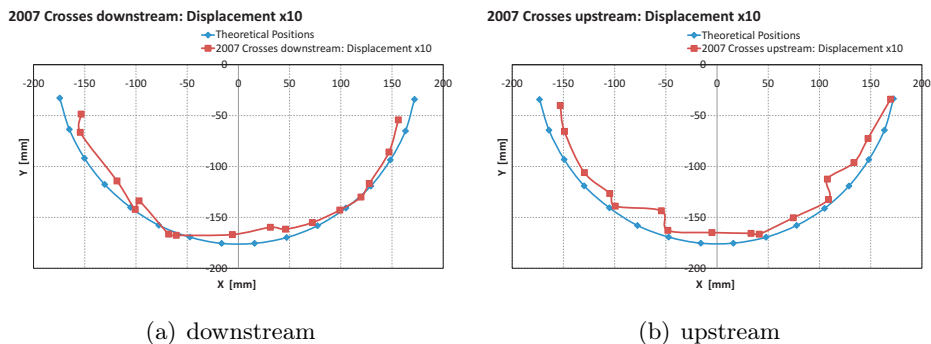


Figure 7.12: Diagram with expected and measured coordinates of downstream and upstream drift chamber crosses 2007.

Of course it is necessary to understand these big deviations of up to 3.9 mm from expected values. This is the reason why in figures 7.13 and 7.14 the situation at the downstream and upstream side of the support structure is shown in other diagrams. In the following paragraphs these diagrams will be explained in detail.

These diagrams show black lines with a starting point and an endpoint. The starting point marks the calculated center of the connecting line between surveyed adjacent support structure pins. The endpoint corresponds to the expected position of the drift chamber cross. This means that the black lines show the expected location of each drift chamber inside COBRA.

The starting point of the colored lines are again the calculated center between two measured support structure pins. But the endpoint is now the measured position of the drift chamber cross with 5 times displacement from expected values. These lines show therefore the real location of the drift chamber inside COBRA.

It is immediately obvious that the gravitational force takes effect on the outermost drift chambers, mainly on the connections as pre-amplifier cards and so on because the drift chamber itself is very light. The amazing exception is drift chamber dc00 at the upstream side which shows a deviation in y direction of only 0.04 mm which is below the measuring precision.

If one compares the diagrams for the upstream and downstream situation, it is obvious that for example drift chamber dc00 is contorted between upstream

and downstream. It is clear that such a fact has to be implemented in the calculation of anode wire positions.

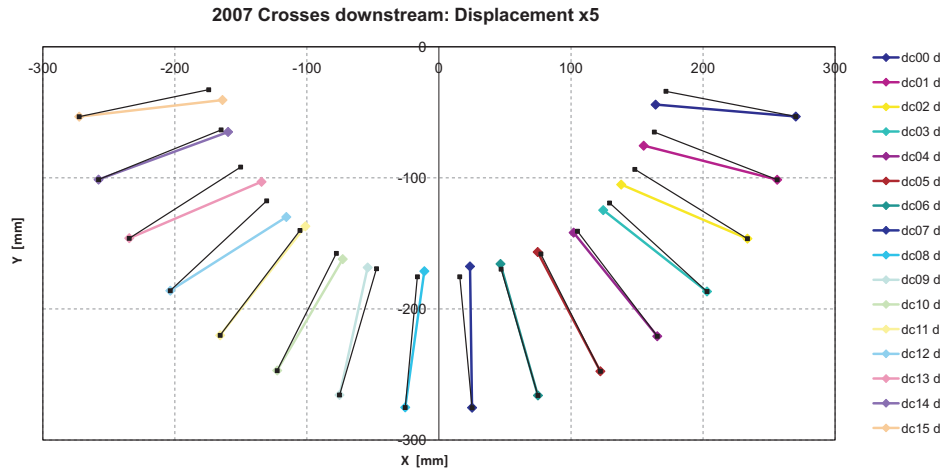


Figure 7.13: Diagram with expected locations of the drift chambers (black) and measured drift chamber crosses with 5 times displacement (colored) at the downstream side of the support structure in 2007.

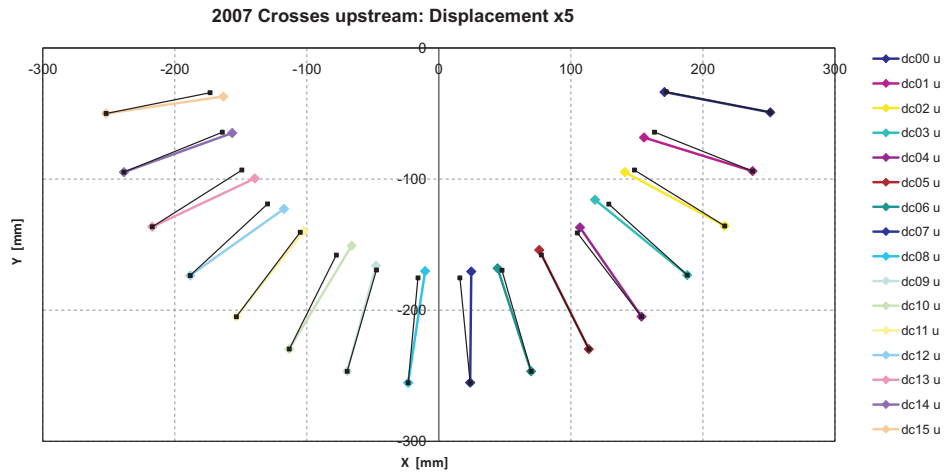


Figure 7.14: Diagram with expected locations of the drift chambers (black) and measured drift chamber crosses with 5 times displacement (colored) at the upstream side of the support structure in 2007.

7.3.2 Drift Chamber Mounting in 2008

The same analysis as in subsection 7.3.1 for 2007 can now be done with data from the optical survey 2008. In figures 7.15(a) and 7.15(b) are diagrams which show the expected values and measured cross positions with 10 times displacement for downstream and upstream in 2008.

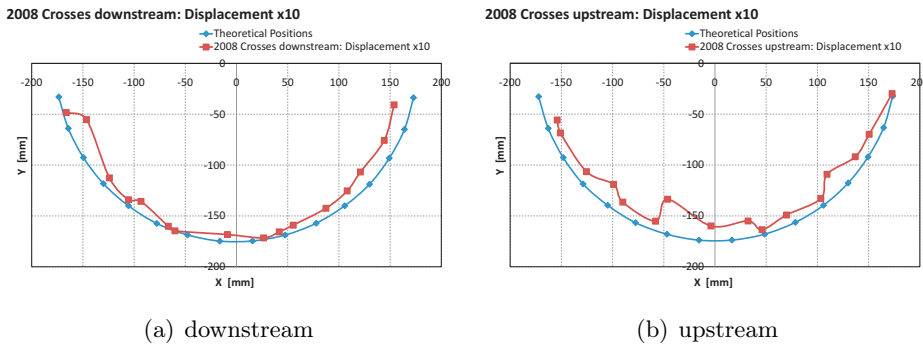


Figure 7.15: Diagram with expected and measured coordinates of downstream and upstream drift chamber crosses 2008.

Again, these diagrams show big deviations of up to 3.4 mm from expected values. In figures 7.16 and 7.17 are therefore diagrams of the expected and real position of each drift chamber at the downstream and upstream side as it was measured in 2008.

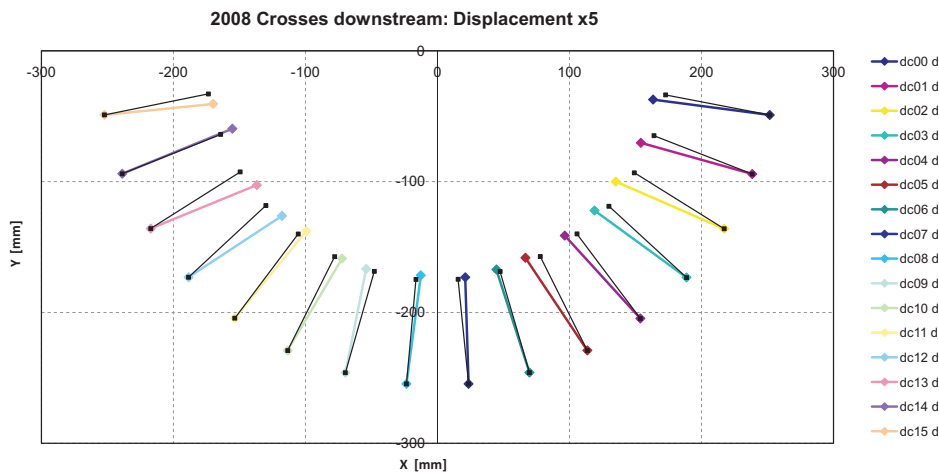


Figure 7.16: Diagram with expected locations of the drift chambers (black) and measured drift chamber crosses with 5 times displacement (colored) at the downstream side of the support structure in 2008.

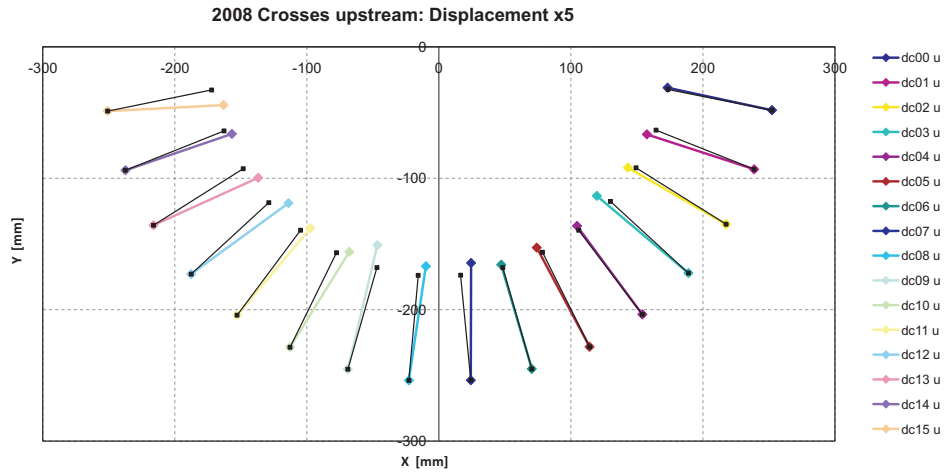


Figure 7.17: Diagram with expected locations of the drift chambers (black) and measured drift chamber crosses with 5 times displacement (colored) at the upstream side of the support structure in 2008.

The same conclusions as for 2007 are also valid for the drift chamber situation in 2008. Again the diagrams show the effect of the gravitational force on the chambers and again drift chamber dc00 at the upstream side is the amazing exception.

Additionally, the cross of drift chamber dc09 is at the upstream side 3.4 mm higher as the expected position. It seems therefore that in 2008 something with the mounting of this chamber is wrong. But this fact has also another consequence: Drift chamber dc09 and hence all anode wires of this chamber have a slope in z direction of about 3 mm. The alignment of 2007 considered no z dependence of the positions of anode wires which is in the case of dc09 a bad assumption. An important improvement of the alignment 2008 compared to last year is therefore to implement such z dependencies.

7.4 Measured z Coordinates of Crosses and Pins

In all discussions before it was assumed that drift chamber crosses and support structure pins have theoretical z coordinates. Because it is dissatisfying to use theoretical values to get results of optical surveys, the measuring principle should be improved in 2008. This is the reason why in 2008 it was tried to survey all measuring points from at least two different total station positions (see chapter 5). With this method not only the x and y coordinates of measuring points can be determined but also the real z positions. The measured z positions will be analyzed in this section.

7.4.1 Cross Distance Check

As already mentioned in section 5.5 it was possible to determine the z coordinate of each drift chamber cross with the optical survey 2008. In figures 7.18 and 7.19 are diagrams with the measured z positions of the downstream and upstream drift chamber crosses which show big differences from theoretical values. Recall that the PCB plates with the crosses were glued on the drift chambers with the help of positioning devices. But nevertheless, it is possible that the flags are not at theoretical positions as the results of the measurements of the mechanical workshop survey 2007 (see chapter 6) already demonstrated. This fact is the reason why the measured z coordinates in diagrams 7.18 and 7.19 are scattered. But additionally these measurements show an overall shift of about 1.8 mm in beam direction, i.e. in $+z$ direction. This shift will be discussed later in subsection 7.4.2 with more details. The error for z measurements is not shown in these figures but it is given by 0.5 mm, see subsection 5.5.5.

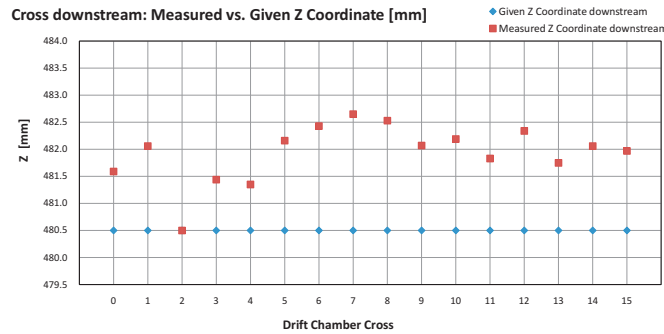


Figure 7.18: Diagram with theoretical and measured z coordinates of downstream drift chamber crosses 2008.

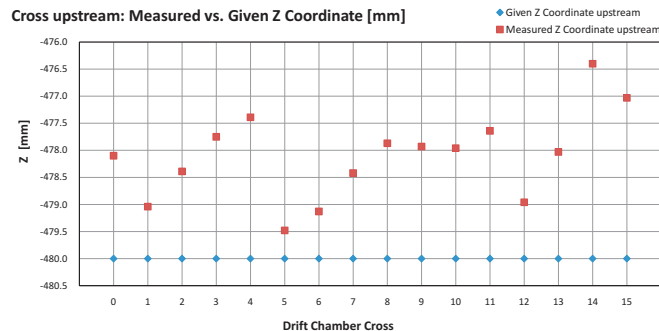


Figure 7.19: Diagram with theoretical and measured z coordinates of upstream drift chamber crosses 2008.

In consideration of the differences between upstream and downstream positions in x and y directions the cross distances can be calculated and can be compared with the values of the mechanical workshop survey 2007 (see subsection 6.1.3). Both results are shown in figure 7.20 with error bars of 0.7 mm due to propagation of uncertainty.

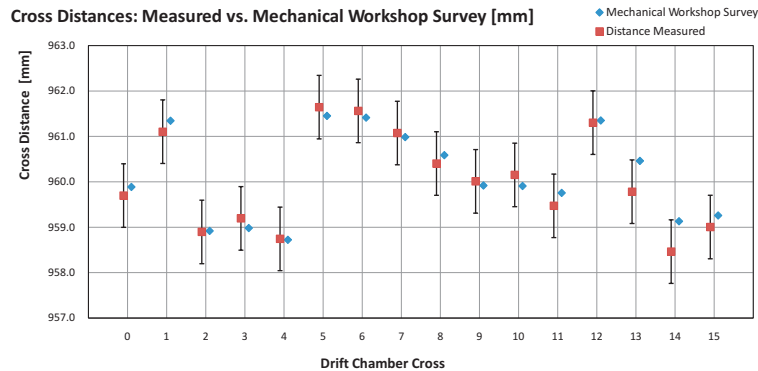


Figure 7.20: Diagram of cross distances measured with mechanical workshop survey 2007 and optical survey 2008 with error bars of 0.7 mm.

This diagram shows that all measured cross distances are much closer to the values of the mechanical workshop survey than the big error bars of 0.7 mm suggest. The only exceptions of this tendency are given by dc13 and dc14. By using the mechanical workshop survey measurements as values, the root mean square (rms) of the pull distribution gives 0.4 and is therefore much smaller than 1. This result indicates that the errors determined by the Survey Group are too big. To reach a rms value of 1 one needs a distance uncertainty of about 0.3 mm. In figure 7.21 is therefore the same diagram as in 7.20 but now with error bars which are given by 0.3 mm.

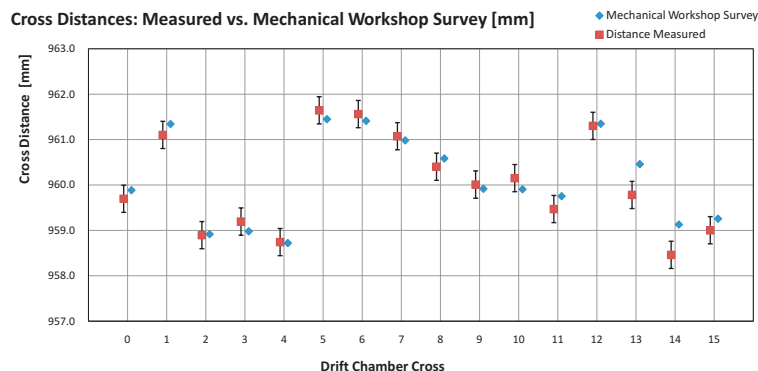


Figure 7.21: Diagram of cross distances measured with mechanical workshop survey 2007 and optical survey 2008 with error bars of 0.3 mm.

The drift chamber cross distances which were determined with the optical survey 2008 are therefore consistent with the results of the mechanical workshop survey 2007 even with smaller error bars. The only exceptions are given by dc13 and dc14. It is therefore reasonable to use drift chamber cross data with measured z coordinates as starting point for the geometrical drift chamber alignment.

7.4.2 Consequence of $+z$ Shift

The z coordinates of all drift chamber crosses which were measured with the optical survey 2008 show an overall shift of about 1.8 mm in $+z$ direction, as already presented in subsection 7.4.1. The differences between theoretical and measured z coordinates of all drift chamber crosses were already shown in figures 7.18 and 7.19. Now, it is interesting to analyze the consequences of these differences for the x and y coordinates of the drift chamber crosses. In figures 7.22 and 7.23 are therefore diagrams with x and y coordinates of drift chamber crosses at downstream and upstream which were determined by using theoretical z positions. Additionally the measured coordinates with 50 times displacement are also shown in these figures. The average deviation in x and y is given by $\Delta = 0.17$ mm for the downstream crosses whereas it is $\Delta = 0.14$ mm for upstream crosses due to smaller measured angles.

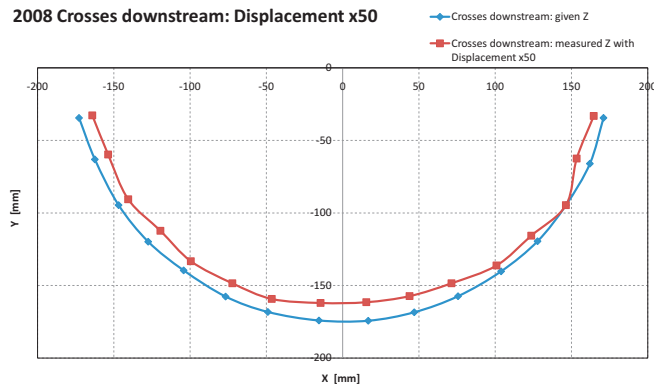


Figure 7.22: Diagram with x and y coordinates of downstream drift chamber crosses 2008. These values are determined by using theoretical and measured z coordinates.

Unfortunately it was only possible to determine the z coordinates of 3 downstream and 5 upstream pins (see section 5.5). The measured and theoretical z positions as well as the obtained x and y coordinates are listed in appendix D. The measured z coordinates show again an overall offset in $+z$ direction of about 1.8 mm. This shift has the following consequences for x and y coordinates: the averaged deviation of downstream pins is given by

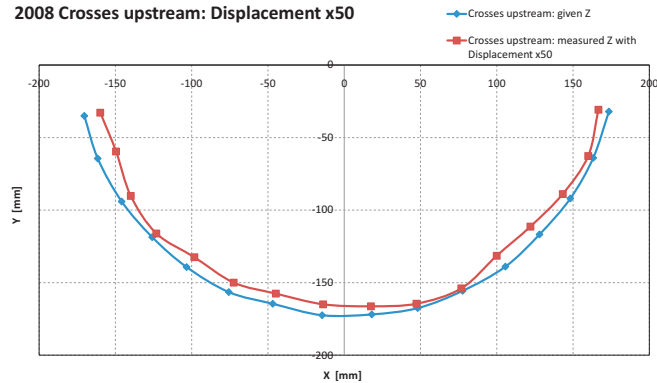


Figure 7.23: Diagram with x and y coordinates of upstream drift chamber crosses 2008. These values are determined by using theoretical and measured z coordinates.

$\Delta = 0.30$ mm whereas the deviation of upstream pins is $\Delta = 0.20$ mm due to smaller measured angles.

It seems therefore that the whole support structure is shifted with about 1.8 mm in $+z$ direction. The theoretical z positions which were used for optical surveys to obtain x and y coordinates are therefore wrong. But one has to note that a shift of nearly 2 mm against downstream is impossible because the support structure would then be no longer supported by the centering mechanism which is mounted inside COBRA (see subsection 4.3.3). And of course after the insertion of the drift chamber system it was checked if the support structure is located correctly inside COBRA. Unfortunately, the mystery about these 2 mm is not yet understood.

For the geometrical anode wire alignment 2008 it seems that it is reasonable to use the drift chamber cross coordinates which are obtained by measuring the z coordinates because this data set is consistent with the results of the mechanical workshop survey 2007. For the support structure pin coordinates exist several possibilities: one can calculate the average z position of the three downstream and five upstream pins and then assume that all other pins are located in planes which are aligned normal to the beam line with these calculated z positions. This means that with this method the theoretical z positions introduced in subsection 7.1.1 are changed to averaged z positions of the measured pins. The other possibility is given by calculating fit planes for the measured five upstream and three downstream pins and assume that all other pins are located in this plane. Which possibility will be used for the geometrical drift chamber alignment 2008 is not yet decided.

Chapter 8

Geometrical Alignment of the Drift Chamber System

The detailed construction of a drift chamber was already shown in chapter 4 and the mechanical workshop survey 2007 which measured the geometry of each drift chamber was also described (see chapter 6). Then, in chapter 5 the optical survey 2008 was explained and the data obtained by this survey was analyzed in chapter 7.

This means that at this point all information to derive the geometrical alignment of the drift chamber system is gathered. To obtain the geometrical alignment one has to find the correlation between coordinates of measuring points (drift chamber crosses and support structure pins) which were determined by the optical survey and the position of each anode wire.

How the geometrical alignment of the drift chamber system is obtained and which assumptions or simplifications are used for the calculation will be described in this chapter.

8.1 Calculation of the Corrected Cross Position

To calculate each anode wire position it is necessary to determine the center line of each drift chamber. As already mentioned in subsection 5.2.2, it has to be assumed that the midpoint of the connecting line of adjacent support structure pins corresponds to the center of the drift chamber. Theoretically, the bull's eye of the cross on the PCB plate marks also the center of the drift chamber. But as the analysis of the mechanical workshop survey 2007 demonstrated, the PCB plate can be shifted against the drift chamber. As already shown in subsection 6.1.1, the displacement of the PCB flag with

respect to the drift chamber is given by the following formulas:

$$\text{downstream:} \quad \chi_d = \text{No.5} - \text{No.4} \quad (8.1)$$

$$\text{upstream:} \quad \chi_u = \text{No.8} - \text{No.7} \quad (8.2)$$

It is important to take the correct algebraic sign into account. In figure 8.1 are schematics with marked PCB displacements χ_d and χ_u . Note that the drift chamber in this figure is viewed from downstream.

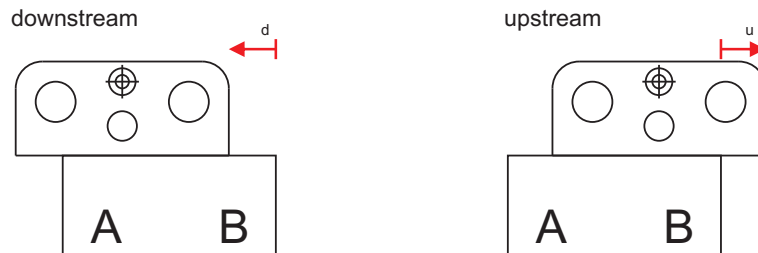


Figure 8.1: Schematics of PCB plate displacements χ_d and χ_u viewed from downstream. Note that for this example the algebraic sign of χ is positive for the downstream situation whereas it is negative for the upstream case.

Of course it is necessary to consider these shifts to determine the center line of the drift chamber. This can be achieved by calculating a so-called corrected cross which marks the real center line. It can now be assumed that the corrected cross position can be obtained by shifting the measured cross position with χ parallel to the connecting line of the corresponding measured pins. But of course this strategy induces an error if the drift chamber is not aligned perpendicular to the pin connecting line.

But fortunately an exact determination of the position of the corrected drift chamber cross is also possible. After the optical survey, the following coordinates of measuring points for each drift chamber dc_i are known:

$$\overrightarrow{\text{cross}}_i = (x_{\text{cross}i}, y_{\text{cross}i}), \quad (8.3)$$

$$\overrightarrow{\text{pin}}_i = (x_{\text{pin}i}, y_{\text{pin}i}), \quad (8.4)$$

$$\overrightarrow{\text{pin}}_{i+1} = (x_{\text{pin}i+1}, y_{\text{pin}i+1}). \quad (8.5)$$

Of course two such data sets exist for each drift chamber, one for upstream and one for downstream. Note that the z coordinates of these measuring points have no effect on this corrected cross calculation. The index i for the drift chamber dc_i is skipped from now on to simplify formulas. In figure 8.2 is a schematic to visualize the situation. Additionally all definitions which will be introduced in the following calculations are shown in this figure.

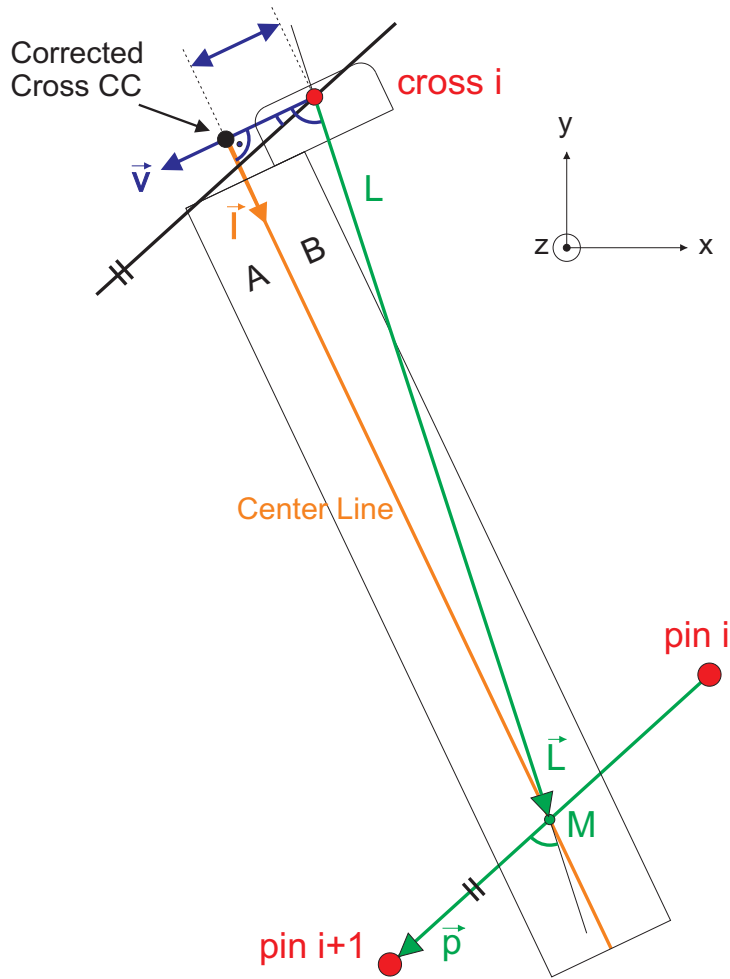


Figure 8.2: Schematic drawing with variables which are mentioned in section 8.1. It is important to note that the situation is viewed from downstream.

With the data set mentioned before one obtains directly the first point of the drift chamber center line provided by the middle of the pin connecting line:

$$\vec{M} = \vec{\text{pin}}_i + 1/2 \cdot (\vec{\text{pin}}_{i+1} - \vec{\text{pin}}_i). \quad (8.6)$$

The normalized pin connecting vector \vec{p} is given by:

$$\vec{p} = \frac{\vec{\text{pin}}_{i+1} - \vec{\text{pin}}_i}{|\vec{\text{pin}}_{i+1} - \vec{\text{pin}}_i|}. \quad (8.7)$$

Additionally, it is possible to determine the distance L between the midpoint \vec{M} and the measured cross position $\vec{\text{cross}}$ as well as the corresponding

normalized vector \vec{L} :

$$L = |\vec{M} - \overrightarrow{\text{cross}}|, \quad (8.8)$$

$$\vec{L} = \frac{\vec{M} - \overrightarrow{\text{cross}}}{|\vec{M} - \overrightarrow{\text{cross}}|}. \quad (8.9)$$

The angle ϕ between the two vectors \vec{p} and \vec{L} can also be determined:

$$\phi = \arccos(\vec{p} \cdot \vec{L}). \quad (8.10)$$

For the next step in the calculation it is assumed that the PCB plate with the cross can only be shifted vertically to the real drift chamber center line. This assumption is tenable because the PCB plate is glued on the connecting pieces of the hood frame (see subsection 4.2.4 for more information). By using this assumption and considering the triangle corrected cross \vec{CC} - measured cross $\overrightarrow{\text{cross}}$ - midpoint \vec{M} which is shown in figure 8.3, one can calculate the angle ψ :

$$\psi = \arccos\left(-\frac{\chi}{L}\right). \quad (8.11)$$

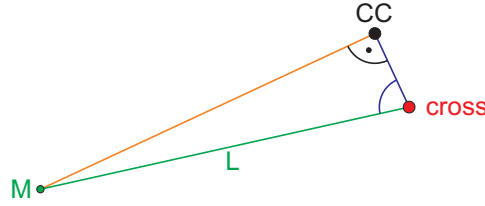


Figure 8.3: Schematic drawing of the triangle \vec{CC} - $\overrightarrow{\text{cross}}$ - \vec{M} to calculate the angle ψ .

Note that the correct algebraic sign of χ is very important for this formula. With the angles ϕ and ψ the difference φ can also be calculated:

$$\varphi = \psi - \phi. \quad (8.12)$$

To obtain the corrected cross position the vector \vec{p} has to be turned by the angle φ :

$$\vec{v} = \begin{pmatrix} \cos(\varphi) & \sin(\varphi) \\ -\sin(\varphi) & \cos(\varphi) \end{pmatrix} \cdot \vec{p}. \quad (8.13)$$

The position of the corrected cross can now be calculated and is given by:

$$\vec{CC} = \overrightarrow{\text{cross}} - \chi \cdot \vec{v}. \quad (8.14)$$

8.2 Determination of Anode Wire Positions

With the corrected cross which is calculated in section 8.1 the center line of the corresponding drift chamber can be determined for the upstream and downstream side of the chamber:

$$\vec{l} = \frac{\vec{M} - \vec{CC}}{|\vec{M} - \vec{CC}|}. \quad (8.15)$$

By comparing the center lines at the upstream and downstream side a possible chamber distortion can be shown. But nevertheless, it is assumed that the geometry inside of a chamber does not change even if the chamber is twisted. To calculate the anode wire positions of the drift layers labeled with A and B it is necessary to determine initially the so-called starting points A and B

$$\vec{A} = \vec{CC} + 5 \cdot \vec{v}, \quad (8.16)$$

$$\vec{B} = \vec{CC} - 5 \cdot \vec{v}, \quad (8.17)$$

which are marked in a schematic drawing shown in figure 8.4. The vector \vec{v} is defined in section 8.1 and describes a unit vector which is vertical to the center line \vec{l} .

For the next calculation step the positions of the outermost anode wires of each plane have to be determined. As shown in figure 8.4 the results of measurements No.10 (for downstream) and No.11 (for upstream) of the mechanical workshop survey 2007 are necessary to determine these anode wire positions for downstream

$$\text{Position A a8 d} = \vec{A} + (\text{No.10} - 1.5 - 3 - 7.76) \cdot \vec{l}, \quad (8.18)$$

$$\text{Position B a8 d} = \vec{B} + (\text{No.10} - 1.5 - 3 - 12.26) \cdot \vec{l}, \quad (8.19)$$

$$(8.20)$$

and upstream

$$\text{Position A a8 u} = \vec{A} + (\text{No.11} - 1.5 - 3 - 7.76) \cdot \vec{l}, \quad (8.21)$$

$$\text{Position B a8 u} = \vec{B} + (\text{No.11} - 1.5 - 3 - 12.26) \cdot \vec{l}. \quad (8.22)$$

The value 1.5 mm corresponds to the distance between the bull's eye of the cross and the upper edge of the PCB plate whereas the radius of a drift chamber bolt is given by 3 mm. The distances between center of drift chamber bolt and outermost anode wire is given by 7.76 mm for plane A and 12.26 mm for plane B as already shown in section 6.2.

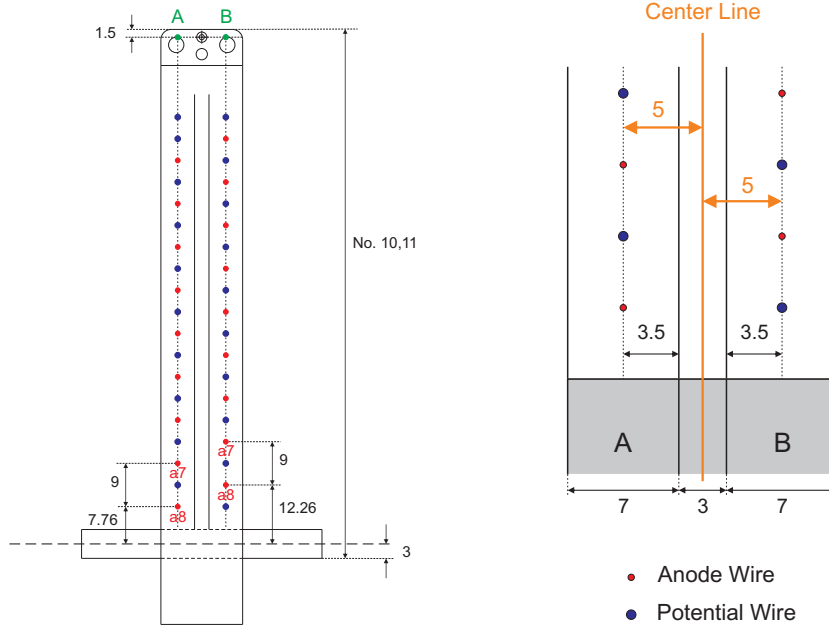


Figure 8.4: Schematic drawings with geometrical specifications which are necessary to calculate anode wire positions.

By considering the fact that the distance between adjacent anode wires in one drift layer is given by 9 mm (see figure 8.4) it is easy to calculate all other anode wire positions:

$$\text{Position A a7} = \text{Position A a8} - 9 \cdot \vec{l}, \quad (8.23)$$

$$\text{Position A a6} = \text{Position A a7} - 9 \cdot \vec{l}, \quad (8.24)$$

$$\vdots \quad \vdots$$

$$\text{Position B a7} = \text{Position B a8} - 9 \cdot \vec{l}, \quad (8.25)$$

$$\text{Position B a6} = \text{Position B a7} - 9 \cdot \vec{l}, \quad (8.26)$$

$$\vdots \quad \vdots$$

During this calculation of the anode wire positions only x and y coordinates were determined by assuming that the z positions are the same as the ones of the drift chamber crosses (measured or theoretical values). But real anode wire positions are aligned in a plane which is normal to the connecting line between corrected cross positions at the upstream and downstream side. Of course this correction was also calculated but because the maximum value of this correction is given by less than $1 \mu\text{m}$ it is neglected to simplify matters.

To implement the anode wire positions into the database, the following information for each anode wire is necessary:

- Unit vector \vec{N} which describes the alignment of the anode wire in direction from upstream to downstream.
- Position \vec{P} of the anode wire center.

In the following calculations the positions of one anode wire at the upstream and downstream side is shortened by \vec{a}_u and \vec{a}_d with

$$\vec{a}_u = (x_{au}, y_{au}, z_{crossu}), \quad (8.27)$$

$$\vec{a}_d = (x_{ad}, y_{ad}, z_{crossd}), \quad (8.28)$$

where $x_{au,d}$ and $y_{au,d}$ are the results of the calculations before whereas $z_{crossu,d}$ are the measured or theoretical z coordinates of the drift chamber crosses upstream and downstream (see discussion before). The unit vector \vec{N} which describes the wire alignment can now be calculated:

$$\vec{N} = \frac{\vec{a}_d - \vec{a}_u}{|\vec{a}_d - \vec{a}_u|}. \quad (8.29)$$

By considering measurement No.9 of the mechanical workshop survey the position of the anode wire center can be determined by the following formula:

$$\vec{P} = \vec{a}_u + (\text{No.9} + 215.75) \cdot \vec{N}. \quad (8.30)$$

Measurement No.9 describes the distance between leading edge of the upstream flag to the center of the upstream drift chamber bolt. The value 431.5 mm corresponds to the theoretical distance between upstream and downstream drift chamber bolts. It is assumed that the center of these two bolts marks the center of the anode wires as shown in figure 8.5.

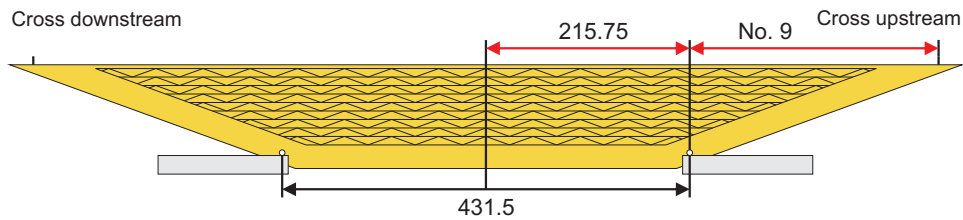


Figure 8.5: Schematic drawing to calculate the center of each anode wire.

It is not necessary to consider the individual length of each anode wire of one drift chamber for this calculation because the corresponding values which are listed in subsection 4.2.4 are already implemented into the database.

With the calculations presented in this chapter the geometrical alignment of the drift chamber system is provided. To visualize these calculations, please see figure 8.6. All anode wire positions of the drift chambers dc00, dc01, dc02 and dc03 at $z = 480.5$ mm are shown in this diagram. Note that data obtained by the optical survey 2008 with given z positions is used for this diagram.

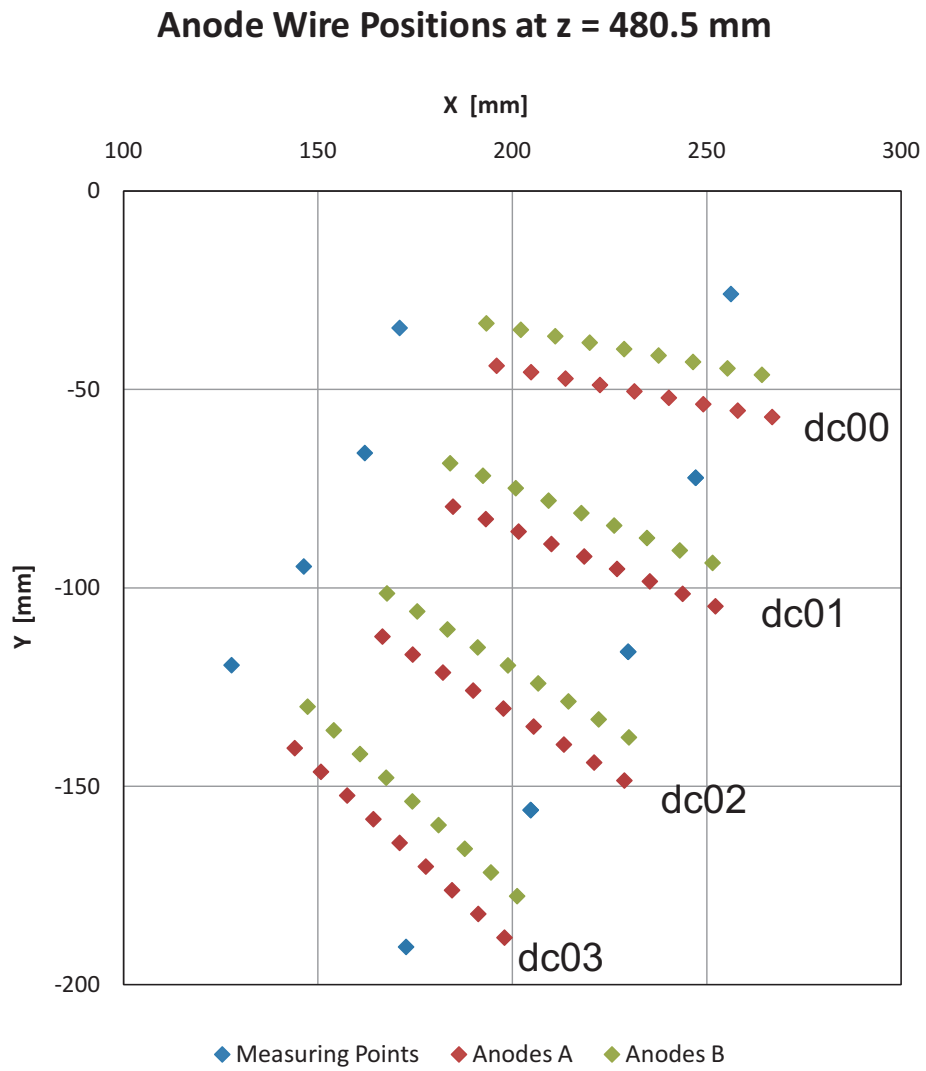


Figure 8.6: Diagram with the anode wire positions of dc00, dc01, dc02 and dc03 at $z = 480.5$ mm. Additionally, the measured drift chamber crosses and support structure pins are also shown.

Chapter 9

Analysis of Target Measurements

In spring 2008, survey marks in the form of crosses were drawn on the target foil for the purpose that the location of the target inside COBRA can be determined by optical surveys (see subsection 5.2.3). Before the target was mounted on the support structure, the coordinates of all target crosses were measured with the help of a microscope and a plane-table. It is clear that with this method only the cross coordinates with respect to the other crosses are known, i.e. the positions are given in a local coordinate system. This system has arbitrary orthogonal axis u and v with origin in cross named target0. In figure 9.1 is a schematic drawing of the target with labeled crosses and the measured positions are also shown.

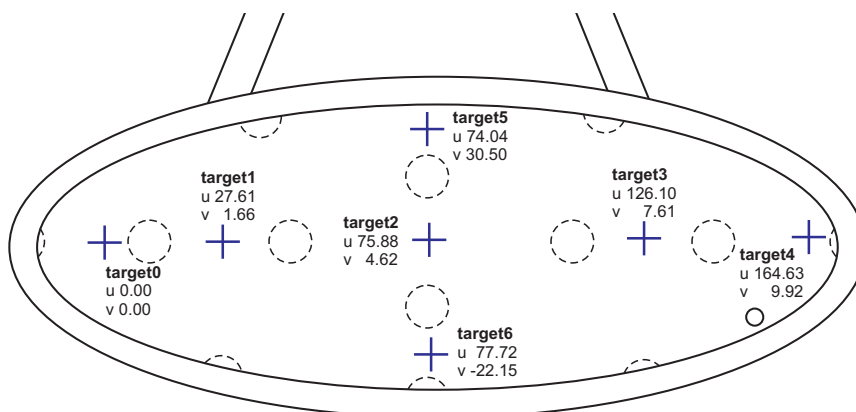


Figure 9.1: Schematic drawing of the target with labeled crosses. Additionally, the measured cross positions in a local coordinate system are also shown.

With the device which was used for this measurement, distances can be determined with an accuracy of $5\ \mu\text{m}$ which is below the measuring precision of an optical survey. The error of this measurement is therefore not relevant compared to the one of the optical survey 2008.

During the optical survey 2008, it was possible to survey each target cross from at least two different total station positions with the consequence that x , y and z coordinates of each cross can be determined. As already discussed in section 5.1, the target has to be moved with an extraction and insertion system. To check the reproducibility of this procedure, the target crosses were measured again after some extraction/insertion movements (see subsection 5.5.4 for a detailed description of this measurement). The error of the optical survey is given by 0.3 mm for x and y coordinates whereas the error for the z coordinate is given by 0.5 mm due to flat angles (see subsection 5.5.5).

The coordinates of the target crosses which were obtained by these measurements are tabulated in appendix F and will be analyzed in this chapter. A consistency check will be applied to the data set of target crosses in section 9.1. Then the reproducibility of the target position after several extraction/insertion movements will be checked in section 9.2. Finally, different measuring methods to determine the target slant angle will be described in section 9.3. Of course the results of these measurements will be also presented in this section.

9.1 Consistency Check

Because we are in possession of exact target cross locations which were measured by the plane-table in spring 2008, it is reasonable to do a consistency check with the cross coordinates which were measured with the optical survey 2008. Of course one has to note that the locations obtained by the plane-table are with respect to a local coordinate system. But one can calculate the distances between a chosen reference point (for example target0) to each other target cross. By comparing the results one gets a consistency check of the measured cross positions which were determined by the optical survey 2008.

The resulting differences between distances measured by the plane-table and the ones determined by the optical survey 2008 before movements are shown in figure 9.2. Of course the bar target1 in diagram "Reference Point: target0" has the same height as target0 in diagram "Reference Point: target1" but nevertheless, these diagrams provide a good method to visualize inconsistencies.

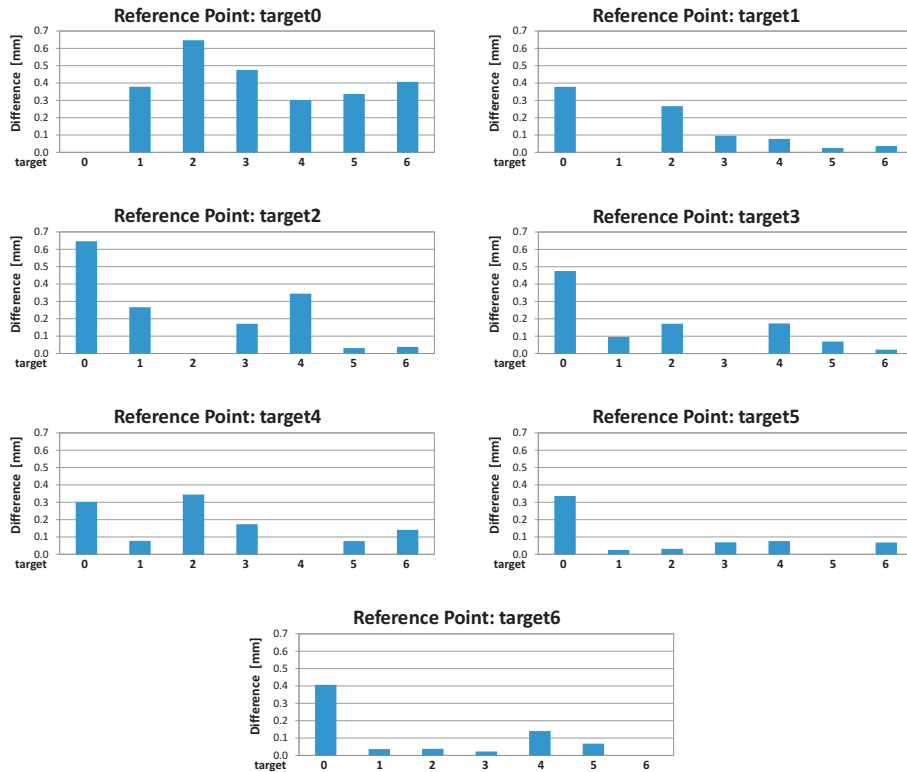


Figure 9.2: Diagrams which show absolute differences between distances which were measured by plane-table and optical survey 2008. Results from data taken before target movements are presented in this figure.

Of course it is also necessary to discuss about errors. Before the target was moved several times the measuring points were surveyed from three different total station positions (Position 1, 2 and 3, see subsections 5.5.2 and 5.5.3 for more information). Most of the target points were measured from all these positions with the consequence that the coordinates of these crosses are reliable because they are obtained by averaging three angle measurements. With errors of 0.3 mm for x and y coordinates and 0.5 mm for the z coordinate, one obtains an error in distance of about 0.7 mm due to propagation of uncertainty. Note that the points target0 and target4 were not visible from Position 3 because they were covered by the ROHACELL frame of the target. This means that the coordinates of target0 and target4 are obtained by using only two angle measurements (from Position 1 and 2). The measuring error is therefore smaller than the one for three surveys but we can not make a statement about the reliability of these coordinates.

By taking account of all these considerations, it seems that the coordinates of target0 are not so precise as the ones of the other target crosses. The surveyor

who measured the target crosses had difficulty to sight cross target0 from Position 1 because it was in the shadow of the ROHACELL frame. Maybe this is the reason why cross target0 fails the consistency check.

During the optical survey after the target movements, the target crosses were measured from only two different total station positions (Position 4 and 5 as already mentioned in subsection 5.5.4). The results of the consistency check with this data is shown in figure 9.3. It seems that in this case each target cross passes the consistency check.

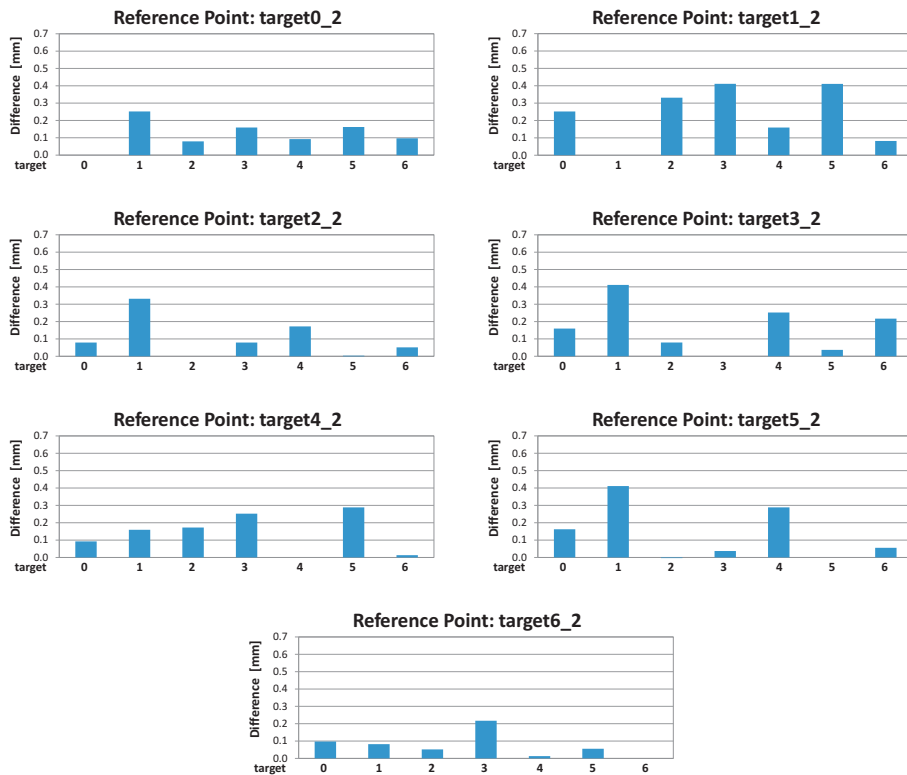


Figure 9.3: Diagrams which show absolute differences between distances which were measured by plane-table and optical survey 2008. Results from data taken after target movements are presented in this figure.

As shown in figures 9.2 and 9.3, the differences between distances measured by plane-table and optical survey are in most cases smaller than the calculated error of 0.7 mm as for example in diagram "Reference Point: target6_2" in figure 9.3. This means that there is evidence that the measurements of the optical survey 2008 are more accurate than expected. Recall that the analysis of drift chamber cross distances in subsection 7.4.1 also indicates that the errors which are determined by the Survey Group (see subsection 5.5.5) are too big.

9.2 Reproducibility

In this section, the reproducibility of the target position before and after extraction/insertion movements should be analyzed. In figures 9.4, 9.5 and 9.6 are diagrams with the differences before - after movements positions in x , y and z coordinates. Of course the ideal values are usually given by differences equal zero. The shown error bars are obtained by using propagation of uncertainties with the conservative errors of 0.3 mm for x and y coordinates and 0.5 mm for the z coordinate. The resulting errors are given by 0.4 mm in the case of x and y differences and 0.7 mm for the z coordinate.

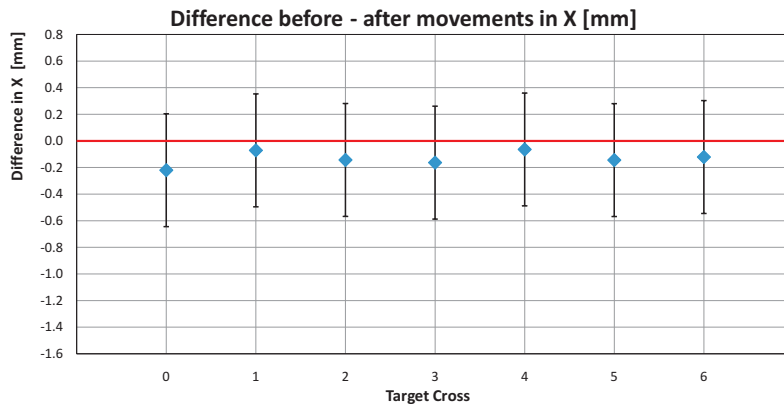


Figure 9.4: Diagram with shown differences between target cross x coordinates before and after target movements.

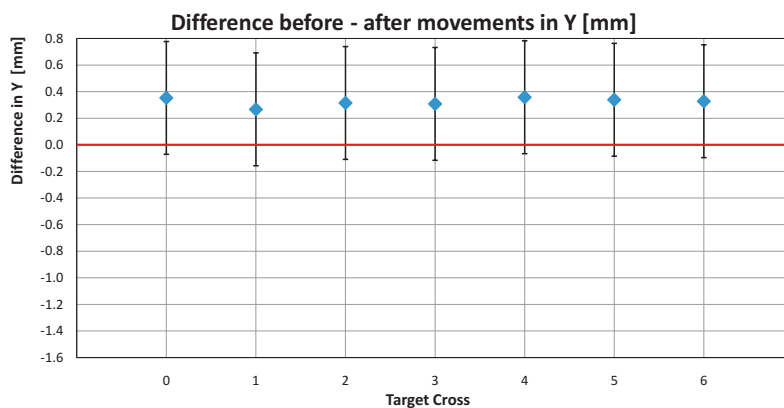


Figure 9.5: Diagram with shown differences between target cross y coordinates before and after target movements.



Figure 9.6: Diagram with shown differences between target cross z coordinates before and after target movements.

Diagram 9.4 shows a systematic offset in $+x$ direction of 0.1 mm. Additionally, the target position after movements seems to be shifted in $-y$ direction with 0.3 mm and in $+z$ direction with 0.4 mm. But nevertheless, all measured coordinates are in the range of reproducibility if errors are considered. The only exception is the z difference of target0, but as already mentioned in section 9.1 the target cross named target0 fails the consistency check.

But recall the analysis of measured drift chamber cross distances (see subsection 7.4.1) as well as the consistency check of target crosses (see section 9.1). These analyses indicate that the errors of measured x , y and z coordinates are maybe smaller than the ones which are determined by the Survey Group (see subsection 5.5.5). The error bars shown in figures 9.4, 9.5 and 9.6 are therefore smaller with the consequence that the target position before and after extraction/insertion movements is maybe not reproducible. To analyze the reproducibility more detailed it is necessary to do more measurements. This means that one would have to move the target, survey it afterwards and repeat this procedure several times.

9.3 Target Slant Angle

As already mentioned in section 3.3, recent simulations show that a target slant angle of about 20° is best suited. This was the reason why in spring 2008 the mounting of the target was changed in a way to reach this angle. But of course it has to be checked how big the real target slant angle is after this modification. There exist several measuring methods which will be described in this section.

9.3.1 Conventional

The target slant angle measurement with the so-called conventional method took place after the mounting of the target on the support structure but before the insertion of the whole drift chamber system. The procedure of this conventional method is shown in figure 9.7.

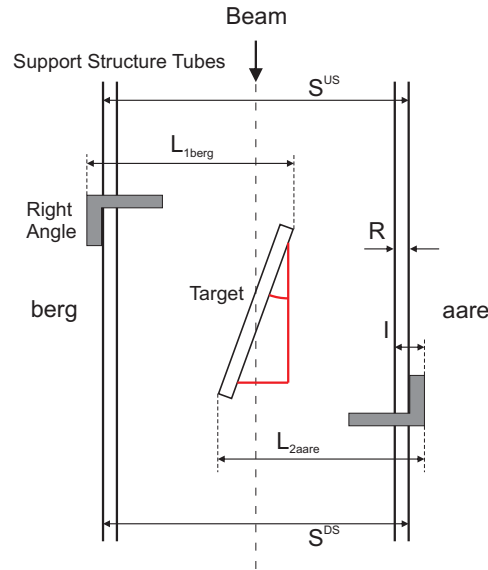


Figure 9.7: Schematic of the conventional measuring method to determine the target slant angle.

On the support structure are tubes consisting of carbon fiber which are aligned parallel to the beam axis on beam height. The distance between these two tubes as well as their thickness were measured with the help of a sliding caliper at the upstream and downstream side of the support structure. By placing a right angle on support tubes the distances between outer edge of this right angle and extremities of the target were measured with the sliding caliper. Of course the thickness of the right angle has also to be known. The length and the thickness of the ROHACELL frame of the target were measured before the target was mounted on the support structure by assuming pessimistic errors of 0.5 mm. See section 3.3 for measured target dimensions.

The target slant angle can be calculated with the help of geometrical considerations with the following result:

$$\text{Conventional: } \alpha = (20.6 \pm 0.2)^\circ \quad (9.1)$$

9.3.2 Photogrammetric

The target slant angle can also be determined by taking photographs of the target. If the camera is aligned to the intersection of the rotational symmetry axis and of the central height of a certain object (for example the MEG target), it is possible to determine the slant angle of this object. Of course the dimensions of the object have to be known.

Dr. Peter-Raymond Kettle determined the target slant angle with this so-called photogrammetric method two times, before and after the insertion into COBRA, with the following results:

$$\text{Photogrammetric outside: } \alpha = (20.4 \pm 0.2)^\circ \quad (9.2)$$

$$\text{Photogrammetric inside: } \alpha = (20.3 \pm 0.3)^\circ \quad (9.3)$$

9.3.3 Optical Survey 2008

Of course it is also possible to determine the target slant angle with the target cross coordinates which were measured by the optical survey 2008. The procedure of this determination will be explained in this subsection.

One has to assume initially that the target foil forms a perfect plane, the so-called target plane. It is clear that the measured cross coordinates are not aligned perfectly on a plane but one can find an optimized plane for the measured data set. To find this optimization one has to choose a combination of three target crosses which determine a unique plane. By calculating the Hessian normal form the distances from the other four target crosses to the calculated plane can be determined and totaled. The target cross combination with the smallest total distance is used as target plane.

For the data set of target cross coordinates after extraction/insertion movement the following combination is best suited to describe the real target plane:

$$\text{target1_2, target4_2, target6_2.} \quad (9.4)$$

With the plane formed by these three target crosses one can calculate the distances of the other crosses to this plane:

$$\text{target0_2: } d = 0.073 \text{ mm} \quad (9.5)$$

$$\text{target2_2: } d = 0.014 \text{ mm} \quad (9.6)$$

$$\text{target3_2: } d = 0.145 \text{ mm} \quad (9.7)$$

$$\text{target5_2: } d = 0.018 \text{ mm} \quad (9.8)$$

Each distance is therefore much smaller as the measuring precision. To calculate the target slant angle the intersection line of the target plane with the xz plane has to be determined. In figure 9.8 is a schematic of the situation and the target slant angle α is also marked. The calculated target slant angle is given by:

$$\text{Optical Survey 2008: } \alpha = (20.6 \pm 0.2)^\circ \quad (9.9)$$

The error for this result is derived from other target cross combinations and the resulting target slant angles.

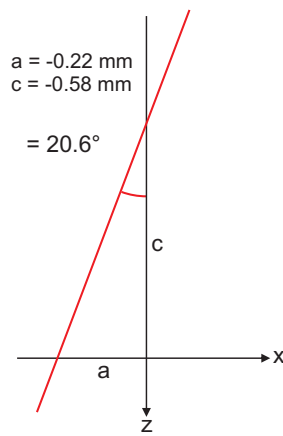


Figure 9.8: Schematic of the xz plane with marked target slant angle α .

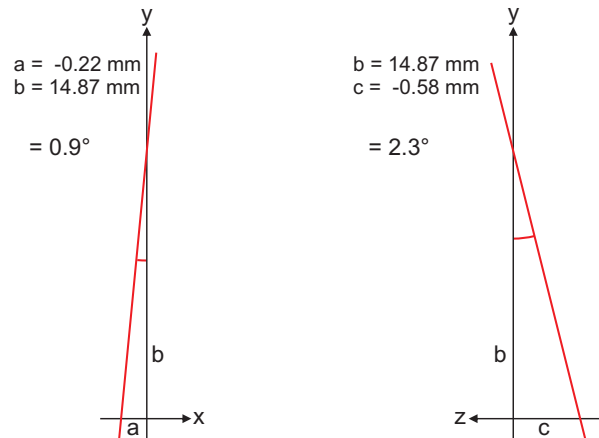


Figure 9.9: Schematics of xy and zy planes with marked angles β and γ .

All axis intercepts of the target plane and the corresponding angles are visualized in figures 9.8 and 9.9 and are listed in table 9.1.

Table 9.1: Axis intercepts and angles of the target plane.

Plane	Axis Intercept 1	Axis Intercept 2	Angle
xz plane	$a = -0.22$ mm	$c = -0.58$ mm	$\alpha = 20.6^\circ$
xy plane	$a = -0.22$ mm	$b = 14.87$ mm	$\beta = 0.9^\circ$
zy plane	$c = -0.58$ mm	$b = 14.87$ mm	$\gamma = 2.3^\circ$

Of course it is possible to apply the procedure described before to the coordinates of target crosses which were measured before extraction/insertion movements. But as already mentioned in section 9.1 the coordinates of cross target0 fails the consistency check. Nevertheless, one can calculate the optimized target plane by using only the six other target crosses. The best suited combination is given by target2, target4 and target6 with a resulting target slant angle of $\alpha = 20.65^\circ$.

Finally, all results of the different target slant angle determination methods are listed in table 9.2. The mean value of all these results is used as target slant angle for run 2008:

$$\alpha_{2008} = (20.5 \pm 0.3)^\circ \quad (9.10)$$

Table 9.2: Results of the different target slant angle determination methods.

Measuring Method	Target Slant Angle
Conventional:	$\alpha = (20.6 \pm 0.2)^\circ$
Photogrammetric outside:	$\alpha = (20.4 \pm 0.2)^\circ$
Photogrammetric inside:	$\alpha = (20.3 \pm 0.3)^\circ$
Optical Survey 2008:	$\alpha = (20.6 \pm 0.2)^\circ$

Chapter 10

Conclusion

In this thesis the optical survey 2008 is described and the analysis of the obtained data is presented. Additionally, the correlation between surveyed measuring points and signal wire positions is derived in this thesis. The geometrical alignment of the drift chamber system is therefore provided. Finally, the target cross measurements are analyzed and the corresponding results are presented in this thesis.

The construction of the MEG drift chambers was studied and understood with the main focus on details which have an effect on anode wire positions. Additionally the mounting of the chambers on the support structure as well as the placing of this support structure inside COBRA were also studied. The focus was again on components which affect the position of the support structure and the drift chambers as for example the centering mechanism inside COBRA or the asymmetric cable disposition.

To obtain the geometrical alignment it is necessary that the measured coordinates of the used survey marks (drift chamber crosses and support structure pins) are available. The optical survey 2008 took place on 30th of April 2008 and was done by the Survey Group of the Paul Scherrer Institute. The measuring procedures of the optical surveys 2007 and 2008 were documented to make these measurements reconstructible and this thesis serves as documentation. Additionally, the limits of an optical survey were also presented as the example of the support structure pins shows. It was not possible to measure all pins from at least two different total station positions with the consequence that the z coordinates of these pins can not be determined.

It is necessary to understand the mechanical workshop survey 2007 to get a correlation between measured drift chamber crosses and anode wire positions. This thesis serves again as documentation for this survey. The most important result of this mechanical workshop survey is given by the fact that

the distances between upstream and downstream crosses are not constant. They vary with up to 1.8 mm from theoretical values. For the optical survey 2007 it was assumed that all upstream crosses have the same theoretical z coordinate and all downstream crosses have the same theoretical z coordinate. After the analysis of the mechanical workshop survey 2007, it is clear that the assumption of constant cross distances is not sufficient. But nevertheless, the only possibility to compare the positions of the support structure and the drift chambers in 2007 with the ones in 2008 is given by comparing data which was obtained by using theoretical z coordinates. With this comparison it is at least possible to realize tendencies.

To do extensive analyses with data provided by the optical survey it is of course necessary to know the theoretical positions of the measuring points. The theoretical positions of the pins were calculated in this theses. For the drift chamber crosses I calculated expected positions depending on a possible support structure deformation. The detailed derivation is presented in this thesis.

By comparing measured coordinates of support structure pins with theoretical values, extensive analyses of a possible support structure deformation can be done. The results show that the centering at the bottom of the support structure worked fine in 2007 as well as in 2008 but nevertheless, it seems that the support structure is rotated at the upstream side due to the asymmetric cable disposition. At the outermost regions of the support structure one can realize big differences between the position in 2007 and 2008. While in 2007 the support structure was deformed at these regions the situation is improved in 2008 due to the additional centering mechanism. But it seems that in 2008 the support structure is raised at the upstream side.

In this thesis the mounting of the drift chambers on the support structure was also analyzed. The measured data of 2007 and 2008 show effects of the gravitational force and that the position of some drift chambers at the upstream and downstream side differs by up to 4 mm. It is clear that such differences have to be considered to obtain the geometrical alignment.

In 2008 the optical survey was improved with the consequence that the z coordinate of some measuring points was also determined. Because the x , y and z coordinate of each cross were measured it is possible to check if the distances between upstream and downstream crosses fit with the mechanical workshop survey, with the result that these two measurements are consistent. It is therefore reasonable to use this data set to determine the geometrical alignment of the drift chamber system.

But unfortunately it was only possible to measure a few support structure pins. There exist several strategies: One can determine an optimized plane for the measured pins and the other pins can be obtained by cutting the

angle measurement with this plane, or one assumes that all pins are aligned in a plane orthogonal to the beam axis with a z coordinate which is given by the mean value of the measured pins. It is not yet decided which strategy will be used.

All measured z coordinates of crosses and pins show an overall offset of almost 2 mm in $+z$ direction but such a displacement is impossible because otherwise the support structure would not be supported by the centering mechanism which was not the case. The problem with these 2 mm is still not solved.

But nevertheless, I developed a strategy to derive the anode wire positions if the coordinates of the pins and crosses are known. The detailed calculation as well as all assumptions and simplifications are presented in this thesis. With this calculation the geometrical alignment of the drift chamber system is provided.

A first positron track analysis of Feng Xiao gives a mean wire displacement from the geometrical alignment of about $50 \mu\text{m}$. As already mentioned in section 6.2, this displacement corresponds to the accuracy of the drift chamber production. This analysis was done by using measured x , y and z coordinates of drift chamber crosses and by using pin planes with z coordinates which are determined by the average z positions of three downstream and five upstream pins.

Additionally to drift chamber crosses and support structure pins the coordinates of target crosses were also measured. With the help of cross positions which were measured by a plane-table it was possible to apply a consistency check on cross coordinates which were measured by the optical survey 2008. The result shows that all crosses passed the check with the exception of cross named target0.

The reproducibility of the target position before and after target movements was also tested. With the result that the data sets show systematic shifts but within the error margin. To check the reproducibility more detailed it is necessary to do more measurements.

By using the data set which was obtained by the optical survey after target movements it was possible to determine the target plane and therefore the location of the target inside COBRA. With the help of this plane the target slant angle was also determined:

$$\alpha = (20.6 \pm 0.2)^\circ \quad (10.1)$$

This value is compatible with the results of other target slant angle determination methods. The mean value of all these results is used as target slant angle for run 2008:

$$\alpha_{2008} = (20.5 \pm 0.3)^\circ \quad (10.2)$$

Appendix A

Labeling and Numbering

To prevent confusion about the used labeling and numbering, this chapter will give a detailed overview about this issue. In this thesis I will use this introduced labeling without any comments or references to this appendix A.

A.1 Orientation in Area $\pi E5$

To orientate oneself in area $\pi E5$ the naming convention shown in figure A.1 is used. The labels berg and aare are normally used by the PSI Hallendienst and describe the geographical alignment of the experimental hall.

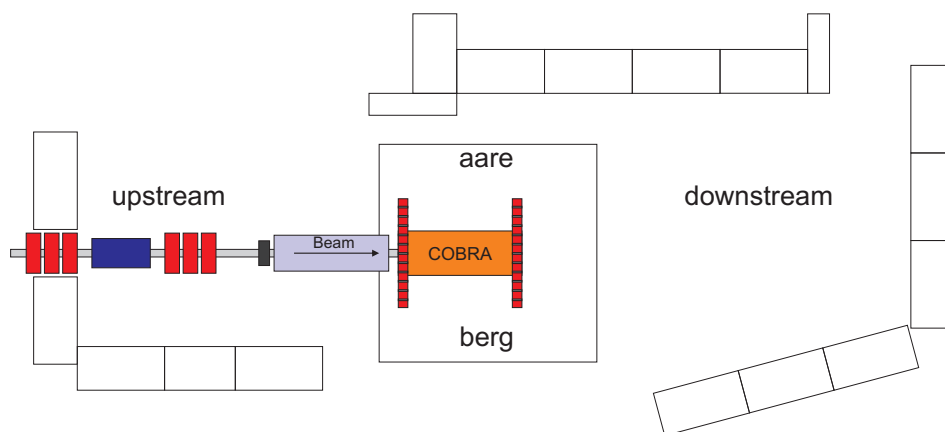


Figure A.1: Outline of area $\pi E5$ with labels upstream, downstream, berg and aare.

A.2 MEG Coordinate System

The following right-handed orthogonal coordinate system is normally used in the MEG experiment (see for example figure 3.6 or 3.7):

- x axis: from berg to aare
- y axis: height
- z axis: in beam direction
- origin: center of COBRA main magnet

A.3 Drift Chamber Labeling and Numbering

A.3.1 upstream / downstream

All cables, pre-amplifier cards, gas connections and measuring points for optical surveys (see section 5.2) at each edge of the drift chamber are labeled with upstream or downstream as shown in figure A.2.

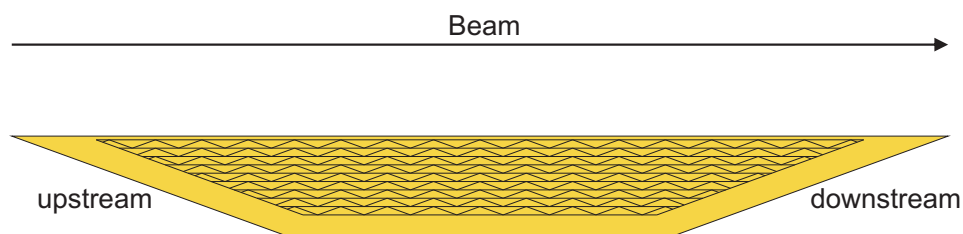


Figure A.2: Schematic drawing of one drift chamber and beam direction. Additionally, the labels upstream and downstream used for drift chamber connections and survey marks are also shown.

A.3.2 Drift Chamber Numbering

The numbering of drift chambers is very easy because it is defined on the order in which positrons fly through modules, starting with dc00 and ending with dc15 as shown in figure A.3.

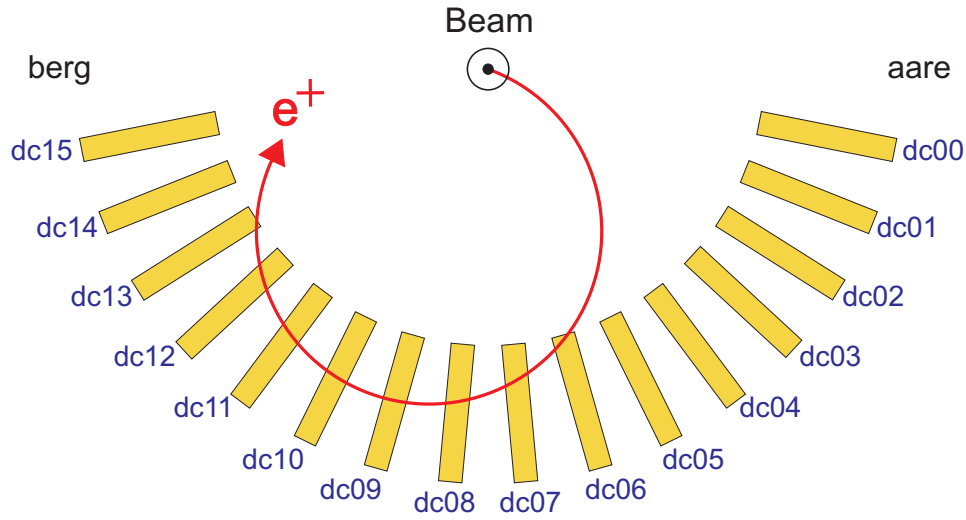


Figure A.3: Schematic drawing of the drift chamber system viewed from downstream with numbered modules starting with dc00 and ending with dc15.

A.3.3 plane A / plane B

Each drift chamber consists of two drift layers shifted against each other. The layer with the outermost anode wire is called plane A whereas plane B is the name of the other one as shown in figure A.4. This convention is maybe a little bit confusing because positrons always traverse firstly plane B and then plane A of each chamber.

A.3.4 Anode Wire Numbering

Anode wire numbering of each drift layer is again very easy because the innermost wire is called a0 whereas the outermost is labeled with a8 as shown in figure A.4.

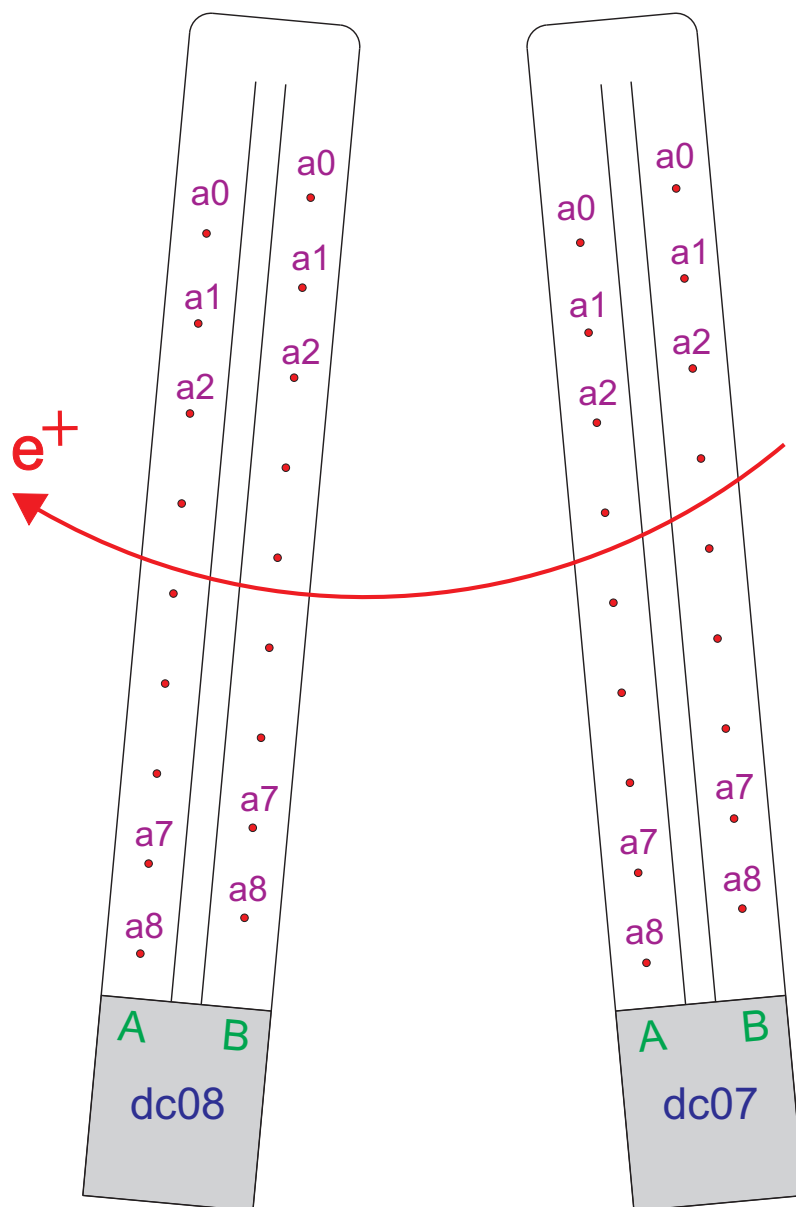


Figure A.4: Schematic drawing of drift chambers dc07 and dc08 viewed from downstream with labeled planes A and B. Additionally, the numbering of anode wires is also shown.

Appendix B

Data Mechanical Workshop Survey 2007

B.1 Data No.4/No.5 and No.7/No.8

Table B.1: Data of measurements No.4/No.5 and No.7/No.8 of the mechanical workshop survey 2007. All values are given in millimeter.

ID	No.4 [mm]	No.5 [mm]	No.7 [mm]	No.8 [mm]
dc00	0.855	0.972	0.959	1.042
dc01	-0.283	-0.033	-0.330	-0.339
dc02	0.018	-0.022	-0.618	-0.582
dc03	-0.859	-0.706	-1.086	-1.133
dc04	0.148	0.332	0.466	0.506
dc05	-0.505	-0.291	-0.499	-0.340
dc06	0.306	0.600	-0.489	-0.325
dc07	1.419	1.795	1.596	1.793
dc08	0.999	1.192	0.505	0.509
dc09	-1.529	-1.549	-0.635	-0.677
dc10	1.638	1.997	1.094	1.113
dc11	-0.312	-0.464	-0.141	-0.300
dc12	1.639	1.948	1.253	1.416
dc13	0.854	0.975	0.899	1.062
dc14	-1.111	-1.185	-0.525	-0.455
dc15	0.320	0.543	0.759	0.886

B.2 Data No.10/No.11 and No.6/No.9

Table B.2: Data of measurements No.10/No.11 and No.6/No.9 of the mechanical workshop survey 2007. All values are given in millimeter.

ID	No.10 [mm]	No.11 [mm]	No.6 [mm]	No.9 [mm]
dc00	110.539	110.571	-696.085	263.800
dc01	110.211	110.253	-696.173	265.170
dc02	110.658	110.748	-695.203	263.714
dc03	110.320	110.524	-696.313	262.667
dc04	110.672	110.419	-695.565	263.156
dc05	110.440	110.536	-696.161	265.289
dc06	110.538	110.436	-696.392	265.020
dc07	110.596	110.572	-696.037	264.946
dc08	110.398	110.560	-696.189	264.396
dc09	110.649	110.660	-695.978	263.939
dc10	110.277	110.271	-696.140	263.766
dc11	110.543	110.769	-695.972	263.782
dc12	110.427	110.311	-696.549	264.800
dc13	110.613	110.696	-696.090	264.369
dc14	110.564	110.692	-696.049	263.080
dc15	110.501	110.578	-695.549	263.708

Appendix C

Data Optical Survey 2007

C.1 Pins with given z Positions

Table C.1: Data of support structure pins downstream obtained by optical survey 2007 with given z positions.

2007: Pin d with given z			
ID	X [mm]	Y [mm]	Z [mm]
pin00 d	275.14	-28.53	253.00
pin01 d	265.42	-77.96	253.00
pin02 d	246.97	-124.87	253.00
pin03 d	220.28	-167.96	253.00
pin04 d	185.80	-205.49	253.00
pin05 d	145.01	-236.17	253.00
pin06 d	99.44	-258.99	253.00
pin07 d	50.43	-272.99	253.00
pin08 d	-0.23	-277.52	253.00
pin09 d	-50.87	-272.74	253.00
pin10 d	-99.76	-258.54	253.00
pin11 d	-145.33	-235.47	253.00
pin12 d	-186.11	-204.76	253.00
pin13 d	-220.93	-167.40	253.00
pin14 d	-248.29	-124.74	253.00
pin15 d	-267.42	-77.93	253.00
pin16 d	-277.63	-28.71	253.00

Table C.2: Data of support structure pins upstream obtained by optical survey 2007 with given z positions.

2007: Pin u with given z			
ID	X [mm]	Y [mm]	Z [mm]
pin00 u	255.63	-26.13	-245.00
pin01 u	246.41	-72.10	-245.00
pin02 u	228.95	-115.78	-245.00
pin03 u	204.02	-155.72	-245.00
pin04 u	172.26	-190.64	-245.00
pin05 u	134.73	-219.17	-245.00
pin06 u	92.50	-240.20	-245.00
pin07 u	47.18	-253.05	-245.00
pin08 u	0.21	-257.50	-245.00
pin09 u	-46.72	-253.14	-245.00
pin10 u	-92.16	-240.13	-245.00
pin11 u	-134.47	-219.10	-245.00
pin12 u	-172.28	-190.86	-245.00
pin13 u	-204.41	-156.26	-245.00
pin14 u	-229.70	-116.45	-245.00
pin15 u	-247.43	-72.98	-245.00
pin16 u	-256.68	-26.95	-245.00

C.2 DC Crosses with given z Positions

Table C.3: Data of drift chamber crosses downstream obtained by optical survey 2007 with given z positions.

2007: DC cross d with given z			
ID	X [mm]	Y [mm]	Z [mm]
cross00 d	170.36	-36.06	480.50
cross01 d	161.56	-67.17	480.50
cross02 d	146.32	-95.87	480.50
cross03 d	128.35	-120.28	480.50
cross04 d	104.35	-140.96	480.50
cross05 d	76.72	-157.85	480.50
cross06 d	47.02	-168.90	480.50
cross07 d	17.34	-173.86	480.50
cross08 d	-15.30	-174.62	480.50
cross09 d	-48.65	-169.14	480.50
cross10 d	-76.78	-158.55	480.50
cross11 d	-104.49	-139.53	480.50
cross12 d	-127.53	-120.06	480.50
cross13 d	-147.10	-94.06	480.50
cross14 d	-163.98	-63.79	480.50
cross15 d	-172.35	-34.36	480.50

Table C.4: Data of drift chamber crosses upstream obtained by optical survey 2007 with given z positions.

2007: DC cross u with given z			
ID	X [mm]	Y [mm]	Z [mm]
cross00 u	171.97	-33.45	-480.00
cross01 u	161.81	-65.05	-480.00
cross02 u	146.73	-93.46	-480.00
cross03 u	126.68	-118.46	-480.00
cross04 u	105.33	-140.25	-480.00
cross05 u	77.36	-157.15	-480.00
cross06 u	47.14	-169.23	-480.00
cross07 u	17.64	-174.38	-480.00
cross08 u	-14.75	-174.32	-480.00
cross09 u	-47.36	-168.69	-480.00
cross10 u	-75.39	-156.52	-480.00
cross11 u	-104.51	-140.42	-480.00
cross12 u	-127.30	-119.72	-480.00
cross13 u	-147.28	-94.38	-480.00
cross14 u	-162.60	-64.39	-480.00
cross15 u	-171.31	-34.71	-480.00

Appendix D

Data Optical Survey 2008

D.1 Pins with given z Positions

Table D.1: Data of support structure pins downstream obtained by optical survey 2008 with given z positions.

2008: Pin d with given z			
ID	X [mm]	Y [mm]	Z [mm]
pin00 d	256.22	-25.94	253.00
pin01 d	247.15	-72.26	253.00
pin02 d	229.77	-116.11	253.00
pin03 d	204.71	-156.01	253.00
pin04 d	172.66	-190.50	253.00
pin05 d	134.78	-218.55	253.00
pin06 d	92.35	-239.49	253.00
pin07 d	47.09	-252.35	253.00
pin08 d	0.09	-256.77	253.00
pin09 d	-47.03	-252.41	253.00
pin10 d	-92.28	-239.64	253.00
pin11 d	-134.51	-218.48	253.00
pin12 d	-172.45	-190.27	253.00
pin13 d	-204.45	-155.83	253.00
pin14 d	-229.86	-115.86	253.00
pin15 d	-247.53	-72.11	253.00
pin16 d	-256.81	-25.99	253.00

Table D.2: Data of support structure pins upstream obtained by optical survey 2008 with given z positions.

2008: Pin u with given z			
ID	X [mm]	Y [mm]	Z [mm]
pin00 u	256.93	-25.10	-245.00
pin01 u	247.61	-71.25	-245.00
pin02 u	230.09	-115.01	-245.00
pin03 u	204.96	-154.85	-245.00
pin04 u	173.05	-189.41	-245.00
pin05 u	135.27	-217.86	-245.00
pin06 u	93.07	-238.70	-245.00
pin07 u	47.70	-251.52	-245.00
pin08 u	0.75	-255.96	-245.00
pin09 u	-46.24	-251.79	-245.00
pin10 u	-91.56	-238.94	-245.00
pin11 u	-133.95	-218.21	-245.00
pin12 u	-171.73	-190.24	-245.00
pin13 u	-203.56	-155.68	-245.00
pin14 u	-228.72	-115.77	-245.00
pin15 u	-246.20	-72.03	-245.00
pin16 u	-255.60	-25.70	-245.00

D.2 DC Crosses with given z Positions

Table D.3: Data of drift chamber crosses downstream obtained by optical survey 2008 with given z positions.

2008: DC cross d with given z			
ID	X [mm]	Y [mm]	Z [mm]
cross00 d	170.99	-34.49	480.50
cross01 d	162.07	-66.04	480.50
cross02 d	146.36	-94.62	480.50
cross03 d	127.76	-119.51	480.50
cross04 d	103.87	-140.26	480.50
cross05 d	75.64	-157.40	480.50
cross06 d	46.93	-168.47	480.50
cross07 d	16.77	-174.31	480.50
cross08 d	-15.54	-174.13	480.50
cross09 d	-49.03	-168.27	480.50
cross10 d	-76.74	-157.65	480.50
cross11 d	-104.24	-139.61	480.50
cross12 d	-127.48	-119.84	480.50
cross13 d	-146.88	-94.63	480.50
cross14 d	-162.43	-63.11	480.50
cross15 d	-172.82	-34.54	480.50

Table D.4: Data of drift chamber crosses upstream obtained by optical survey 2008 with given z positions.

2008: DC cross u with given z			
ID	X [mm]	Y [mm]	Z [mm]
cross00 u	173.47	-32.11	-480.00
cross01 u	163.19	-64.03	-480.00
cross02 u	148.18	-92.01	-480.00
cross03 u	127.99	-116.80	-480.00
cross04 u	105.65	-138.96	-480.00
cross05 u	77.61	-155.65	-480.00
cross06 u	48.19	-167.56	-480.00
cross07 u	18.04	-171.93	-480.00
cross08 u	-14.47	-172.50	-480.00
cross09 u	-46.87	-164.59	-480.00
cross10 u	-75.65	-156.55	-480.00
cross11 u	-103.34	-139.30	-480.00
cross12 u	-125.88	-118.67	-480.00
cross13 u	-145.91	-94.08	-480.00
cross14 u	-161.60	-64.43	-480.00
cross15 u	-170.40	-35.06	-480.00

D.3 Pins with measured z Positions

Table D.5: Data of support structure pins downstream obtained by optical survey 2008 with measured z positions.

2008: Pin d with measured z			
ID	X [mm]	Y [mm]	Z [mm]
pin00 d	255.89	-25.91	255.21
pin01 d	246.83	-72.17	255.16
pin16 d	-256.57	-25.96	254.58

Table D.6: Data of support structure pins upstream obtained by optical survey 2008 with measured z positions.

2008: Pin u with measured z			
ID	X [mm]	Y [mm]	Z [mm]
pin00 u	256.72	-25.08	-243.29
pin01 u	247.43	-71.20	-243.38
pin14 u	-228.54	-115.67	-243.31
pin15 u	-245.93	-71.96	-242.60
pin16 u	-255.41	-25.68	-243.39

D.4 DC Crosses with measured z Positions

Table D.7: Data of drift chamber crosses downstream obtained by optical survey 2008 with measured z positions.

2008: DC cross d with measured z			
ID	X [mm]	Y [mm]	Z [mm]
cross00 d	170.86	-34.46	481.59
cross01 d	161.89	-65.97	482.06
cross02 d	146.36	-94.62	480.50
cross03 d	127.68	-119.44	481.44
cross04 d	103.81	-140.18	481.35
cross05 d	75.55	-157.22	482.16
cross06 d	46.87	-168.24	482.43
cross07 d	16.74	-174.06	482.65
cross08 d	-15.52	-173.89	482.53
cross09 d	-48.97	-168.09	482.07
cross10 d	-76.65	-157.46	482.19
cross11 d	-104.14	-139.48	481.83
cross12 d	-127.32	-119.69	482.34
cross13 d	-146.75	-94.55	481.75
cross14 d	-162.26	-63.04	482.06
cross15 d	-172.64	-34.50	481.97

Table D.8: Data of drift chamber crosses upstream obtained by optical survey 2008 with measured z positions.

2008: DC cross u with measured z			
ID	X [mm]	Y [mm]	Z [mm]
cross00 u	173.33	-32.08	-478.10
cross01 u	163.13	-64.00	-479.04
cross02 u	148.09	-91.94	-478.39
cross03 u	127.87	-116.69	-477.75
cross04 u	105.54	-138.81	-477.39
cross05 u	77.60	-155.62	-479.48
cross06 u	48.17	-167.50	-479.13
cross07 u	18.03	-171.82	-478.42
cross08 u	-14.46	-172.35	-477.87
cross09 u	-46.83	-164.45	-477.93
cross10 u	-75.59	-156.42	-477.96
cross11 u	-103.24	-139.16	-477.64
cross12 u	-125.83	-118.62	-478.96
cross13 u	-145.79	-94.00	-478.03
cross14 u	-161.36	-64.34	-476.40
cross15 u	-170.19	-35.02	-477.03

Appendix E

Data Theoretical Positions

E.1 Theoretical Positions Pins

Table E.1: Theoretical positions of support structure pins downstream for 2007 and 2008.

ID	2007			2008		
	X [mm]	Y [mm]	Z [mm]	X [mm]	Y [mm]	Z [mm]
pin00 d	275.98	-29.01	253.00	256.09	-25.92	253.00
pin01 d	266.07	-78.81	253.00	246.90	-72.13	253.00
pin02 d	247.25	-125.98	253.00	229.43	-115.90	253.00
pin03 d	220.16	-168.93	253.00	204.29	-155.76	253.00
pin04 d	185.68	-206.22	253.00	172.30	-190.36	253.00
pin05 d	144.99	-236.61	253.00	134.54	-218.56	253.00
pin06 d	99.45	-259.07	253.00	92.28	-239.40	253.00
pin07 d	50.57	-272.85	253.00	46.93	-252.19	253.00
pin08 d	0.00	-277.50	253.00	0.00	-256.50	253.00
pin09 d	-50.57	-272.85	253.00	-46.93	-252.19	253.00
pin10 d	-99.45	-259.07	253.00	-92.28	-239.40	253.00
pin11 d	-144.99	-236.61	253.00	-134.54	-218.56	253.00
pin12 d	-185.68	-206.22	253.00	-172.30	-190.36	253.00
pin13 d	-220.16	-168.93	253.00	-204.29	-155.76	253.00
pin14 d	-247.25	-125.98	253.00	-229.43	-115.90	253.00
pin15 d	-266.07	-78.81	253.00	-246.90	-72.13	253.00
pin16 d	-275.98	-29.01	253.00	-256.09	-25.92	253.00

Table E.2: Theoretical positions of support structure pins upstream for 2007 and 2008.

ID	2007			2008		
	X [mm]	Y [mm]	Z [mm]	X [mm]	Y [mm]	Z [mm]
pin00 u	256.09	-26.92	-245.00	256.09	-25.92	-245.00
pin01 u	246.90	-73.13	-245.00	246.90	-72.13	-245.00
pin02 u	229.43	-116.90	-245.00	229.43	-115.90	-245.00
pin03 u	204.29	-156.76	-245.00	204.29	-155.76	-245.00
pin04 u	172.30	-191.36	-245.00	172.30	-190.36	-245.00
pin05 u	134.54	-219.56	-245.00	134.54	-218.56	-245.00
pin06 u	92.28	-240.40	-245.00	92.28	-239.40	-245.00
pin07 u	46.93	-253.19	-245.00	46.93	-252.19	-245.00
pin08 u	0.00	-257.50	-245.00	0.00	-256.50	-245.00
pin09 u	-46.93	-253.19	-245.00	-46.93	-252.19	-245.00
pin10 u	-92.28	-240.40	-245.00	-92.28	-239.40	-245.00
pin11 u	-134.54	-219.56	-245.00	-134.54	-218.56	-245.00
pin12 u	-172.30	-191.36	-245.00	-172.30	-190.36	-245.00
pin13 u	-204.29	-156.76	-245.00	-204.29	-155.76	-245.00
pin14 u	-229.43	-116.90	-245.00	-229.43	-115.90	-245.00
pin15 u	-246.90	-73.13	-245.00	-246.90	-72.13	-245.00
pin16 u	-256.09	-26.92	-245.00	-256.09	-25.92	-245.00

E.2 Expected Positions DC Crosses

Table E.3: Expected positions of drift chamber crosses downstream for 2007 and 2008.

ID	2007			2008		
	X [mm]	Y [mm]	Z [mm]	X [mm]	Y [mm]	Z [mm]
cross00 d	171.94	-34.04	480.50	172.88	-33.79	480.50
cross01 d	163.17	-65.09	480.50	164.04	-64.96	480.50
cross02 d	148.37	-93.55	480.50	149.18	-93.27	480.50
cross03 d	129.31	-119.19	480.50	129.94	-118.86	480.50
cross04 d	104.94	-140.76	480.50	105.71	-140.02	480.50
cross05 d	77.22	-158.16	480.50	77.89	-157.21	480.50
cross06 d	47.13	-169.72	480.50	47.50	-168.78	480.50
cross07 d	15.80	-175.43	480.50	15.69	-174.61	480.50
cross08 d	-16.35	-175.49	480.50	-16.28	-174.78	480.50
cross09 d	-47.32	-169.32	480.50	-47.80	-168.66	480.50
cross10 d	-77.74	-157.68	480.50	-77.87	-157.36	480.50
cross11 d	-105.32	-140.17	480.50	-105.46	-140.04	480.50
cross12 d	-130.51	-117.61	480.50	-129.93	-118.26	480.50
cross13 d	-150.27	-91.83	480.50	-149.41	-92.63	480.50
cross14 d	-165.05	-63.49	480.50	-164.21	-63.98	480.50
cross15 d	-174.45	-32.78	480.50	-173.55	-33.00	480.50

Table E.4: Expected positions of drift chamber crosses upstream for 2007 and 2008.

ID	2007			2008		
	X [mm]	Y [mm]	Z [mm]	X [mm]	Y [mm]	Z [mm]
cross00 u	172.26	-33.41	-480.00	173.53	-32.37	-480.00
cross01 u	163.41	-64.23	-480.00	164.59	-63.39	-480.00
cross02 u	148.18	-93.17	-480.00	149.43	-92.02	-480.00
cross03 u	128.79	-119.14	-480.00	130.07	-117.65	-480.00
cross04 u	104.95	-141.12	-480.00	105.91	-139.63	-480.00
cross05 u	77.69	-157.90	-480.00	78.48	-156.38	-480.00
cross06 u	47.81	-169.53	-480.00	48.43	-168.00	-480.00
cross07 u	15.92	-175.34	-480.00	16.46	-173.81	-480.00
cross08 u	-15.83	-175.36	-480.00	-15.64	-173.89	-480.00
cross09 u	-47.28	-169.35	-480.00	-46.93	-168.02	-480.00
cross10 u	-77.72	-157.96	-480.00	-77.61	-156.69	-480.00
cross11 u	-105.07	-140.58	-480.00	-104.82	-139.60	-480.00
cross12 u	-129.80	-118.97	-480.00	-128.87	-118.62	-480.00
cross13 u	-149.25	-93.09	-480.00	-148.18	-92.69	-480.00
cross14 u	-164.11	-64.27	-480.00	-162.79	-63.98	-480.00
cross15 u	-173.33	-34.12	-480.00	-172.21	-32.76	-480.00

Appendix F

Data Target Measurements

F.1 Target Crosses in Local Coordinate System

Table F.1: Data of target crosses in a local coordinate system.

Local Coordinate System		
ID	u [mm]	v [mm]
target0	0.00	0.00
target1	27.61	1.66
target2	75.88	4.62
target3	126.10	7.61
target4	164.63	9.92
target5	74.04	30.50
target6	77.72	-22.15

F.2 Measured Target Crosses in 2008

Table F.2: Data of target crosses measured by the optical survey 2008 before movements.

Before Movements			
ID	X [mm]	Y [mm]	Z [mm]
target0	-28.39	2.01	73.67
target1	-18.48	1.43	48.26
target2	-1.66	0.45	3.21
target3	16.14	-0.68	-44.01
target4	29.79	-1.51	-80.30
target5	-1.27	26.42	2.77
target6	-2.03	-26.42	3.22

Table F.3: Data of target crosses measured by the optical survey 2008 after movements.

After Movements			
ID	X [mm]	Y [mm]	Z [mm]
target0_2	-28.17	1.65	74.51
target1_2	-18.41	1.16	48.36
target2_2	-1.52	0.14	3.42
target3_2	16.31	-0.99	-43.53
target4_2	29.85	-1.86	-79.94
target5_2	-1.13	26.08	3.39
target6_2	-1.91	-26.74	3.44

Bibliography

- [1] Bogdan Povh u.a. *Teilchen und Kerne - Eine Einführung in die physikalischen Konzepte*. Springer Verlag, 6th edition, 2004. ISBN: 3-540-21065-2.
- [2] Francis Halzen and Alan D. Martin. *Quarks and Leptons: An Introductory Course in Modern Particle Physics*. John Wiley & Sons, 1984. ISBN: 0-471-88741-2.
- [3] Particle Data Group: W. M. Yao et. al. Review of Particle Physics. *Journal of Physics G: Nuclear and Particle Physics*, 33(1), July 2006. Website: <http://pdg.lbl.gov>.
- [4] SNO Collaboration: Q. R. Ahmad et.al. Measurement of the Rate of $\nu_e + d \rightarrow p + p + e^-$ Interactions Produced by ^8B Solar Neutrinos at the Sudbury Neutrino Observatory. *Physical Review Letters*, 87(7):071301, August 2001.
- [5] Super-Kamiokande Collaboration: Y. Fukada et.al. Evidence for Oscillation of Atmospheric Neutrinos. *Physical Review Letters*, 81(8):1562–1567, August 1998.
- [6] Super-Kamiokande Collaboration: S. Fukada et.al. Solar ^8B and hep Neutrino Measurements from 1258 Days of Super-Kamiokande Data. *Physical Review Letters*, 86(25):5651–5655, June 2001.
- [7] W. Fetscher and A. Rubbia. *Physik der Neutrinos*. Lecture Notes, WS 2006.
- [8] T. P. Cheng and L. F. Li. $\mu \rightarrow e \gamma$ in Theories with Dirac and Majorana Neutrino-Mass Terms. *Physical Review Letters*, 45(24):1908–1911, December 1980.
- [9] C. H. Albright and M. C. Chen. Lepton flavor violation in predictive supersymmetric GUT models. *Physical Review D*, 77(113010):1–14, June 2008.

- [10] MEGA Collaboration: M. L. Brooks et.al. New Limit for the Lepton-Family-Number Nonconserving Decay $\mu^+ \rightarrow e^+\gamma$. *Physical Review Letters*, 83(8):1521–1524, August 1999. arXiv:hep-ex/9905013.
- [11] P. Depommier et.al. New Limit on the Decay $\mu^+ \rightarrow e^+\gamma$. *Physical Review Letters*, 39(18):1113–1116, October 1977.
- [12] A. van der Schaaf et.al. A search for the decay $\mu^+ \rightarrow e^+\gamma$. *Nuclear Physics A*, 340(2):249–270, May 1980.
- [13] W. W. Kinnison et.al. Search for $\mu^+ \rightarrow e^+\gamma$. *Physical Review D*, 25(11):2846–2868, June 1982.
- [14] R. D. Bolton et.al. Search for rare muon decays with the Crystal Box detector. *Physical Review D*, 38(7):2077–2101, October 1988.
- [15] MEG Collaboration: Stefan Ritt. Meg Home Page. <http://meg.psi.ch> [11th June 2008].
- [16] PSI - Paul Scherrer Institute. Accelerator Facilities. <http://abe.web.psi.ch/facilities/facilities.php> [4th June 2008].
- [17] PSI - Paul Scherrer Institute: Laboratory for Particle Physics (LTP). Welcome to the Detector Group of Particle Physics. http://ltp.web.psi.ch/organisation_of_ltp/detector_group.htm [11th June 2008].
- [18] PSI - Paul Scherrer Institute: Laboratory for Particle Physics (LTP). LTP Home. <http://ltp.web.psi.ch> [11th June 2008].
- [19] PSI - Paul Scherrer Institute: TEM - Research Department Particles and Matter. TEM Home. <http://tem.web.psi.ch> [11th June 2008].
- [20] Hajime Nishiguchi. *An Innovative Positron Spectrometer to Search for the Lepton Flavour Violating Muon Decay with a Sensitivity of 10^{-13}* . PhD thesis, University of Tokyo, 2008.
- [21] PSI - Paul Scherrer Institute: Abteilung Technik / Koordination / Betrieb. PSI Vermessung. <http://atk.web.psi.ch/8842/index.html> [21th June 2008].
- [22] PSI - Paul Scherrer Institute: Abteilung Technik / Koordination / Betrieb. PSI Vermessung: Instrumentarium. <http://atk.web.psi.ch/8842/instrumente.html> [12th July 2008].
- [23] Leica Geosystems. Home - Leica Geosystems. <http://www.leica-geosystems.com> [21th June 2008].
- [24] PSI - Paul Scherrer Institute: Abteilung Technik / Koordination / Betrieb. PSI Vermessung: Referenzpunkte. <http://atk.web.psi.ch/8842/referenzpunkte.html> [22th June 2008].

Acknowledgements

First of all I would like to thank Prof. Dr. Urs Langenegger for giving me the opportunity to do my diploma thesis in the MEG experiment at PSI.

I'm especially grateful for the support and advice of Dr. Malte Hildebrandt. During our discussions I learned a lot about the MEG experiment and especially about the MEG drift chamber system. I would also like to thank Dr. Malte Hildebrandt for reading my diploma thesis carefully and making useful suggestions. Special thanks go to Dr. Stefan Ritt for supporting and helping me whenever necessary. My thanks also go to Dr. Peter-Raymond Kettle for answering all my questions about the target. I would also like to thank Dieter Fahrni and Andreas Hofer for explaining me a lot about the drift chamber assembly, the support structure and the mechanical workshop survey. Thanks go also to the PSI Survey Group especially to Karsten Dreyer and Tino Hoewler who gave me an introduction about optical surveys.

Finally, I would like to thank my family and my friends for their support during my studies.